Department of Precision and Microsystems Engineering

A new concept in bearing technology: Magnetorheological texturing

M.C. de Graaf

Report no	:	2019.001
Coach	:	S.G.E. Lampaert
Professor	:	R.A.J. van Ostayen
Specialisation	:	Mechatronic System Design
Type of report	:	Master of Science Thesis
Date	:	January 2019

TU Delft Delft University of Technology

Challenge the future

A new concept in bearing technology: Magnetorheological texturing

by

M.C. de Graaf

to obtain the degree of Master of Science
at the Delft University of Technology,
to be defended publicly on Tuesday January 29, 2019 at 14:00.

Student number:	4286758	
Project duration:	September, 2017 – January, 2019	
Thesis committee:	Dr. ir. R.A.J. van Ostayen,	TU Delft, chairman
	Ir. S.G.E. Lampaert,	TU Delft, supervisor
	Prof. dr. ir. W. van de Water,	TU Delft
	Ir. F. Quenci,	AEGIR-Marine

TU Delft Delft University of Technology

"The best things in life are on the other side of terror, on the other side of your maximum fear, are all of the best things in life."

— *Will Smith*

Preface

September 2012, the beginning of my final year before going to university. Still not knowing what to choose, being scared of making the wrong decision. The one thing I knew at that time was that I already had a passion for technology. I wanted to understand and get to the bottom of new technologies and wanted to understand the underlying principles. During this last year before going to university I researched with a friend of mine the possibility of riding a Formula-1 car upside down through a tunnel. We made a small wind tunnel in order to simulate the velocity of a Formula-1 car, and in it a small scale model of the car. Optimizing this set-up, ultimately, the Formula-1 car did stick to the top! Observing my own joy doing this, I was determined to go to an university of technology but still feared the choices I had to make.

Ultimately choosing for Mechanical Engineering at the Delft University of Technology, was until now one of the best decisions in my life. During my years I have learned that fear can be good and can bring you great things. It is fear of failure, fear of losing, but failure is sometimes better than succeeding immediately. You learn so much more from failure and what to improve. For this you need people around you that care for you, and these I have met. They give you the last push in order to overcome your fears, at the moment you do not expect it.

Looking back I have not only gained a lot of new knowledge which prepared me for the future, but saw the importance of good people around you who want to push you to this new knowledge. My time in Delft was awesome, thank you.

> "Somebody opens the door, and in that moment, you realize you have never been in a freaking airplane with the door open. You are looking out down to death. They say, 'On three,' and they say, 'One, two,' and he pushes you on two because people grab on three. You fall out of the airplane. In one second, you realize that it is the most blissful experience of your life. You are flying. There is zero fear. *You realize at the point of maximum danger is the point of minimum fear. It is bliss.*"
>
> — *Will Smith, Skydiving experience*

Delft, University of Technology — M.C. de Graaf
January, 2018

Acknowledgements

First of all of course I want to thank my parents and my family for supporting me throughout my studies. You have always showed interest in my progress and my life here in Delft. You kept faith in me, and having people around you that have faith in you, really motivates you to succeed and keep on going.

Another person that really kept faith in me and I want to thank is my girlfriend Iris Heijboer. During the progress towards graduation, students experience highs but also many lows. During these 'lows', you were really there for me and convinced me to stop worrying, and that everything is going to be alright.

I want to thank the people of the Taylor board, Gijs van der Velden, Richard Pleeging, Justin Smid, and Ad Huisjes. During the year we were the board many good memories were made unrelated to my graduation, for which I am grateful. Being all together in one office for one whole year was good for the variation between education and some fun.

I want to thank the technical support staff of PME for helping me with my experiments. From time to time I knew what I wanted in theory but could not translate it to something practical which could be used for my experiments. For this translation I really needed you, you knew exactly what to get to make it work.

I want to thank everyone attending the full film meetings for all the discussions we have had regarding our research. When I was stuck at some points, you really helped me out from time to time. Sometimes you need a fresh perspective on the problem, and that is what you provided me with.

I want to thank Ron van Ostayen, Willem van de Water, Stefan Lampaert, and Federico Quinci for being on my graduation committee. I appreciate it that you make time for this and help me finish my graduation successfully.

I want to thank Ron van Ostayen for all the help and advice you gave me throughout my graduation. You exactly asked the right questions in order for me to notice something that needed more attention and improvement, resulting in better work.

At last I of course want to thank my supervisor Stefan Lampaert. The moment I needed help, you were there for me. Not only your criticism I am thankful for, but the advice you always gave with it. Every time I was really stuck, you always had some advice which directed me in a new direction to overcome this obstacle. Besides the many discussions regarding the project, we also had many conversations regarding many other things. It was never pure 'business' and you really showed interest in other things, and that is what I really appreciate. You really helped and motivated me throughout my graduation, and I will always be thankful for that.

Abstract

In fluid bearings the load is supported by a pressurized thin film of fluid. The bearing faces are separated by this thin film allowing for lower friction, wear and vibration than many other types of bearings. Fluid bearings have superior wear behavior but still the lifetime of this concept is in not infinite. Hydrostatic bearings do rely on pumps which are sensitive to failure and contribute to the system energy loss. Wear in hydrodynamic bearings is generally caused by poor lubrication during high loading conditions or low speeds. This wear gets especially troublesome when surface textures are used that can get worn away completely.

In this thesis two mechanisms utilizing surface textures for pressure buildup in a lubricating film using magnetorheological (MR) fluids are studied. The first uses local viscosity variation resulting in so-called virtual surface textures. These surface textures can be created using an MR fluid because their flow behavior can be controlled in presence of a magnetic field. The variable rheological properties of an MR fluid add an extra design variable to the system which can increase the performance of bearings. The second is also a new mechanism introduced in this thesis, the use of local sedimentation of magnetic particles in locations of higher magnetic field strengths resulting in physical surface textures. This second method can be considered as an initial step in the development of self-healing bearings, that is, bearings with a surface texture that is resistant to wear.

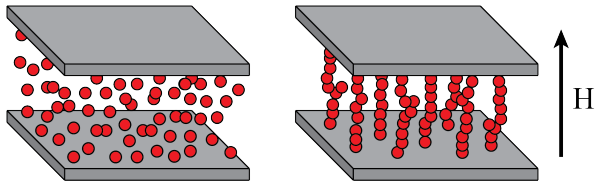

Figure 1: Formation of chain-like agglomerates in an MR fluid when subjected to a magnetic field.

In this thesis it is demonstrated that it is possible to create self-healing physical surface textures using an MR fluid as lubricant. It is demonstrated that these surface textures pressurize the fluid in order to obtain a load carrying capacity. The magnetic properties of an MR fluid are obtained when particles that have magnetic properties are suspended in a carrier fluid. When subjected to a magnetic field, the fluid greatly increases its apparent viscosity, to the point of becoming a solid. The strength of the solid phase is caused by the formation of certain structures by the particles, such as chain-like agglomerates (Fig. 1).

The first example studied to show the potential of virtual MR texturing is similar to a step geometry (Fig. 2). This in combination with a local varying magnetic field. This step shows

an antisymmetric pressure distribution which indicates pressurization of the fluid which can result in a load carrying capacity (Fig. 3). This demonstrates that it is possible to create surface textures using solely an MR fluid and a local varying magnetic field. This step cannot be obtained using a magnetic field that is constant across the film thickness. A constant magnetic field only results in a solid part in the middle of the channel for flow mode.

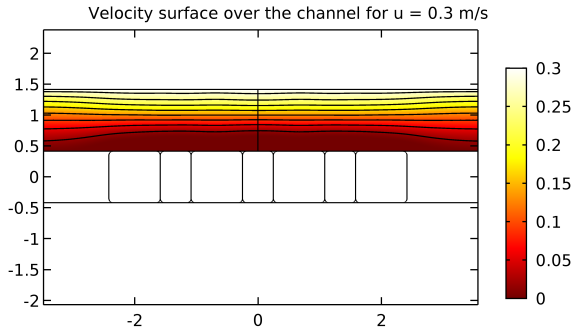

Figure 2: Solid part created at the middle of the length of the channel.

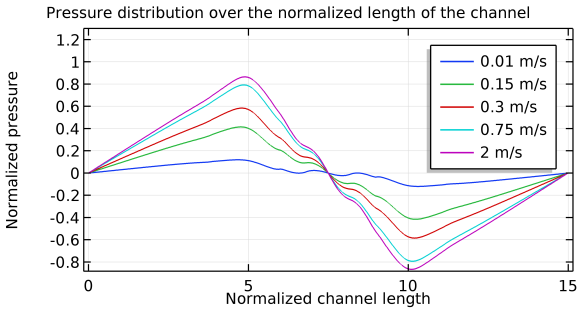

Figure 3: The normalized pressure distribution in the MR fluid with a solid part in the middle of the channel for different velocities of the moving wall.

A proof of concept for a hydrodynamic thrust bearing lubricated with an MR fluid in order to create surface textures is modeled and produced. For the models virtual and physical surface textures are considered which correspond to two extremes respectively, the case that the particles stay completely in suspension and for the case that the particles show complete sedimentation. The experimental results correspond to the situation where the magnetic particles are completely sedimented (Fig. 4). These sedimented particles form the physical surface textures over which the carrier fluid flows.

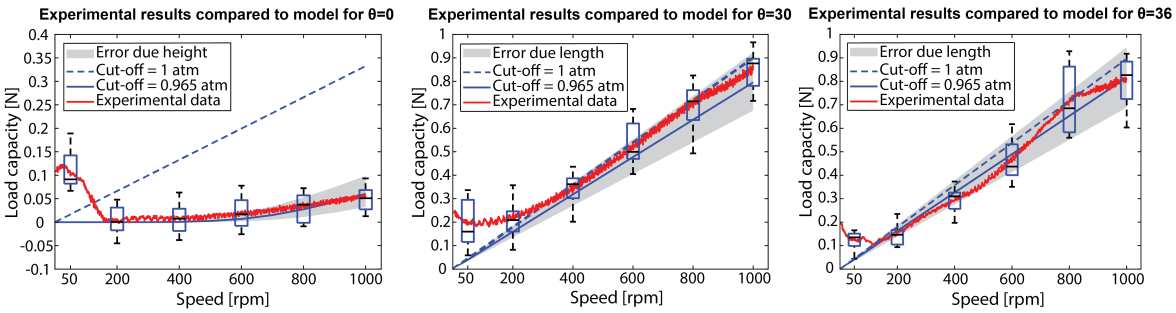

Figure 4: Comparison of the experimental results to numerical simulations for complete sedimentation.

It is demonstrated that the surface textures created are self-healing (Fig. 5). During the experiments the sedimented particles agglomerate around the magnets, because here the magnetic field is the strongest. These magnetic particles do not wear down and do not leave the system. These steps are self-healing, because magnetic particles are traded among these steps. The carrier fluid is pressurized by these textures which results in a load carrying capacity.

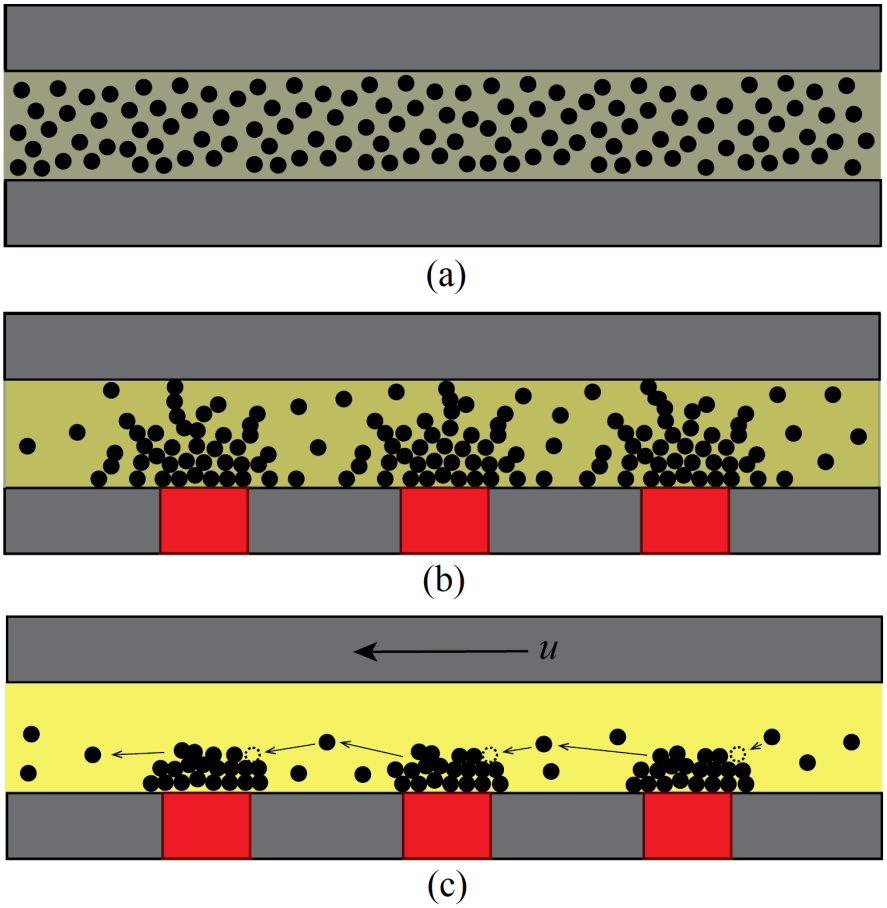

Figure 5: Illustration of the self-healing bearing. (a) MR fluid is trapped between the bearing surfaces and no magnetic field is applied. (b) Agglomerates are formed around the magnets. (c) During operation magnetic particles are traded among the self-healing steps.

Table of Contents

Chapter 1

Introduction

1-1 Introduction of the project

In 1929 the definition *"the study of the deformation and flow of matter"* for the new term "rheology" was accepted the moment the American Society of Rheology was founded. This term was invented by Professor Bingham [4]. Since the discoveries of Rabinow and Winslow in the 1940's [28, 64], the importance of magnetorheological (MR) fluids started to grow. Rabinow invented a high-speed magnetic fluid clutch (Fig. 1-1). He used a mixture of paramagnetic particles, for example iron, and a carrier fluid such as oil. When this mixture was exposed to a magnetic field it acted as a transmission for the force between two independently movable members. On top of that, since 1939 Winslow begun some experiments where it was established that when acted upon by an electric field an oil-occluding fibrous mass was formed by certain particles suspended in low viscosity oils.

Currently MR fluids are applied in many different fields. In the field of Mechanical Engineering they are used for damping in different applications, such as damping in vehicles used in the heavy industry. A good example is the MagneRide [12], which is a computer controlled suspension system that uses MR fluids. Here the amount of damping is controlled with magnetic energy. Besides this MR fluids are used for creating damping in prosthetic legs, where the fluid damps the shocks created when the patient for example is walking normally or jumps [14]. In [26] it is seen that the technology is also used in aerospace. Here it is implemented in a helicopter seat design to minimize the shock load-induced injury. These injuries are caused by harsh vertical landings or crash landings. MR fluids are even used for the military and defense, US Special Operations Command (SOCOM) is working with the Massachusetts Institute of Technology (MIT) to develop a new type of suit. This suit is called The Tactical

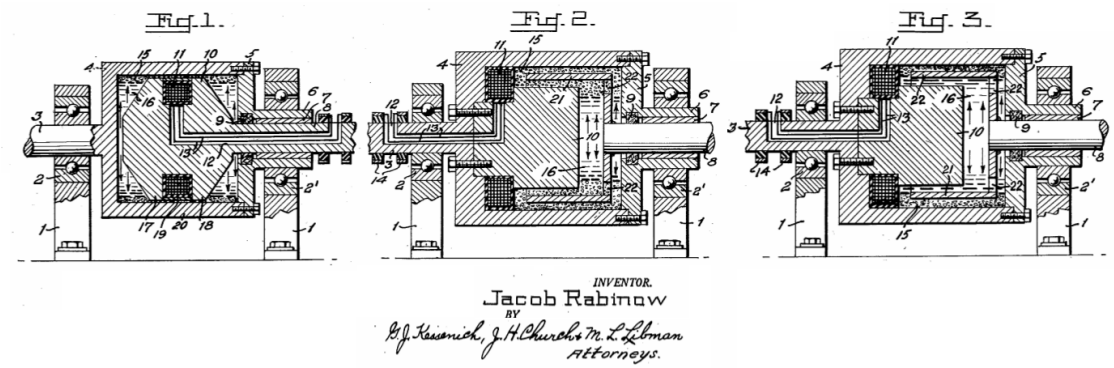

Figure 1-1: Different types of the electromagnetic clutches designed by Rabinow that use the magnetic fluid. Picture from [28].

Assault Light Operator Suit (TALOS) and it is required that this suit will be bulletproof and enhance the strengths of the wearer [63]. At last there is the magnetorheological finishing technology, this is a technology used for polishing optical surfaces, where a magnetorheological finishing slurry is used for the polishing [55].

As seen MR fluids are used in many different applications and bring great potential. Nevertheless, the use of magnetic fluids in rotational bearings is not that well developed yet and this brings great opportunity. The science behind bearings is well developed but still most bearings are basically the same as years ago [56]. Optimizing the geometry and the properties of the possible lubricants used, did improve the performance of the bearings. Despite this optimization and years long of development, wear and lifetime of bearings still occur to be big problems. To overcome this, big changes are required to solve this. In fluid bearings the load is supported by a pressurized thin film of fluid. The bearing faces are separated by this thin film allowing lower friction, wear and vibration than many other types of bearings [54].

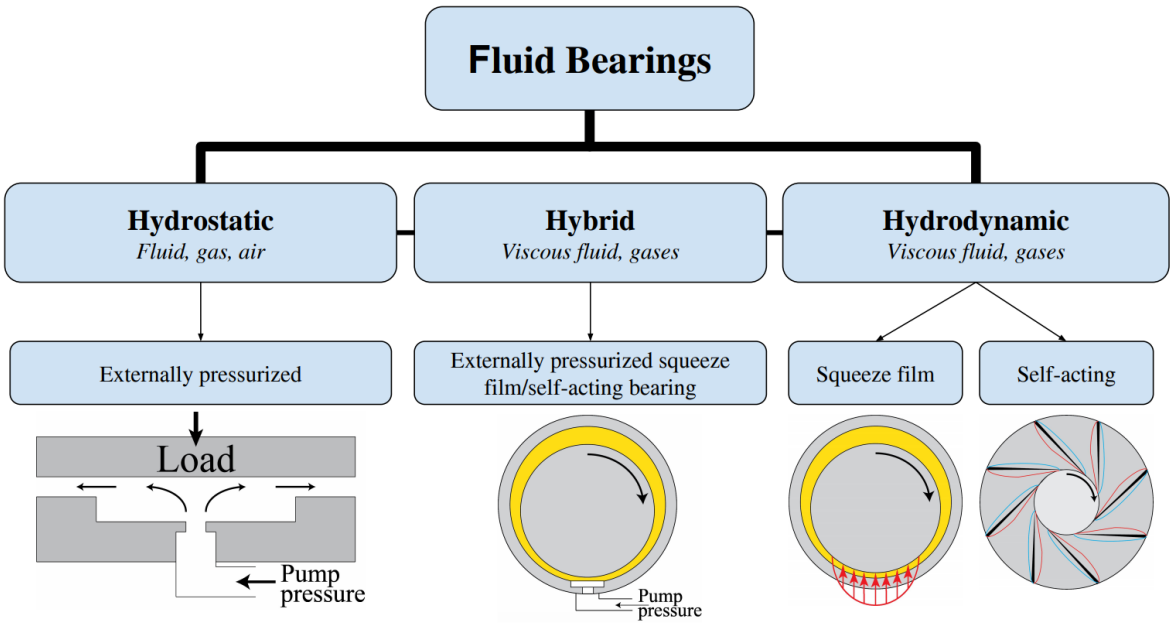

Figure 1-2: Categorization of fluid bearings.

Fluid bearings can be categorized as in figure 1-2. For hydrostatic bearings the fluid is externally pressurized by a pump. These pumps required, are sensitive to failure and contribute to the system energy loss, just as bearing friction otherwise would. For a good performance a hydrostatic bearing has to be equipped with a shaft position control system [27]. Hydrodynamic bearings pressurize the fluid due rapid movement of the bearing faces and thus rely on high speed. A squeeze film is where a film exists due to relative normal motion. Self-acting bearings pressurize the fluid using certain surface textures as seen in spiral groove bearings. At low speeds the bearings have a high friction and short life. This high friction is especially happening during starts and stops where the speed is not sufficient to maintain the thin fluid film. This can be prevented by externally pressurizing the fluid at lower speeds. These bearings can be categorized as hybrid bearings, and are a combination of hydrostatic and hydrodynamic bearings. A pump is used to prevent sliding friction at low speeds, then again these are sensitive to failure and contribute to the system energy loss.

1-2 Problem definition & research objective

Fluid bearings minimize friction and wear but still encounter different problems. The main causes of failure for lubricated bearings can be summarized as the following [7]:

- Pumps required for externally pressurization of the fluid are sensitive to failure and contribute to the system energy loss.
- At lower speeds, starts, and stops, metal to metal contact in the bearing cannot be avoided due to a not sufficient oil pressure and viscosity.
- Metal to metal contact occurs when the variation of the load and vibration exceed the acceptable level due to which the fluid film breaks.
- There can be a decrease in viscosity and load carrying capacity of the lubricant caused by the temperature increase of the lubricant during operation.

Smart fluids, like magnetic fluids, have the potential to improve the performance of these bearings and overcome these drawbacks. In literature it is seen that the tuneability for the rheological properties of ferrofluids is low and currently the load capacity is limited, in contrary to MR fluids. The variable rheological properties of an MR fluid add an extra design variable to the system which can increase the performance of bearings. MR fluids in combination with a constant magnetic field are used in fluid bearings in order to globally control the viscosity. This is already used to lower vibrations and prevent a decrease in viscosity and load carrying capacity for example caused by a temperature increase during operation. This is done in hydrodynamic bearings, and so a pump is also excluded from the system. Hydrodynamic bearings have superior wear behavior but still it is seen that the lifetime of this concept is not infinite. Wear of this bearing concept is generally caused by poor lubrications during high loading conditions or low speeds. This wear gets especially troublesome when surface textures are used that can get worn away completely. Considering textured hydrodynamic bearings, using an MR fluid in this application can be beneficial regarding wear and controllability of these surface textures. These bearings do not require external pressurization of the fluid, but utilize surface textures to pressurize the fluid. This pressurization results in a load carrying capacity. Whether using the limiting shear stress of an MR fluid to form local solid textures, or, using sedimentation of magnetic particles from an MR fluid to form local solid textures in order to pressurize the fluid (Fig. 1-3). These surface textures consist of magnetic particles that do not wear down and do not leave the system. Therefore the objectives in this thesis are as following:

- Demonstrate the possibility to create surface texturing using an MR fluid as lubricant with a new concept in bearing technology.
- Demonstrate that these surface textures pressurize the fluid resulting in a load carrying capacity.

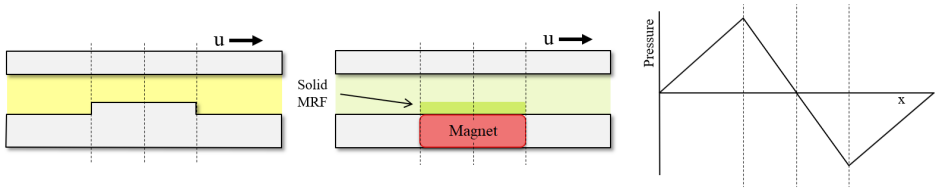

Figure 1-3: A step which can be recreated with the use of magnets (red) and MR fluid (green) in order to obtain a pressure distribution over the length of the channel.

1-3 Thesis organization

In figure 1-4 the organization of this thesis is shown. The first chapter is a general introduction with some background, an introduction to the current problems in bearing technology which have to be overcome, and the research objectives. The most important information is found in chapter 2 and 3. Here the research done regarding a textured hydrodynamic bearing using an MR fluid is presented. In chapter 2 several numerical simulations using different 2D fluid models incorporating an MR fluid are discussed. Here the possibility of using an MR fluid in order to create surface texturing which can pressurize the fluid is investigated. In chapter 3 the work done in chapter 2 is elaborated into 3D fluid models. Based on these models a hydrodynamic thrust bearing is made in order to validate the models. In chapter 4 all the work is discussed, and links everything together. At last there are chapter 5 and 6, containing the main conclusions and recommendations for further research respectively.

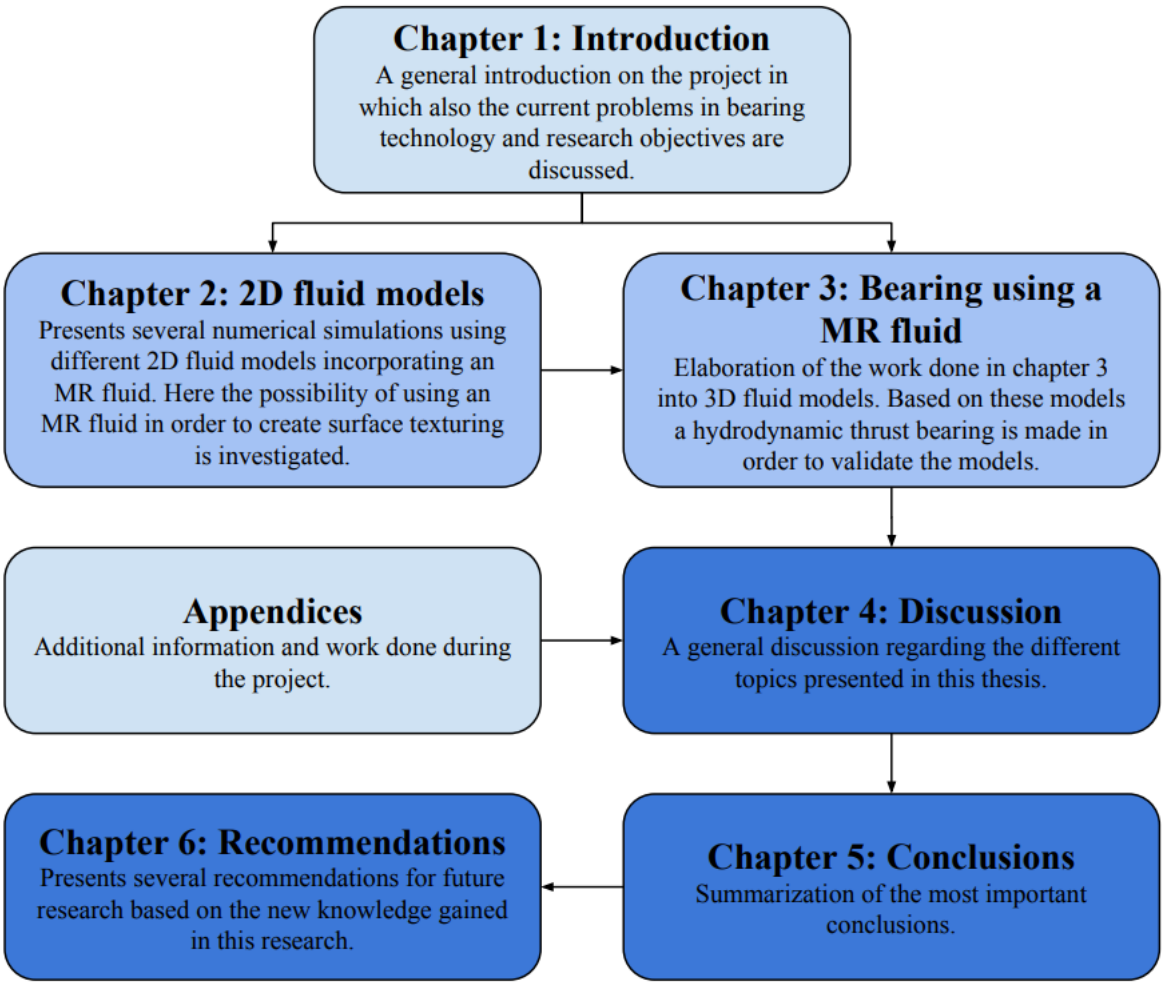

Figure 1-4: Organization of the thesis.

Chapter 2

A new concept in bearing technology: Magnetorheological texturing

A new concept in bearing technology: Magnetorheological texturing

M.C. de Graaf

Delft University of Technology, Mekelweg 2, 2628 CD Delft, the Netherlands

Abstract

Hydrodynamic bearings have superior wear behavior but still the lifetime of this concept is not infinite. Wear of this bearing concept is generally caused by poor lubrication during high loading conditions or low speeds. This wear gets especially troublesome when surface textures are used to improve lubrication that can get worn away completely. The concept discussed in this work is that of creating the behavior of surfaces textures with the use of a magnetorheological (MR) fluid. The fluid together with a local magnetic field can locally create solid like behavior of the lubricant resulting in a so-called virtual surface texture that is not sensitive to wear.

This work presents several numerical simulations using different 2D fluid models incorporating an MR fluid. A configuration of a step geometry using MR fluid shows an antisymmetric pressure distribution. This indicates pressurization of the fluid which can result in a load carrying capacity. This demonstrates that it is possible to create virtual surface textures using solely an MR fluid and a local magnetic field.

Keywords:
Magnetorheology, Hydrodynamic bearing, Tribology, Numerical simulation

1. Introduction

A hydrodynamic bearing is a type of fluid bearing in which the load is supported by a thin layer of rapidly moving pressurized liquid between the bearing surfaces [1]. Hydrodynamic bearings use the squeeze film principle or surface textures to pressurize the fluid (a changing fluid film height). At lower speeds hydrodynamic bearings have high wear and short life. This high wear especially occurs during starts and stops where the speed is not sufficient to maintain the thin fluid film.

Surface textures can be used to pressurize the fluid in hydrodynamic bearings. In [2] the friction characteristic of a journal bearing with dimpled bushings is investigated. These dimples contribute to the load carrying capacity and improve the frictional performance of journal bearings. In [3]-[5] textured thrust bearings are demonstrated. It is shown that the presence of the textures can provide better lubrication efficiency through both a reduction of friction and an increase in load carrying capacity. Also there are hydrodynamic bearings that utilize grooves textured in the bearing faces in order to obtain a load carrying capacity [6, 7]. Nevertheless, at lower speeds, starts, and stops these surface textures do wear down and the contribution to the bearing performance is lost. Therefore a surface texture is desired that is not sensitive to wear.

In the work of [8] a bearing is proposed where the resistance is increased locally by using an MR fluid and a local magnetic field. Here the resistance is modified locally in the lubricating film, however at a certain location in the lubricating film, the magnetic field is uniform across the full film gap. This concept cannot be used for textured hydrodynamic bearings, because for this a varying resistance over the bearing gap is required.

The magnetic properties of a magnetic fluid are obtained when particles that have magnetic properties are suspended in a carrier fluid. The magnetic particle material often used for an MR fluid is carbonyl iron since this has a saturation magnetization equal to 2.1 tesla, the highest value of known elements [9]. MR fluids can appear as a liquid but can also act solid, depending on the strength of the magnetic field applied to it. This solid phase is due to the attractive dipolar forces between the particles that have been magnetized by the applied magnetic field. The strength of the solid phase is caused by the formation of certain structures by the particles, such as chain-like agglomerates (Fig. 1) [10]. The particles of MR fluids are normally around the size of micrometers [11]. The aggregation process for an MR fluid is more intense in presents of a field, that is why their flow behavior can be controlled [12].

In [14] a new concept of hydrostatic bearings is presented that is lubricated with an MR fluid. A constant gap size for alternating payloads is achieved due to the fact that when an MR fluid is exposed to an external magnetic field the rheological properties change. In [15] a test bench has been developed to demonstrate

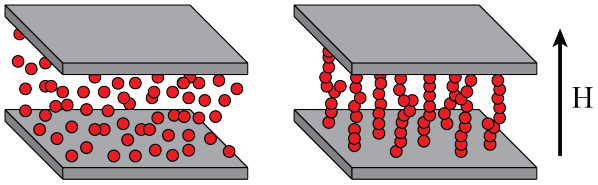

Figure 1: Formation of chain-like agglomerates in an MR fluid when subjected to a magnetic field.

that magnetic fluids can be used to develop active journal bearings. In [16] experiments are done with a constructed MR fluid film bearing. The dynamic properties of this bearing are evaluated both in its active and its inactive state. What the former concepts all have in common is that the magnetic field is constant and applied globally and not locally.

Numerical simulations can be used to predict the performance of MR fluid based applications. Literature reports several works in which a numerical simulation is used for modeling an MR fluid. In [17] and [18] only the magnetic field is considered for an MR fluid brake and clutch. In [19] and [20] the flow of the MR fluid is also considered but only at microscopic level. In [21] a higher level model coupled with magnetic simulation is presented which successfully describes MR fluids behavior in flow mode. Considering textured hydrodynamic bearings, using an MR fluid in this application can be beneficial regarding wear and controllability of these surface textures. For textured hydrodynamic fluid bearings using an MR fluid a model regarding shear mode is required. In this sense it is desired to create a model which can describe MR fluids at a higher level and in shear mode.

For a textured hydrodynamic bearing one surface is moving tangentially relative to the other which results in a shear flow (Fig. 2). In the situation that the fluid has a constant yield stress across the full height of the channel, either no flow or a complete Newtonian flow happens. However, in order to create a solid part at the bottom of the channel, the yield stress at the bottom has to be higher than at the top of the channel. This varying yield stress cannot be obtained with a constant magnetic field. Now, a gradient in magnetic field is required, which results in a decreasing yield stress over the channel height.

A solid part at the bottom for the full length of the channel, does not show a change in pressure distribution over the length of the channel. To obtain a pressure distribution, only locally the channel must behave as a solid while the other part of the channel behaves as a fluid (Fig. 3). This creates a difference in fluid transport along the length of the channel resulting in a changing pressure over the length of the bearing. This pressurization of the fluid results in a load carrying capacity in a bearing [13].

In this paper it is demonstrated that these surface

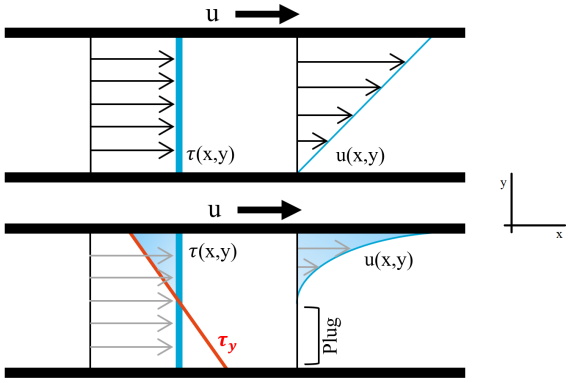

Figure 2: Shear mode for a Newtonian fluid (top) and an MR fluid (bottom) between two parallel surfaces where one surface is moving relative to the other surface.

textures can be created with an MR fluid with a local magnetic field. This is done with several numerical simulations using different 2D fluid models. At the end using a local magnetic field a configuration of a step geometry using MR fluid is created. Over this step an antisymmetric pressure distribution is obtained that indicates pressurization of the MR fluid. This step consists of the magnetic particles in the MR fluid and these do not wear down and do not leave the system.

2. Method

In order to create virtual surface textures with an MR fluid, a non-Newtonian fluid model which is able to describe the behavior of an MR fluid has to be validated. Therefore first a fluid model regarding the flow mode is made. This is followed by a model which can describe an MR fluid in shear mode. Finally a self created magnetic field is applied locally in order to obtain a virtual surface texture which is able to pressurize the fluid.

2.1. Fluid model

A model that is used to describe these non-Newtonian fluids is the Bingham model (Eq. 1 and 2) [22].

$$\tau = \tau_y + \eta\dot{\gamma}, \qquad |\tau| > \tau_y \tag{1}$$

$$\dot{\gamma} = 0, \qquad |\tau| \leq \tau_y \tag{2}$$

Here τ is the shear stress, τ_y is the yield stress, η is the viscosity, and $\dot{\gamma}$ is the shear rate. Compared to the Newtonian model, it is seen that the shear stress now dependents on the yield stress of the fluid. For an MR fluid this yield stress is caused by a magnetic field, and with a change in magnetic field this yield

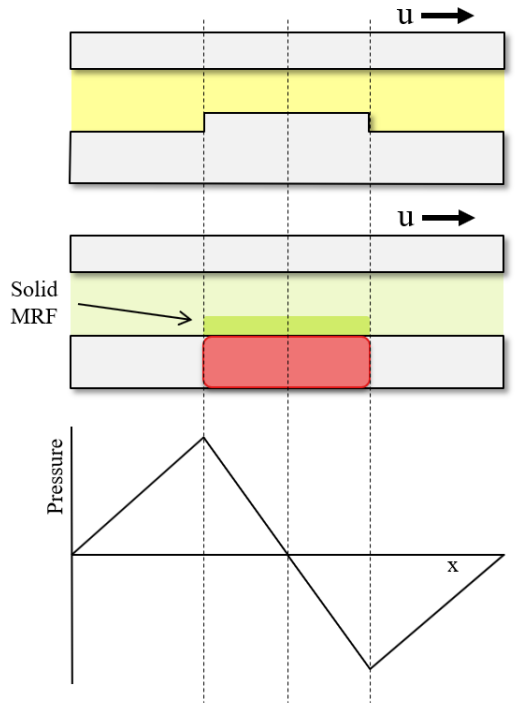

Figure 3: The step geometry (top graph) leads to a sawtooth pressure profile (lower graph). The combination of a magnetic field and MRF (middle graph) also produces a similar geometry and therefore pressure.

stress changes (Fig. 4). This yield stress causes the solid phase of the MR fluid. The moment this yield stress is exceeded, the MR fluid starts to flow just like a Newtonian fluid.

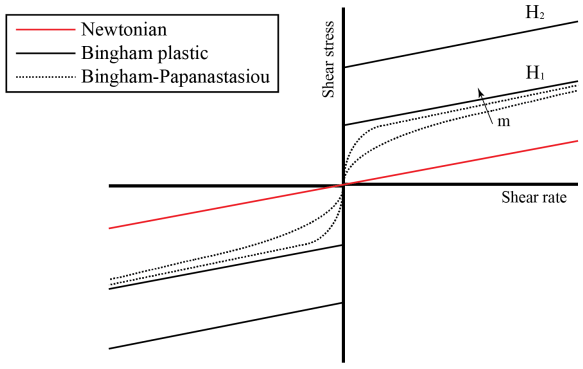

Figure 4: Different models where the shear stress versus the shear rate is shown. Here $H_2 > H_1$ and m is the regularization parameter.

To simulate this behavior a numerical simulation is made in COMSOL Multiphysics [23] where the Bingham-Papanastasiou model is implemented [24]. The Bingham-Papanastasiou model proposes an exponential regularization for the Bingham model (Eq. 3).

$$\tau = \tau_y(1 - e^{-m|\dot{\gamma}|}) + \eta_0\dot{\gamma} \tag{3}$$

$$\eta = \frac{\tau_y}{\dot{\gamma}}(1 - e^{-m|\dot{\gamma}|}) + \eta_0 \tag{4}$$

Here η_0 represents the viscosity when no magnetic field is applied, and m is the regularization parameter. The value of m controls the exponential growth of the shear stress. The higher the value, the faster the shear stress growths (Fig. 4). When there is no magnetic field present, the yield stress in the fluid is equal to 0 and then the apparent viscosity (Eq. 4) is equal to the viscosity when no magnetic field is applied, $\eta = \eta_0$.

2.2. *Flow mode with a constant yield stress*

To validate the model used, first a pure pressure driven flow (Poiseuille flow) is modeled using an MR fluid for different yield stresses. For this the parameters in [21] are considered. The dimensions used for this model are normalized (Table 1). Here the height of the channel is taken equal to 1, and the ratios between parameters used in [21] are used for further parameterization. The simulation for the flow mode evaluates the MR fluid for different yield stresses, which correspond to a certain constant magnetic field.

Table 1: Normalized parameters from [21] used for simulating the MR fluid in flow mode

Parameters	
Channel (l x h) $[L_{norm} \cdot h]$	10 x 1
Regularization parameter $[m_{norm} \cdot h]$	1250
Viscosity $[\eta_{norm}]$	0.28
Pressure drop $[\Delta p_{norm} \cdot (1/h)]$	60
Yield stress $[\tau_{y,norm} \cdot (1/h)]$	0, 1,2, $\frac{13}{5}$, 3

2.3. *Shear mode with a varying magnetic field*

Pure shear flow for both a Newtonian fluid and MR fluid are seen in figure 2, this mode is also referred to as Couette flow. In order to create a solid part at the bottom of the channel, a varying yield stress is used. In the model a linear decrease in yield stress over the channel height is applied. For the model normalized parameters are used (Table 2). To simulate the shear mode the MR fluid is evaluated for different velocities of the moving surface.

2.4. *Step bearing configuration*

Local solidification in the MR fluid is created with a local magnetic field. To realize this an array of magnets and metal blocks is used. Using different parameters (table 3) an environment is simulated representing a bearing consisting of 4 layers (Fig. 5). The MR

Table 2: Normalized parameters used for simulating an MR fluid in shear mode.

Parameters	
Channel (l x h) $[L_{norm} \cdot h]$	10 x 1
Regularization parameter $[m_{norm} \cdot h]$	10^4
Viscosity $[\eta_{norm}]$	1
Yield stress bottom $[\tau_{y,norm} \cdot (1/h)]$	1
Yield stress top $[\tau_{y,norm} \cdot (1/h)]$	0
Surface velocity $[u_{norm}]$	$\frac{1}{100}$, $\frac{3}{20}$, $\frac{3}{10}$, $\frac{3}{4}$, 2

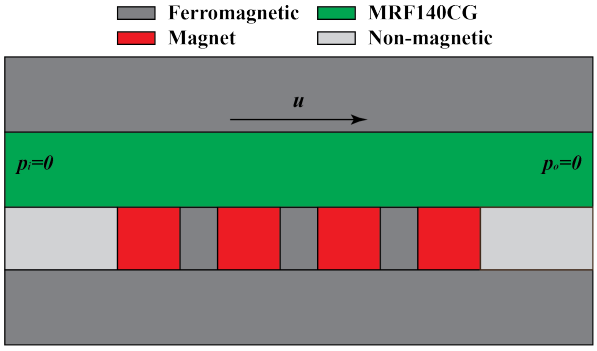

Figure 5: An environment representing a bearing consisting of 4 layers: 2 layers of metal, a layer containing square magnets and metal blocks, and a layer of MR fluid. Here the top metal surface represents the moving shaft and the bottom two layers the fixed bearing surface.

Table 3: Normalized parameters used for simulating the MR fluid MRF140CG

Parameters	
Channel (l x h) $[L_{norm} \cdot h]$	15 x 1
Ferromagnetic layer (l x h) $[L_{norm} \cdot h]$	15 x 1
Magnets (l x h) $[L_{norm} \cdot h]$	$\frac{5}{6}$ x $\frac{5}{6}$
Ferromagnetic blocks (l x h) $[L_{norm} \cdot h]$	$\frac{1}{2}$ x $\frac{5}{6}$
Flux density $[B_{norm} \cdot (1/h)]$	10^{-5}
Regularization parameter $[m_{norm} \cdot h]$	10^4
Viscosity $[\eta_{norm}]$	1
Surface velocity $[u_{norm}]$	$\frac{1}{100}$, $\frac{3}{20}$, $\frac{3}{10}$, $\frac{3}{4}$, 2

fluid used is MRF140CG provided by Lord Corporation [25].

The magnetic field that is created is related to the flow of the MR fluid. This means a relation has to be found between the magnetic field strength and the yield stress of the MR fluid which can be implemented into COMSOL. In [26]-[31] different models and approaches are presented to obtain the yield stress depending on the magnetic field. For the purpose of this model the relation between yield stress and magnetic field strength for MRF140CG is used. Implementing this and coupling the fluid and magnetic analysis, the behavior of the MR fluid is obtained. To simulate the shear mode the MR fluid is evaluated for different velocities of the moving surface.

Using this magnetic field, local solid zones are formed, located where the shear stress is lower than the local yield stress. These local solid zones act as a virtual surface texture, and influence the flow of the fluid and thus increase the pressure. To see if obtaining a load capacity from this is an possibility with an MR fluid, an antisymmetric pressure distribution over the surface textures has to be obtained (Fig. 3). The surface textures created have a step geometry. This step geometry is represented by the solid part in the MR fluid and can be created by a locally applied magnetic field.

3. Results and discussion

3.1. Flow mode with a constant magnetic field

The results for the velocity profiles for pressure driven flow (Poiseuille flow) are seen in figure 6. A parabolic velocity is observed for no yield stress applied, and is becoming flatter for increasing yield stress. No yield stress corresponds to the behavior of a Newtonian fluid. The situations where a yield stress is applied correspond to the behavior of an MR fluid subjected to a certain magnetic field. This also applies to results for the apparent viscosity, shear stress, and shear rate seen in figure 7, 8, and 9 respectively.

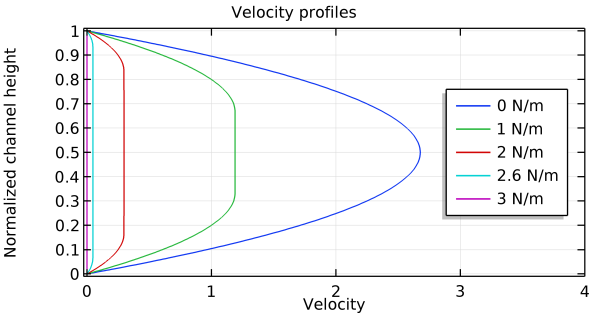

Figure 6: The velocity profiles for a Poiseuille flow of the MR fluid for different yield stresses.

The results are as expected and correspond to the results in [21]. For no yield stress the apparent viscosity stays constant and the shear rate goes linearly to zero in the middle all according to the Newtonian model. For the MR fluid where a yield stress is applied different behavior is observed. In the regions the yield stress exceeds the shear stress, the velocity is constant, the apparent viscosity increases, and the shear rate is equal to zero. In these regions the

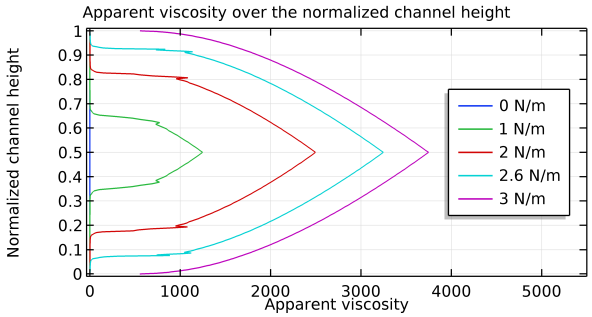

Figure 7: The apparent viscosity for a Poiseuille flow of the MR fluid for different yield stresses.

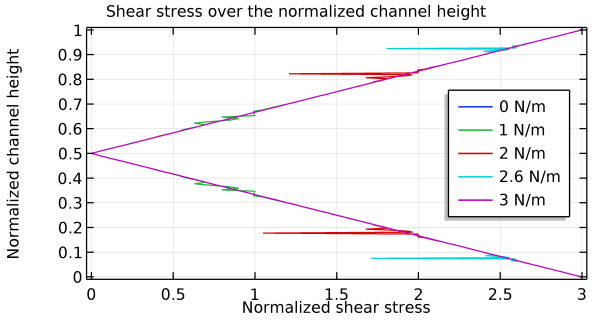

Figure 8: The absolute normalized shear stress for a Poiseuille flow in the MR fluid for different yield stresses.

MR fluid can be seen as one solid moving through the channel. No change is seen in the shear stress which is expected, only some irregularities are seen at some points. These irregularities happen at the point where the shear stress is equal to the yield stress applied in the different situations. This position is the boundary between fluid and solid.

3.2. Shear mode with a varying magnetic field

For shear mode the MR fluid is subjected to a varying yield stress in order to obtain the solid phase. In figure 10 the results for the velocity profiles are seen

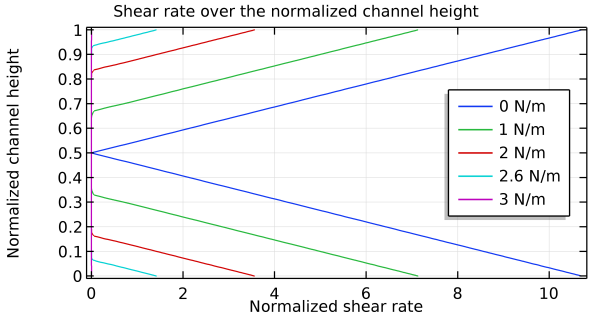

Figure 9: The normalized shear rate for a Poiseuille flow in the MR fluid for different yield stresses.

for different velocities of the moving wall using a linear decrease in yield stress over the channel height. The results for the apparent viscosity, shear stress, and shear rate are seen in figure 11, 12 and 13 respectively.

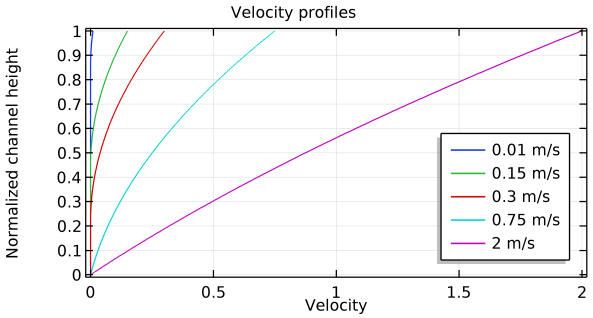

Figure 10: The velocity profiles of the MR fluid for different velocities of the moving wall.

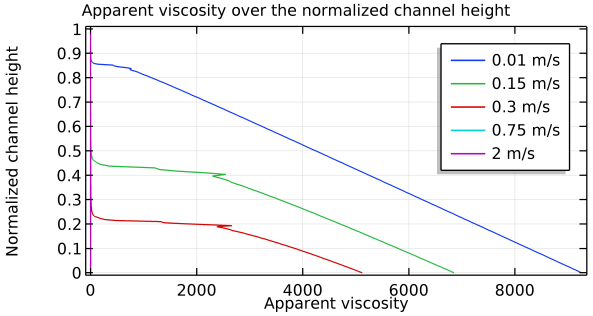

Figure 11: The apparent viscosity of the MR fluid for different velocities of the moving wall.

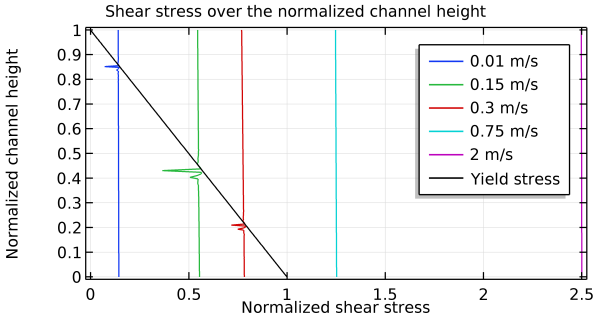

Figure 12: The normalized shear stress in the MR fluid for velocities of the moving wall. Also the yield stress in the fluid is plotted here, this one is the same for every velocity.

The applied yield stress has a large impact on the velocity of the fluid, the apparent viscosity and the shear rate. At the region the yield stress exceeds the shear stress the velocity of the MR fluid is zero, the apparent viscosity is high, and the shear rate is approaching zero. This indicates that in this region the

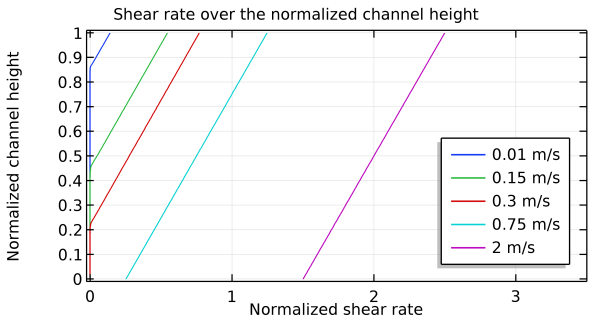

Figure 13: The normalized shear rate in the MR fluid for different velocities of the moving wall.

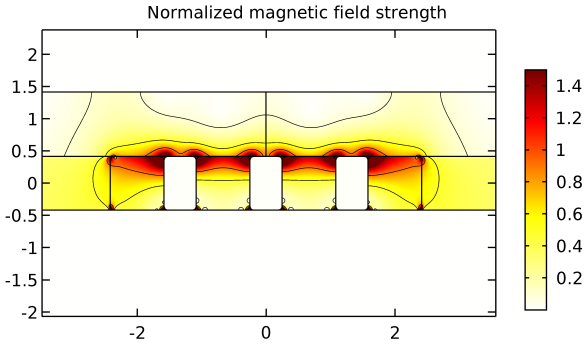

Figure 14: Simulated array of magnets and metal blocks.

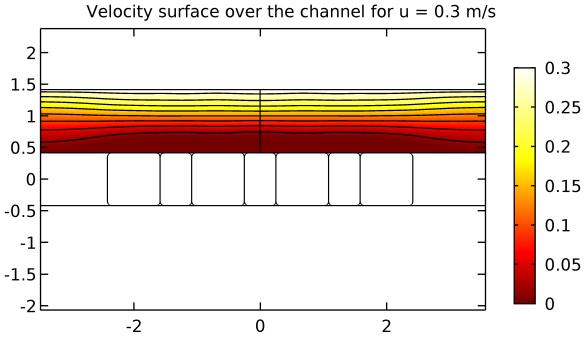

Figure 15: Solid part created in the middle of the length of the channel at a velocity for the moving wall of 0.3.

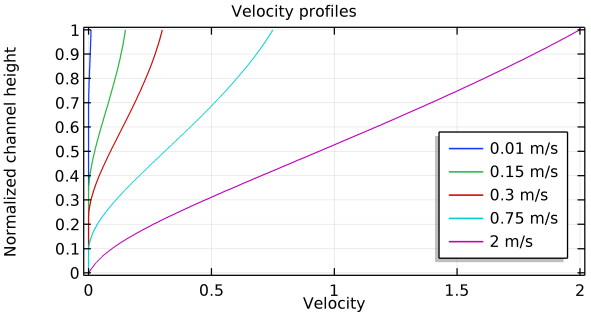

Figure 16: The velocity profiles of the MR fluid with a solid part in the middle of the length of the channel for different velocities of the moving wall.

MR fluid appears solid and a virtual surface texture is created over the whole length of the channel. At a higher velocity the impact of the yield stress is less and the size of the virtual surface textures decrease. This is because for higher velocities the shear stress in the fluid is greater. The regions where the yield stress is dominant over the shear stress are becoming smaller and more fluid starts to flow. At one moment the shear stress exceeds the yield stress completely in the MR fluid and no solid phase is present. Still the effect of the yield stress is seen in the velocity profile. At the bottom of the channel the liquid is still more viscous than at the top where it approaches the viscosity of the MR fluid where a lower yield stress is applied. This more viscous liquid results in more resistance to flow and therefore no perfectly linear velocity profile is obtained.

3.3. Step bearing configuration

The result for the magnetic field strength of the created array is seen in figure 14. For this array a quite evenly spread magnetic field strength is obtained. Using the metal blocks in between the magnets, the magnetic field is deflected and a high magnetic field is obtained at the bottom of the channel. Due to this local magnetic field a local solid part, a virtual surface texture, is created in the middle of the length of the channel (Fig. 15). In figure 16 to 19 the results for the velocity profile, apparent viscosity, shear stress, and shear rate respectively are seen. Everything is obtained at the middle of the length of the channel.

The relation between the different results for a solid part in the middle of the length of the channel (figure 16 to 19) is the same as for the results discussed for where the solid part is present over the length of the whole channel (figure 10 to 13). Although these relations are still there, compared to the earlier results the velocity starts to increase less at the top of the channel, the shear stress is not constant anymore, and the shear rate does not increase linearly because of the not linear yield stress. Here the physics of a pressure driven flow and shear flow are now combined. Due to the step, the fluid is pressurized which causes a shear stress due to a pressure driven flow which is added to the constant shear stress due to shear flow. This should result in a linear decrease in shear stress over the channel height. This trend is seen in with some irregularities (Fig. 18). At the edges of the created array the magnetic field strength is higher (Fig. 14). Here the resistance to flow is higher than at middle of the length of the solid part. This is what causes the irregularities observed. This is also affecting the shape of velocity profile and the shear rate.

The result for the pressure distribution over this virtual surface texture is seen in figure 20. The pressure

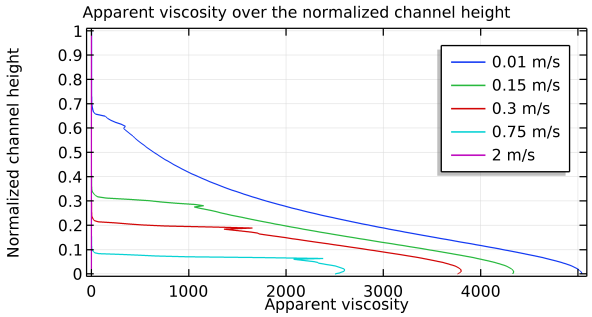

Figure 17: The apparent viscosity in the MR fluid with a solid part in the middle of the length of the channel for different velocities of the moving wall.

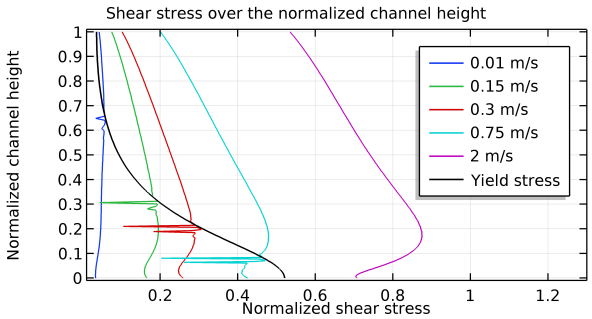

Figure 18: The normalized shear stress in the MR fluid with a solid part in the middle of the length of the channel for different velocities of the moving wall.

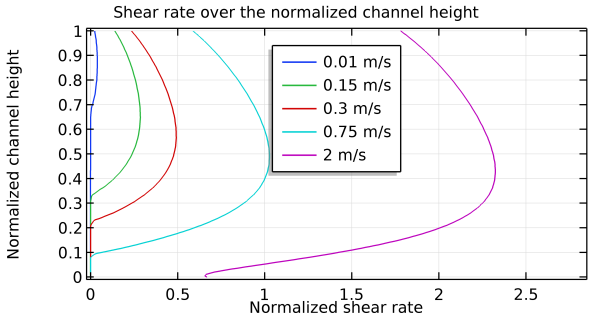

Figure 19: The normalized shear rate in the MR fluid with a solid part in the middle of the length of the channel for different velocities of the moving wall.

distribution obtained indicates that there is the possibility to create a load carrying capacity. Even when the shear stress in the MR fluid exceeds the yield stress (Fig. 18), and no solid part is present, a pressure distribution is observed (Fig. 20). This is because the magnetic field still influences the viscosity of the MR fluid. Instead of a solid part at the bottom in the middle of the length of the channel, a more viscous fluid than in rest of the channel is observed. This means that at the bottom the fluid flows with more resistance than at the top which causes the observed pressure distribution. So even for this situation it is possible to obtain a load carrying capacity.

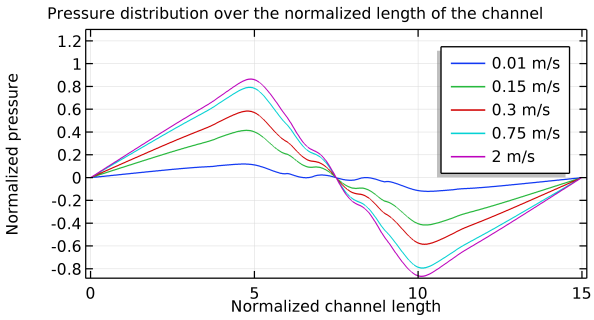

Figure 20: The normalized pressure distribution in the MR fluid with a solid part in the middle of the length of the channel for different velocities of the moving wall.

4. Conclusion

A magnetic field that is constant across the film height cannot be used to create a solid part in shear mode. Therefore a magnetic field that varies across the film height needs to be applied. For a fluid that is depending on a magnetic field a solid part is created at the bottom over the whole length of the channel, where the yield stress is the highest. As a result to an increase in velocity, this solid part decreases in size.

A virtual surface texture is obtained by applying a magnetic field that varies across the film height locally at the middle of the length of the channel. Due to this surface texture a pressure distribution is obtained which indicates that creating a load carrying capacity is possible using an MR fluid. It is interesting to note that for where the shear stress exceeds the yield stress and no solid part is observed, still a pressure distribution is obtained. This indicates that also a load carrying capacity can be obtained if no solid part is present. This is due to the more viscous MR fluid at the location of the previous solid part resulting in more resistance to flow.

References

[1] W.B. Rowe, *Hydrostatic, Aerostatic and Hybrid Bearing Design*. Butterworth-Heinemann, 2012.

[2] X. Lu, M.M. Khonsari, "An Experimental Investigation of Dimple Effect on the Stribeck Curve of Journal Bearings," *Tribology Letters*, vol. 27, no. 2, pp. 169176, 2007.

[3] I. Etsion, G. Halperin, V. Brizmer, Y. Kligerman, "Experimental Investigation of Laser Surface Textured Parallel Thrust Bearings," *Tribology Letters*, vol. 17, no. 2, pp. 295300, 2004.

[4] Y. Qiu, M.M. Khonsari, "Experimental investigation of tribological performance of laser textured stainless steel rings," *Tribology International*, vol. 44, no. 5, pp. 635644, 2011.

[5] Y. Henry, J. Bouyer, M. Fillon, "An experimental analysis of the hydrodynamic contribution of textured thrust bearings during steady-state operation: A comparison with the untextured parallel surface configuration," *Proceedings of the Institution of Mechanical Engineers, Part J: Journal of Engineering Tribology*, vol. 229, no. 4, pp. 362375, 2015.

[6] E.A. Muijderman, "Spiral Groove Bearings," *Industrial Lubrication and Tribology*, vol. 17, no. 1, pp. 1217, 1965.

[7] C.W. Wong, X. Zhang, S.A. Jacobson, A.H. Epstein, "A Self-Acting Gas Thrust Bearing for High-Speed Microrotors," *Journal of Microelectromechanical Systems*, vol. 13, no. 2, pp. 158164, 2004.

[8] S.G.E. Lampaert and R.A.J. van Ostayen, "Virtual Textured Hybrid Bearings," *44^{th} Leeds-Lyon Symposium on Tribology*, 2017.

[9] M. Aslam, Y. Xiong-Liang, D. Zhong-Chao, "Review of magnetorheological (MR) fluids and its applications in vibration control," *Journal of Marine Science and Application*, vol. 5, no. 3, pp 17-29, 2006.

[10] S. Odenbach, *Ferrofluid. Magnetically Controllable Fluids and Their Applications*. Springer Berlin Heidelberg, 2002.

[11] S. Genc and B. Derin, "Synthesis and rheology of ferrofluids: A review," *Current Opinion in Chemical Engineering*, vol. 3, pp. 118-124, 2014.

[12] I.G. Kim, K.H. Song, B.O. Park, B.I. Choi, and H.J. Choi, "Nano-sized Fe soft-magnetic particle and its magnetorheology," *Colloid and Polymer Science*, vol.289, no. 1, pp. 79-83, 2011.

[13] D.B. Hamilton, J.A. Walowit, C.M. Allen, "A theory of lubrication by micro- irregularities," *Journal of Basic Engineering*, vol. 8, pp. 177-185, 1966.

[14] J. Hesselbach and C. Abel-Keilhack, "Active hydrostatic bearing with magnetorheological fluid," *Journal of Applied Physics*, vol. 93, no. 10, pp. 8441-8443, 2003.

[15] H. Urreta, Z. Leicht, A. Sanchez, A. Agirre, P. Kuzhir, and G. Magnac, "Hydrodynamic Bearing Lubricated with Magnetic Fluids," *Journal of Intelligent Material Systems and Structures*, vol. 21, no. 15, pp. 1491-1499, 2010.

[16] D. Bompos and P. Nikolakopoulos, "Experimental and Analytical Investigations of Dynamic Characteristics of Magnetorheological and Nanomagnetorheological Fluid Film Journal Bearing," *Journal of Vibration and Acoustics, Transactions of the ASME*, vol. 138, no. 3, pp. 1-7, 2016.

[17] D. Senkal, H. Gurocak, "Compact MR-brake with serpentine flux path for haptics applications," *Third Joint EuroHaptics conference and Symposium on Haptic Interfaces for Virtual Environment and Teleoperator Systems*, pp. 9196, 2009.

[18] X. Xu, C. Zeng, "Design of a Magneto-rheological Fluid Clutch Based on Electromagnetic Finite Element Analysis," *2nd International Conference on Computer Engineering and Technology*, vol. 5, 2010.

[19] E. Climent, M.R. Maxey, G.E. Karniadakis, "Dynamics of Self-Assembled Chaining in Magnetorheological Fluids," *Langmuir*, vol. 20, pp. 507513, 2004.

[20] Y. Pappas, D.J. Klingenberg, "Simulations of magnetorheological suspensions in Poiseuille flow," *Rheologica Acta*, vol. 45, no. 5, pp. 621629, 2006.

[21] G. Daniel, C. Yoan, P. Zoltan, and P. Yves, "Bingham-papanastasiou and approximate parallel models comparison for the design of magneto-rheological valves," *IEEE/ASME International Conference on Advanced Intelligent Mechatronics, AIM*, pp. 168-173, 2014.

[22] K. Walters, "An Introduction to Rheology," *Elsevier Science Publishers*, firs ed., 1989

[23] *COMSOL Multiphysics*, available at https://www.comsol.com/.

[24] T.C. Papanastasiou, "Flows of Materials with Yield," *Journal of Rheology*, vol. 31, no. 5, pp. 385-404, 1987.

[25] *Lord Corporation*. available at https://www.lord.com/.

[26] J. M. Ginder and L.C. Davis, Shear stresses in magnetorheological fluids: Role of magnetic saturation, *Applied Physics Letters*, vol. 65, pp. 3410-3412, 1994.

[27] S. Genc and P.P. Phule, Rheological properties of magnetorheological fluids, *Smart Materials & Structures*, vol. 11, no. 1, pp. 140-146, 2002.

[28] G. Bossis, S. Lacis, A. Meunier, and O. Volkova, Magnetorheological fluids, *Journal of Magnetism and Magnetic Materials*, vol. 252, pp. 224-228, 2002.

[29] S. Chen, J. Huang, H. Shu, T. Sun, and K. Jian, Analysis and testing of chain characteristics and rheological properties for magnetorheological fluid, *Advances in Materials Science and Engineering*, vol. 2013, pp. 1-7, 2013.

[30] C.W. Guo, F. Chen, Q. R. Meng, and Z.X. Dong, Yield shear stress model of magnetorheological fluids based on exponential distribution, *Journal of Magnetism and Magnetic Materials*, vol. 360, pp. 174-177, 2014.

[31] S.G. Sherman, A.C. Becnel, and N.M. Wereley, Relating Mason number to Bingham number in magnetorheological fluids, *Journal of Magnetism and Magnetic Materials*, vol. 380, pp. 98-104, 2015.

Chapter 3

A self-healing hydrodynamic thrust bearing using a magnetorheological fluid

A self-healing hydrodynamic thrust bearing using a magnetorheological fluid

M.C. de Graaf

Delft University of Technology, Mekelweg 2, 2628 CD Delft, the Netherlands

Abstract

Fluid bearings do have several disadvantages which have to be overcome. Some fluid bearings require an external pump which is sensitive to failure, others have fixed surface textures which are sensitive to wear, especially during starting and stopping. By applying a magnetic field the viscosity of a magnetorheological (MR) fluid can be altered, up to the point it becoming a solid. Using an MR fluid in combination with a magnetic field, local and controllable surface textures can be created which are less sensitive to wear.

In this work a proof of concept for a hydrodynamic thrust bearing lubricated with an MR fluid is modeled and produced. For the models two mechanisms utilizing surface textures for pressure buildup in a lubricating film using MR fluids are studied. The first uses local viscosity variation resulting in so-called virtual surface textures. The second uses local sedimentation of magnetic particles in locations of higher magnetic field strengths resulting in physical surface textures. The experimental results correspond to the situation where the magnetic particles are completely sedimented. Here self-healing surface textures are created, over which the carrier fluid flows. The carrier fluid is pressurized by these textures which results into a load carrying capacity.

Keywords:
Magnetorheology, Hydrodynamic, Tribology, Numerical, simulation

1. Introduction

To minimize friction and prevent wear are the main reasons why lubricants are used in fluid bearings. In fluid bearings the load is supported by a thin film of fluid which is externally pressurized or which is pressurized by a rapid movement of the bearing faces. But these lubricated bearings encounter different problems [1]. Metal to metal contact cannot be avoided due to a not sufficient oil pressure and viscosity at certain working conditions or due to that the oil film thickness breaks when the variation of the load and vibration exceed the acceptable level [2, 3]. In addition, a decrease in viscosity and load carrying capacity is possible due to the temperature increase of the lubricant during operation. Smart fluids, like magnetic fluids, have the potential to improve the performance and overcome the drawbacks of fluid bearings [4, 5].

The magnetic properties of a magnetic fluid are obtained when particles that have magnetic properties are suspended in a carrier fluid. MR fluids are fluids that can have a liquid behavior but can also act solid, depending on the strength of the magnetic field applied to it. MR fluids becoming a solid is due to the attractive dipolar forces between the particles which have been magnetized by the applied magnetic field [6]. The strength of the solid phase is caused by the formation of certain structures, such as chain-like agglomerates. The aggregation process for an MR fluid is more intense in presents of a field than for ferrofluids, another well known magnetic fluid [7]. Due to this more intense aggregation process the flow behavior can be controlled [8].

In [9] an MR fluid film bearing is constructed, which is capable of exciting the MR fluid. The purpose is to evaluate the dynamic properties of this bearing both in its active and its inactive state. In [10] a virtual textured hydrostatic bearing is proposed where the resistance is increased locally by using an MR fluid and a local magnetic field. In [5] it is seen that the critical pressures of the proposed thrust bearing using a magnetic fluid are larger than those of the normal lubricated bearing under high speeds. In [11] it is shown that the load capacity of a magnetic-fluid-based porous inclined slider bearing is found to be greater than the configuration using a conventional lubricant seen in [12]. The research in [13] elaborated on [11] considering a slider consisting of an inclined pad and a flat pad. It was seen that the magnetic fluid increases the load capacity, and does not alter the friction.

In [14]-[17] journal bearings lubricated with a ferrofluid are presented. There it is concluded that the bearing performance is modified significantly, like increase in stiffness and load capacity, but only only for certain conditions. Far from these conditions, an insignificant effect is obtained for the magnetic lubrication. In [18] it is investigated if magnetic fluids can

be used as active lubricants in a hydrodynamic journal bearing, here both a ferrofluid and an MR fluid are tested. It is seen that the rheological change of the ferrofluid is negligible for the purpose of a tunable lubricant. On the other hand, the MR fluid has good potential to be used as an tunable lubricant. In [19] an active hydrostatic bearing with MR fluid is presented. Here it is shown that the drawbacks (stiffness, response time and variation in bearing gap) of conventional hydrostatic bearings are overcome with the use of an MR fluid.

Ferrofluids already show potential to overcome the drawbacks of lubricated bearings, but seen is that the tunability is low and it only works for certain conditions. Therefore it is beneficial to look into MR fluids and their application to overcome the drawbacks of wear present in lubricated bearings. The MR fluid together with a local magnetic field can locally create solid like behavior of the lubricant resulting in surface textures that are not sensitive to wear.

In this paper three different designs of hydrodynamic thrust bearings lubricated with an MR fluid are considered. All of the designs are numerically modeled and experimentally measured. The designs are modeled for the case that the particles stay completely in suspension and for the case that the particles show complete sedimentation, resulting in virtual and physical surface texturing respectively. Comparing the results of the model with the results of the experiments demonstrates which situation is likely to occur.

2. Method

First the model for perfect mixture resulting in virtual surface texturing is discussed followed by the model for complete sedimentation resulting in physical surface texturing, at last the experimental set-up is discussed. The models and proof of concept consist of several layers. In figure 1 a top view configuration is seen of the layer containing the magnets. Here θ is the angle under which the magnets lie, r is the radius of the bearing, l is the length of the magnet, and b is the width of the magnet. In figure 2a the cross section at location A-A in figure 1 is seen for the model used for perfect mixture. In this figure every layer used in the model is shown. In figure 2b the cross section is seen for the model used for complete sedimentation. Here the MR fluid film now consists of steps created by the sedimented magnetic particles over which the carrier fluid flows. In this model only the fluid film containing the steps is considered. The proofs of concept only consist of the layers below the MR fluid in figure 2.

In the numerical simulations a vapor pressure equal to 1 atmosphere is used. Here the vapor pressure as relating to cavitation refers to the vapor pressure in equilibrium conditions. Without cavitation for $\theta = 0$, the negative pressure and the positive pressure will cancel out. However, due to the release of gas entrained in oil, the negative pressure cannot be lower than vapor pressure. In most cases the vapor pressure is nearly ambient due to long time exposure to air [20]. For this reason the vapor pressure is taken equal to 1 atmosphere.

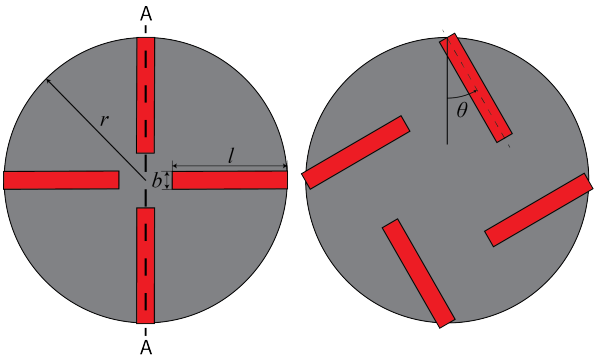

Figure 1: Configuration of the magnets used in the numerical simulations and proofs of concept.

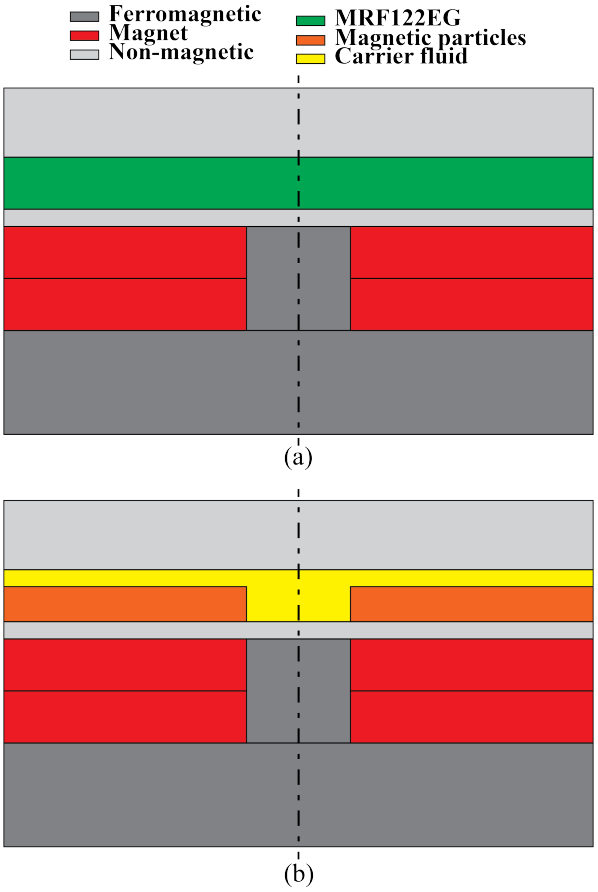

Figure 2: 2D section at location A-A in figure 1 of the geometry used in the numerical simulation. (a) Perfect mixture. (b) Complete sedimentation.

2.1. Model for perfect mixture

A three-dimensional numerical simulation in COMSOL Multiphysics [21] is made. This is done taken into consideration that on this model a proof of concept can be based. A model that is used to describe these non-Newtonian fluids is the Bingham model (Eq. 1 and 2) [22].

$$\tau = \tau_y + \eta\dot{\gamma}, \qquad |\tau| > \tau_y \tag{1}$$

$$\dot{\gamma} = 0, \qquad |\tau| \leq \tau_y \tag{2}$$

Here τ is the shear stress in the fluid and $\dot{\gamma}$ the shear rate. In the Bingham model the shear stress is dependent on the yield stress of the fluid. For an MR fluid this yield stress is depending on the magnetic field, the higher the magnetic field strength the higher the yield stress. Using a local magnetic field the viscosity and fluid pressure of the MR fluid can be controlled locally. To simulate this behavior the Bingham-Papanastasiou model [23] is implemented in the numerical simulation. The Bingham-Papanastasiou model proposes an exponential regularization for the Bingham model (Eq. 3 and 4).

$$\tau = \tau_y(1 - e^{-m|\dot{\gamma}|}) + \eta_0\dot{\gamma} \tag{3}$$

$$\eta = \frac{\tau_y}{\dot{\gamma}}(1 - e^{-m|\dot{\gamma}|}) + \eta_0 \tag{4}$$

Here η_0 represents the viscosity for no applied magnetic field, and m is the regularization parameter. The higher the value of m, the closer the Bingham-Papanastasiou model follows the Bingham plastic model. From this the apparent viscosity is obtained (Eq. 4).

The model for the perfect mixture is build up out of several layers representing a thrust bearing (Fig. 2a). Two layers of ferromagnetic material, one containing the magnets, a non-magnetic layer separating the magnets from the MR fluid, an MR fluid film which in reality is surrounded by air but is not shown in the figure, and a sliding top layer made of non-magnetic material. The MR fluid used is MRF122EG provided by Lord Corporation [24]. The parameters used in the model can be seen in table 1.

For this model a combined study regarding magnetism and fluid flow is used. The magnetic field is simulated for the whole domain. Given every part has its own magnetic properties, a certain magnetic field is formed. After simulating the magnetic field, the fluid flow of the MR fluid is simulated. This is done only for the domain where the MR fluid is present. Because the viscosity is depending on the local magnetic field, the results from the study regarding the magnetic field across the film height are obtained beforehand. The apparent viscosity (Eq. 4) is implemented in the simulation. Here it is seen that the yield stress depends on the magnetic field strength, which is obtained in the study for the magnetic field. The relation between the magnetic field strength and the yield stress for MRF122EG is used. The shear rate, obtained in the numerical simulation is a variable that is obtained during the study for the fluid flow. The viscosity η_0 and the regularization parameter m are known constants. The appropriateness of the chosen regularization parameter is checked with the results.

Table 1: Parameters used for simulating the perfectly mixed MR fluid.

Parameters	
Outer diameter bearing	30 [mm]
Ferromagnetic layer thickness	2 [mm]
Magnet (l x b x h)	7.5x1.1x1 [mm]
Remanent flux density of the magnet	1.28 [T]
Separation layer thickness	0.15 [mm]
MR fluid film height	0.2 [mm]
MR fluid film diameter	20 [mm]
Air surrounding MR fluid thickness	0.2 [mm]
Top layer thickness	2.2 [mm]
Viscosity MRF122EG	0.086 [Pa·s]
Regularization parameter	1
θ	0, 30, and 36 [degree]

Bar magnets are used to create a magnetic field that decreases across the height of the fluid film. Due to the gradient in magnetic field strength, the effective viscosity of the fluid appears to be higher at the bottom. Near the magnets local surface textures are created that influences the tribological performance. This surface texture is used to pressurize the liquid and so a load carrying capacity is obtained.

2.2. Model for complete sedimentation

In an MR fluid where the magnetic particles are completely separated from the carrier fluid the magnetic particles cluster around the magnets. These agglomerates of magnetic particles represent physical steps, and these steps are simulated in a second model. An approximation for the dimensions of these steps is obtained in the previous model where a perfect mixture is assumed. It is assumed that for $\eta > 1000$ the fluid appears solid. Based on this the steps are represented using rectangular blocks with a certain length, width, and height equal to 7.5E-3 mm, 1.1E-3 mm, 1.8E-4 mm respectively. Using these dimensions the particles occupy 19% of the volume. This corresponds to the volume fraction of iron in MRF122EG. This rectangular block is used to approximate the behavior and see if it corresponds to the situation where the carrier fluid separates from the magnetic particles. These

steps are combined with a fluid that has the same viscosity as for the carrier fluid of MRF122EG. This is illustrated in figure 2b, a solid part representing the steps over which an oil flows. These steps pressurize the liquid and so a load carrying capacity is obtained.

In this model only the MR fluid film is simulated using the same angles and dimensions as in the model for perfect mixture. Now the particles are completely sedimented and in the fluid film now physical textures are present over which the carrier fluid flows. The sensitivity for the dimensions and viscosity is considered in this model. A change in value of 10% for the viscosity and dimensions of the step is implemented to obtain the parameter which has the most significant impact on the load capacity.

2.3. Experimental setup

Three proofs of concept seen in figure 3 are build up similar to the model. The Anton Paar rheometer MCR 302 (Fig. 4) is used for the experiments. This rheometer measures the normal force exerted on the parallel plate spindle used. The dimensions of the rheometer determine the diameter of the layer MR fluid, and also the maximum dimensions of the magnets which have to placed under this layer MR fluid. The diameter of the spindle under which the MR fluid is captured is equal to 20 mm.

Figure 3: Proofs of concept used for the experiments. Here $\theta = 0$, $\theta = 30$, and $\theta = 36$.

The proof of concept consists of 2 layers of 2 mm thick steel, one of these layers containing 8 magnets, a layer of 0.15 mm thick glass that separates the MR fluid from the magnets, and several screws and bolts to hold it together. Both the layers of steel are made by laser cutting, where the bottom plate locks the prototype in the rheometer and the top plate contains the magnets. The magnets have a remanent flux density of 1.28 Tesla and the dimensions are 7.5x1.1x1 mm. Because the steel layer containing the magnets is 2 mm thick, 2 magnets have to be stacked on top of each other resulting in the total of 8 magnets.

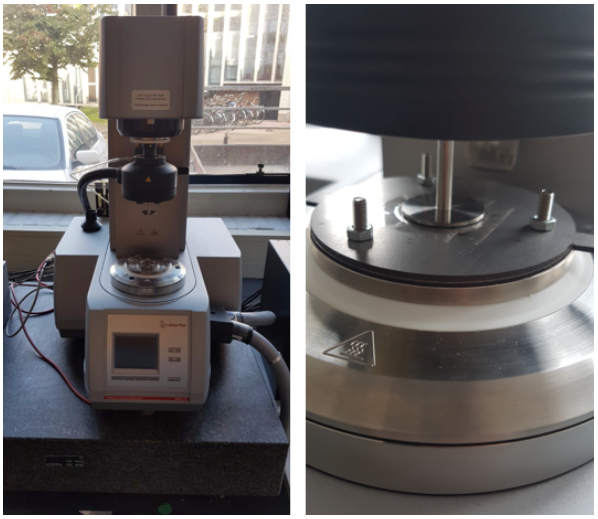

Figure 4: The Anton Paar rheometer MCR 302 used for the experiments and one proof of concept placed in the rheometer.

The measuring position, which is equal to the flying height, is set using the rheometer. The proof of concept is placed in the rheometer, then the zero-gap is set in order to determine the position with respect to the spindle. The rheometer lowers the spindle until first contact is made, this position is equal to a height of 0 mm. This is done without the presence of any liquid.

During operation of the rheometer, the MR fluid is captured between the glass and the spindle of the rheometer. During the experiments the revolutions per minute of the spindle is given as an input and the normal force acting on the spindle is given as an output. A total of 10 measurements are done using an interval of 10 milliseconds between data points, up to a total of 1000 data points. In the end the average of these 10 measurements is taken.

3. Results and discussion

In figure 5 the results for the numerical simulations can be seen. Here both the results for a perfect mixture and complete sedimentation of magnetic particles and carrier fluid are shown for θ equal to 0, 30, 36 degrees and a flying height equal to 200 μm. For perfect mixture the yield stress in the MR fluid is in the order of 10^5. Using an exponential growth factor $m = 1$ the Bingham-Papanastasiou model follows the Bingham plastic model down to a shear rate $\dot{\gamma} = 10s^{-1}$. Shear rates lower than $\dot{\gamma} = 10s^{-1}$ are assumed to be of negligible influence to the solution. The shear rate in the simulation is in order of 10^3, so this is a valid assumption.

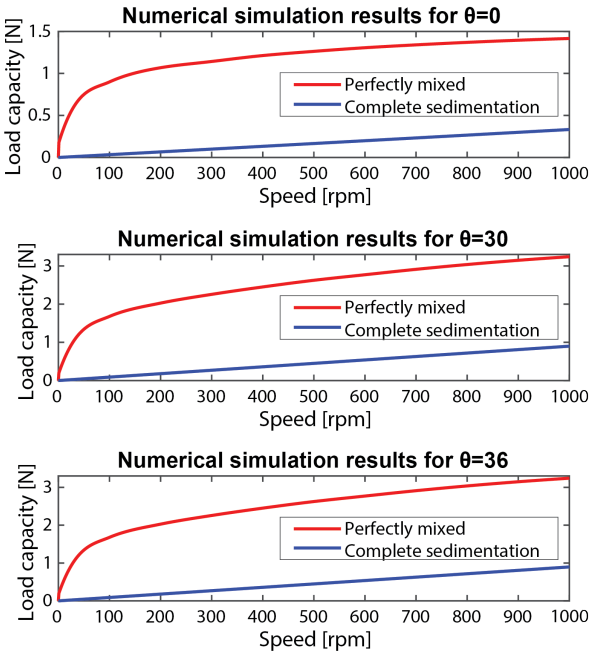

Figure 5: Results for the numerical simulations. Here the results for both perfect mixture and complete sedimentation are shown.

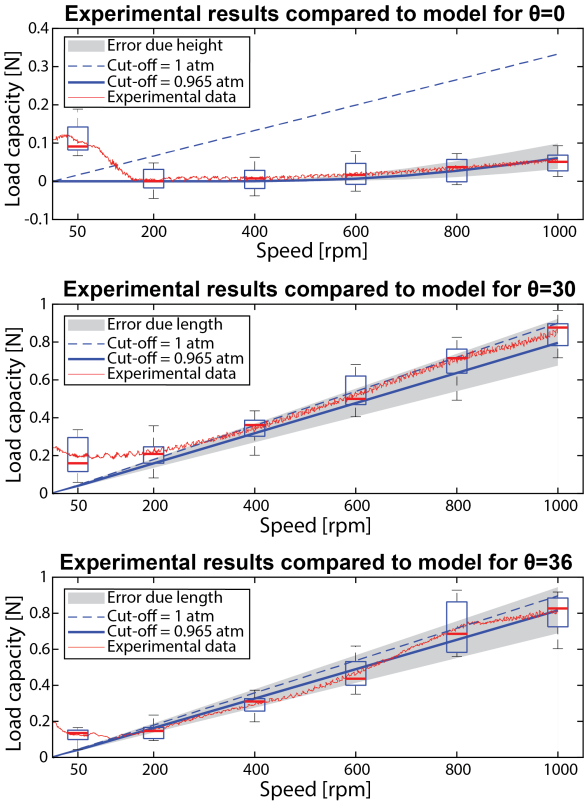

Figure 6: Comparison of the experimental results to numerical simulations for complete sedimentation.

For perfect mixture an exponential decay (increasing form) in load capacity is seen for every configuration. This is due to a trade-off between saturation of the liquid (influencing the viscosity and the geometry of the bearing), and the load capacity due to the pressurization of the fluid for increasing velocity. At low speed the viscosity of the fluid appears higher and size of the textures are larger because of the lower stresses. The moment the velocity increases, the viscosity decreases and also the size of the textures decrease which results in a smaller increase in load capacity.

For complete sedimentation physical surface textures are implemented over which a fluid flows with a viscosity equal to the viscosity of the carrier fluid. This is used to approximate the behavior and see if it corresponds to the situation where the carrier fluid separates from the magnetic particles. Here a linear increase for the load capacity is observed. This is due to that now the geometry of the bearing is fixed and the viscosity is constant.

In figure 6 the experimental results together with the numerical results for complete sedimentation (Fig. 5) are seen for θ equal to 0, 30, 36 degrees and a flying height equal to 200 μm. For the experimental results the average of 10 measurements is shown for an interval of 10 milliseconds between data points up to a total of 1000 data points. A boxplot is shown to indicate the sensitivity of the measurements.

At zero speed, already a normal force is obtained due to the magnetization of the MR fluid. The application of an external magnetic field increases the pressure inside the fluid after which the fluid is capable of carrying loads as already seen for ferrofluid bearings [25]-[28]. The local magnetic field has a strong effect on the fluid and pressurizes the liquid resulting in a load capacity at zero speed. Also the fluid shows viscoelastic behavior due to the higher viscosity of the fluid at zero speed. This viscoelastic behavior results in a stiffness depending on the magnetic field [29, 30] resulting in a load capacity. For an increase in velocity the fluid is sheared and the viscosity decreases and with it less elastic behavior is seen. The load capacity increases at the point pressurization of the liquid due to the rapid movement of the bearing faces overcomes these effects.

It is observed that the experiments where $\theta > 0$ show similar behavior as for a fixed geometry with a fluid flowing over it with a viscosity equal to 0.03. Knowing that the viscosity of the carrier fluid is equal to 0.03 it shows that there is the possibility that what is measured is actually the carrier fluid separated from the magnetic particles flowing over physical surface textures created by the magnetic particles itself. At first the vapor pressure is taken equal to the atmospheric pressure, but for θ equal to zero this shows different behavior. A lower vapor pressure significantly lowers the value of the load capacity for $\theta = 0$. This is

due to the pressure distribution which is antisymmetric for $\theta = 0$. For $\theta > 0$ the vapor pressure has a less significant impact, because here the positive pressurization is dominant. A lower vapor pressure is simulated which does correspond with the experimental data of $\theta = 0$. Seen is that this new vapor pressure which is close to 1 atm, still corresponds for θ equal to 30 and 36 degrees.

The impact of different parameters are considered, these parameters are the width, length, and height of the bearing, and also the viscosity of fluid flowing over the steps. The impact is investigated for a change of 10% for each parameter, and the influence on the load capacity of the parameter which has the most significant impact is obtained (Fig. 6). It is seen that for $\theta = 0$ the height of the step has the most significant impact, besides the vapor pressure. For θ equal to 30 and 36 the length of the step has to most significant impact. The change in load capacity due to the vapor pressure falls within these limits.

Observed is that the experimental results correspond to the situation where the magnetic particles are completely sedimented. This sedimentation is observed after doing the experiments (Fig. 7). Clearly the oil is separated and is laying on top of the magnetic particles, also oil is seen on the spindle. Already in literature this separation of the carrier fluid from the magnetic particles is observed. In [31] this phenomenon is discussed using two terms, Fluid Particle Separation (FPS) in combination with the clumping effect. It is discovered that the magnetic particles of the MR fluid are trapped in the forming chains of the magnetic field, the so called clumping effect [32, 33]. Here the carrier fluid can still flow freely separately. This effect occurs when for a longer period of time a high magnetic field is applied [34].

Figure 7: Oil seen on the spindle and laying on top of the magnetic particles after the experiments.

The FPS is linked to the clumping effect. Experiments done in [35, 36] showed separation of the carrier fluid. This is caused by the distribution in magnetic field, the pressure that is build up due to squeezing and changes in the chain structure of the magnetic particles. From this study, it is concluded that the fluid-particle separation phenomenon increased at low carrier fluid viscosity, low compression speed, and high magnetic field intensity.

It can be stated that during the experiments the particles form self-healing physical surface textures. The agglomerated magnetic particles do not wear down and do not leave the system. Over these textures a fluid flows with a viscosity equal to the viscosity of the carrier fluid (Fig. 8). At the top the MR fluid is trapped between the bearing surfaces and no magnetic field is applied, so the magnetic particles are evenly spread over the volume. Then a magnetic field is applied to the MR fluid by adding permanent magnets indicated with red in the figure. Near these magnets the magnetic field strength is high and therefore agglomerates are formed around the magnets. When the velocity of the bearing is increased, some of the magnetic particles further away from the magnets are sheared off because here the magnetic field is not sufficient to hold them in place. The magnetic particles that are kept in place form steps that pressurize the fluid. These steps are self-healing, because magnetic particles are traded among these steps. A magnetic particle sheared of from the previous step, fills a gap in the following step and so the steps do not decay.

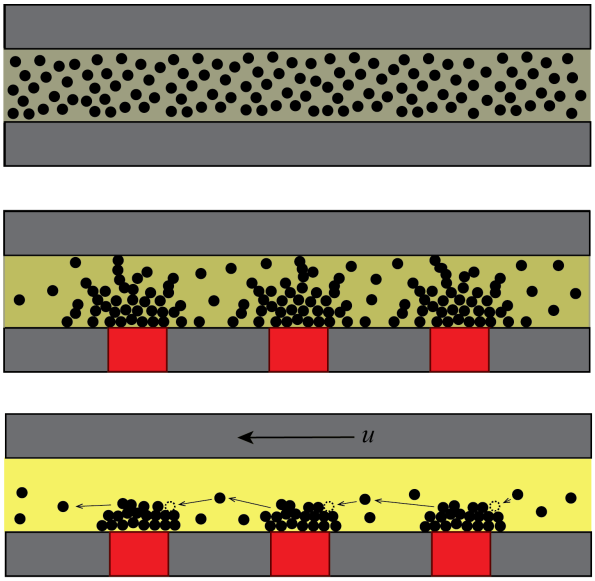

Figure 8: Illustration of the self-healing bearing.

4. Conclusion

It is concluded that a self-healing bearing is created. The surface textures consists of the magnetic particles over which the carrier fluid flows which is pressurized resulting in a load carrying capacity predicted with the numerical model for a complete sedimentation. Near the magnets the magnetic field strength is high and therefore agglomerates are formed around the magnets. During operation the magnetic particles are traded among the created textures. These textures

are self-healing, because the magnetic particles do not wear down and do not leave the system.

References

[1] S.N. Bhore, N.D. Khaire, "Analytical and Experimental investigation of Magnetorheological Fluid in Hydrodynamic journal bearing," *International Engineering Research Journal*, pp. 271277.

[2] A.M. Loeb, "Electric analog study of hydrostatic bearings," *Journal of the Franklin Institute*, vol. 263, no. 5, pp. 450452, 1957.

[3] F.Y. Zeidan, B.S. Herbage, "Fluid Film Bearing Fundamentals and Failure Analysis," *Texas A&M University. Turbomachinery Laboratories*, pp. 161186, 1991.

[4] P.G. Nikolakopoulos, C.A. Papadopoulos, "Controllable Misaligned Journal Bearings, Lubricated with Smart Fluids," *Journal of Intelligent Material Systems and Structures*, vol. 8, no. 2, pp. 125137, 1997.

[5] K. Nagaya, S. Takeda, A. Sato, S. Ikai, H. Sekiguchi, N. Saito, "Thrust bearing using a magnetic fluid lubricant under magnetic fields," *Tribology International*, vol. 26, no. 1, pp. 1115, 1993.

[6] S. Odenbach, *Ferrofluid. Magnetically Controllable Fluids and Their Applications*. Springer Berlin Heidelberg, 2002.

[7] L. Vks, "Ferrofluids and Magnetorheological Fluids," *Advances in Science and Technology*, vol. 54, pp. 127136, 2008.

[8] I.G. Kim, K.H. Song, B.O. Park, B.I. Choi, and H.J. Choi, "Nano-sized Fe soft-magnetic particle and its magnetorheology," *Colloid and Polymer Science*, vol.289, no. 1, pp. 79-83, 2011.

[9] D. Bompos, P. Nikolakopoulos, "Experimental and Analytical Investigations of Dynamic Characteristics of Magnetorheological and Nanomagnetorheological Fluid Film Journal Bearing," *Journal of Vibration and Acoustics, Transactions of the ASME*, vol. 138, no. 3, pp. 1-7, 2016.

[10] S.G.E. Lampaert and R.A.J. van Ostayen, "Virtual Textured Hybrid Bearings," *44th Leeds-Lyon Symposium on Tribology*, 2017.

[11] V.K. Agrawal, "Magnetic-fluid-based porous inclined slider bearing," *Wear*, vol. 107, no. 2, pp. 133139, 1986.

[12] J. Prakash, S.K. Vij, "Hydrodynamic Lubrication of a Porous Slider," *Journal of Mechanical Engineering Science*, vol. 15 no. 3, pp. 232234, 1973.

[13] V.M. Bhat, G.M. Deheri, "Porous Composite Slider Bearing Lubricated with Magnetic Fluid," *Japanese Journal of Applied Physics*, vol.30 ,no. 10, pp. 25132514, 1991.

[14] D.C. Kuzma, "The Magnetohydrodynamic Journal Bearing," *Journal of Basic Engineering*, volume 85, no. 3, 1963.

[15] C.Q. Chi, Z.S. Wang, P.Z. Zhao, "Research on a new type of ferrofluid-lubricated journal bearing," *Journal of Magnetism and Magnetic Materials*, vol 85 no. 13, 257260, 1990.

[16] T.A. Osman, G.S. Nada, Z.S. Safar, "Static and dynamic characteristics of magnetized journal bearings lubricated with ferrofluid," *Tribology International*, vol. 34 no.6, pp. 369380, 2001.

[17] N. Patel, D. Vakharia, G. Deheri, "A Study on the Performance of a Magnetic-Fluid-Based Hydrodynamic Short Journal Bearing," *ISRN Mechanical Engineering*, vol. 2012, 2012.

[18] H. Urreta, Z. Leicht, A. Sanchez, A. Agirre, P. Kuzhir, and G. Magnac, "Hydrodynamic Bearing Lubricated with Magnetic Fluids," *Journal of Intelligent Material Systems and Structures*, vol. 21, no. 15, pp. 1491-1499, 2010.

[19] J. Hesselbach and C. Abel-Keilhack, "Active hydrostatic bearing with magnetorheological fluid," *Journal of Applied Physics*, vol. 93, no. 10, pp. 8441-8443, 2003.

[20] X. Lu, M.M. Khonsari, "An Experimental Investigation of Dimple Effect on the Stribeck Curve of Journal Bearings," *Tribology Letters*, vol. 27, no. 2, pp. 169176, 2007.

[21] *COMSOL Multiphysics*, available at https://www.comsol.com/.

[22] K. Walters, "An Introduction to Rheology," *Elsevier Science Publishers*, firs ed., 1989

[23] T.C. Papanastasiou, "Flows of Materials with Yield," *Journal of Rheology*, vol. 31, no. 5, pp. 385-404, 1987.

[24] *Lord Corporation*. available at https://www.lord.com/.

[25] S.G.E. Lampaert, "Planar Ferrofluid Bearings: Modelling and Design Principles," *DSPE Conference. 20160*, 2016.

[26] S.G.E. Lampaert, J.W. Spronck, R.A.J. van Ostayen, "Load and stiffness of a planar ferrofluid pocket bearing," *Proceedings of the Institution of Mechanical Engineers, Part J: Journal of Engineering Tribology*, vol. 232 no. 1, pp. 1425, 2018.

[27] S.G.E. Lampaert, B.J. Fellinger, J.W. Spronck, R.A.J. van Ostayen, "In-plane friction behaviour of a ferrofluid bearing," *Precision Engineering*, vol. 54, pp. 163170, 2018.

[28] A.S.T. Boots, L.E. Krijgsman, B.J.M. de Ruiter, S.G.E. Lampaert, J.W. Spronck, "Increasing the load capacity of planar ferrofluid bearings by the addition of ferromagnetic material," *Tribology International*, vol. 129, pp. 4654, 2019.

[29] Y. Xue, S. Changgeng, "The stiffness and damping properties of magnetorheological fluid-elastomer composites," *21st International Congress on Sound and Vibration 2014, ICSV 2014*, vol. 5, pp. 43774381, 2014.

[30] J.S. Oh, S.B. Choi, "State of the art of medical devices featuring smart electro-rheological and magneto-rheological fluids," *Journal of King Saud University - Science*, vol. 29 no. 4, pp. 390400, 2017.

[31] S.A. Wahid, I. Ismail, S. Aid, and M.S.A. Rahim, "Magnetorheological defects and failures: A review," *In IOP Conference Series: Materials Science and Engineering*, vol. 114, 2016.

[32] A. Farjoud, R. Cavey, M. Ahmadian, M. Craft, "Magnetorheological fluid behavior in squeeze mode," *Smart Materials and Structures*, vol. 18, no. 9, 2009.

[33] A. Farjoud, M. Craft, W. Burke, and M. Ahmadian, "Experimental Investigation of MR Squeeze Mounts," *Journal of Intelligent Material Systems and Structures*, vol. 22, no. 15, pp. 1645-1652, 2011.

[34] K. Adjerid, "A Study on the Dynamic Characterization of a Tunable Magneto-Rheological Fluid-Elastic Mount in Squeeze Mode Vibration," Virginia Polytechnic Institute and State University, 2011.

[35] I. Ismail, S.A. Mazlan, H. Zamzuri, A.G. Olabi, "FluidParticle Separation of Magnetorheological Fluid in Squeeze Mode," *Japanese Journal of Applied Physics*, vol. 51, 2012.

[36] I. Ismail and S.N. Aqida, "Fluid-Particle Separation of Magnetorheological (MR) Fluid in MR Machining Application", *Key Engineering Materials*, vols. 611-612, pp. 746-755, 2014.

Chapter 4

Discussion

An MR fluid is a type of smart fluid in a carrier fluid. When subjected to a magnetic field, the fluid greatly increases its apparent viscosity, to the point of becoming a viscoelastic solid (appendix A-1 to A-3). MR fluids are non-Newtonian fluids, therefore different models are proposed to model the stress-strain relation in these fluids (appendix A-4). Currently MR fluids bring great potential in many different applications, but still a lot is to be achieved in the bearing technology (chapter 1). Despite years long of development, wear and lifetime of bearings still occur to be big problems.

In fluid bearings (appendix A-5) the load is supported by a pressurized thin film allowing lower friction, wear and vibration than many other types of bearings. Hydrostatic bearings do rely on pumps which are sensitive to failure and contribute to the system energy loss. Hydrodynamic lubrication (appendix A-6) is also used but at lower speeds, starts, and stops, metal to metal contact in the bearing cannot be avoided. The variable rheological properties of an MR fluid add an extra design variable to the system which increases the performance of bearings. What former concepts discussed in literature (appendix B) all have in common is that the applied magnetic field is constant and/or applied globally and not locally. They all improve the performance to a certain extent, but do not discuss the wear which is generally caused by poor lubrications during high loading conditions or low speeds. Therefore the main focus is to consider the possibility of recreating surface textures that pressurize the fluid in a hydrodynamic bearing in order to carry a load. These surface textures consist of magnetic particles that do not wear down and do not leave the system.

In the first paper (chapter 2) several numerical simulations are developed using different 2D fluid models incorporating an MR fluid in flow and shear mode, also referred to as Poiseuille flow and Couette flow. For the flow mode (appendix D) succesfully a numerical simulation (appendix E-1) is developed where the results correspond to the results in [16]. In this model the Bingham-Papanastasiou model is implemented to model the non-Newtonian behavior of an MR fluid. By applying a constant yield stress to the MR fluid a constant magnetic field is simulated. The higher the yield stress, the bigger the region the shear stress does not exceed the yield stress. In this region the MR fluid is in solid phase. This solid phase results in a so-called plug flow at the center of the channel, which grows in size for increasing yield stress.

In the numerical simulation for the shear mode (appendix E-2) a varying yield stress is required to obtain a solid part in the channel. This varying yield stress is linearly decreasing over the channel height. Using this a solid part is created over the length of the channel. Applying a higher velocity to the moving wall in the model, results in a smaller solid part. This is because due the higher velocity the shear stress in the fluid increases. The region where the shear stress exceeds the yield stress grows and less solid phase is seen.

For the model regarding the step bearing configuration (appendix E-4) a local magnetic is created (appendix E-3). Using the magnetic field created by the self created array combined with the MR fluid MRF140CG (appendix I), locally a virtual texture is created (Fig. 4-1). This solid part represents a step geometry which is used to pressurize the MR fluid. A pressure distribution over the length of the channel is observed (Fig. 4-2). This pressure distribution indicates that there is the possibility to create a load carrying capacity. Even for where the shear stress does exceed the yield stress and no solid part is visible, a pressure distribution is observed. This is due that the MR fluid is still more viscous at the bottom of the channel. The flow resistance is higher at the bottom which results in the observed pressure distribution.

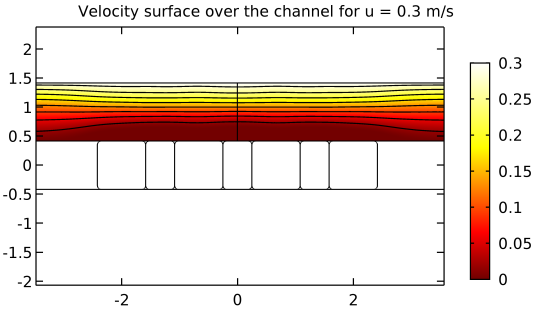

Figure 4-1: Solid part created at the middle of the length of the channel.

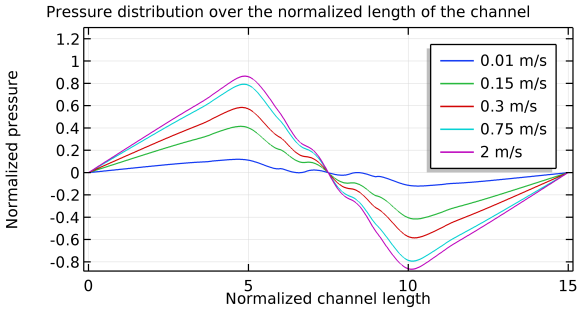

Figure 4-2: The normalized pressure distribution in the MR fluid with a solid part in the middle of the channel for different velocities of the moving wall.

The work done in the first paper is elaborated in the second paper (chapter 3). Here the 2D fluid models are used to create a 3D model. For this numerical simulation the MR fluid MRF122EG (appendix J) is considered. In the configuration used the magnets lie under a certain angle equal to 0, 30, and 36 degrees. The angle equal to 36 degrees is based on the angle for which the highest load capacity is expected (appendix E-7). In one model it is assumed that the magnetic particles are perfectly mixed with the carrier fluid (appendix E-5), resulting in virtual surface textures. For this situation an exponential decay (increasing form) in load capacity is obtained (Fig. 4-3). This is due the the trade-off between saturation of the liquid (influencing the apparent viscosity and the geometry of the bearing), and the load capacity due the rapid movement of the bearing faces. In the numerical simulation where it is assumed that magnetic particles completely separate from the carrier fluid (appendix E-6) a linear increase in load capacity is obtained (Fig. 4-3). Here the physical surface textures that pressurize the fluid consist of the magnetic particles which are completely sedimented. Over these steps a fluid flows of which its viscosity is equal to viscosity of the carrier fluid.

The proofs of concept are made using the same parameters as used for the 3D models. Using these proofs of concept, an experimental set-up is made and experiments are done using the Antor Paar MCR 302 rheometer (appendix F). The alignment error is also taken into consideration, and it is expected that this will have no significant influence on the results (appendix G). Observed is that the experimental results correspond to the situation where the magnetic particles are completely sedimented (Fig. 4-4). This sedimentation is seen after doing the experiments. Clearly the oil is separated and is laying on top of the magnetic particles and also oil is seen on the spindle (appendix H). It can be stated that during

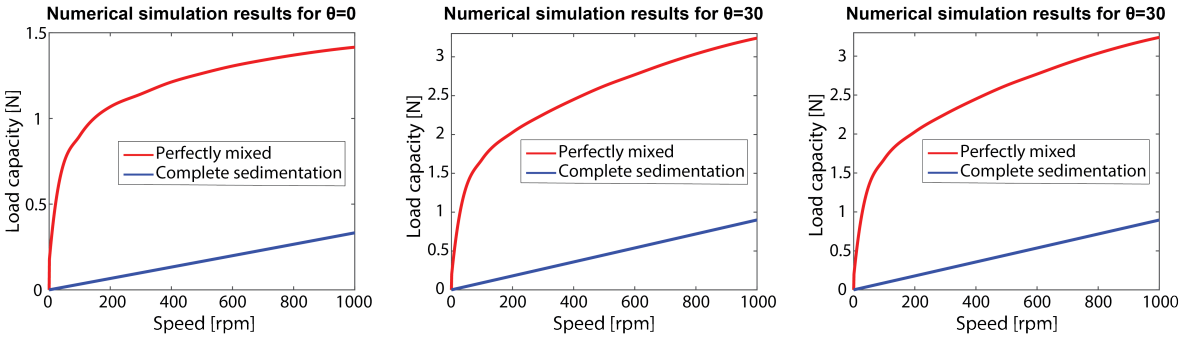

Figure 4-3: Results for the numerical simulations. Here the results for both perfect mixture and complete sedimentation are shown.

the experiments the particles form self-healing physical surface textures. The agglomerated magnetic particles do not wear down and do not leave the system. Over these physical textures a fluid flows with a viscosity equal to the viscosity of the carrier fluid (Fig. 4-5). The magnetic particles are kept in place by the magnetic field and form steps that pressurize the fluid. These steps are self-healing, because magnetic particles are traded among these steps. A magnetic particle sheared of from the previous step, fills a gap in the following step and so the steps do not decay.

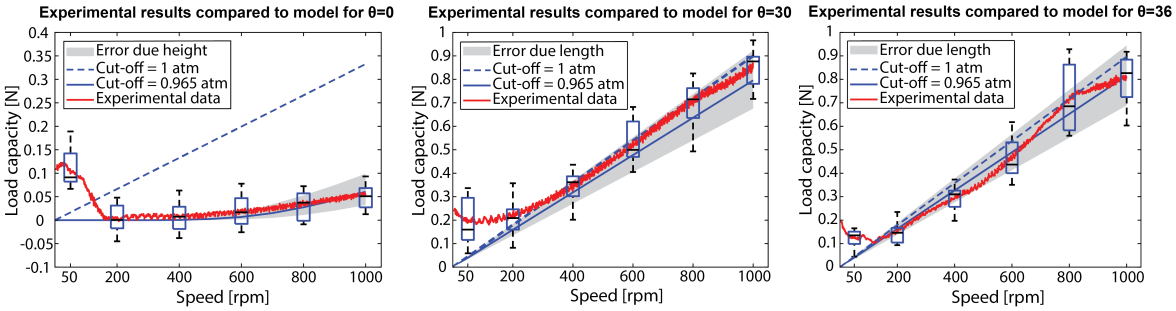

Figure 4-4: Comparison of the experimental results to numerical simulations for complete sedimentation..

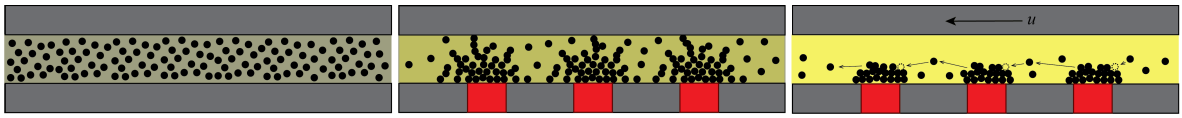

Figure 4-5: Illustration of the self-healing bearing.

Chapter 5

Conclusions

In this thesis the possibility of using MR fluids in fluid bearings is considered. Because fluid bearings still encounter several problems regarding wear and lifetime, magnetic fluids could be used to improve the performance. The goal was to develop a fluid bearing using an MR fluid to solve the different problems seen currently regarding wear and lifetime. Here the most important conclusions are summarized.

5-1 Literature

Here the main conclusions are presented considering information found in literature.

- Despite years long of development, wear and lifetime of bearings still occur to be big problems.
- Fluid bearings allow lower friction, wear and vibration, but still require external pressurization or significant wear occurs at lower speeds, starts, and stops.
- Magnetic fluids have the potential to improve the performance of fluid bearings due their variable rheological properties.
- The tunability for the rheological properties of ferrofluids is low and currently the load capacity is limited.
- Due the more intense aggregation process in an MR fluid the flow behavior can be controlled.
- The variable rheological properties of an MR fluid add an extra design variable to the system which can be used to increase the performance of fluid bearings.
- The resistance in a bearing can be increased locally by using an MR fluid and a local magnetic field.
- Currently MR fluids are only applied in combination with a constant magnetic field.

5-2 Magnetorheological texturing

Here the main conclusions are presented considering the research on the possibility of creating surface textures using an MR fluid.

- A constant yield stress cannot be used to create a solid part in shear mode.
- A varying magnetic field is required to obtain a solid part in the MR fluid in shear mode.
- A virtual surface texture in the MR fluid can be created using a local varying magnetic field.
- This virtual surface texture pressurizes the MR fluid which indicates that creating a load carrying capacity is possible using an MR fluid.
- A pressure distribution is also obtained for no visible solid part.
- The pressure distribution for no visible solid part remains constant for higher velocities.

5-3 Self-healing bearing

Here the main conclusions are presented considering the research on the self-healing hydrodynamic thrust bearing using an MR fluid.

- For a perfectly mixed MR fluid combined with a local varying magnetic field virtual surface textures are created.
- The virtual surface textures result in an exponential decay (increasing form) in load capacity.
- The size of the virtual surface textures for a perfectly mixed MR fluid decreases in size for increasing velocity.
- For a completely sedimented MR fluid combined with a local varying magnetic field the physical surface textures result in a linear increase in load capacity.
- The experimental results do correspond with the situation of complete sedimentation.
- The experimental results show a load capacity at zero speed due the magnetization of the MR fluid.
- A self-healing hydrodynamic thrust bearing is created.

Chapter 6

Recommendations

The results are already promising, but more research can be done to extend on this. Based on the new knowledge gained in this research several recommendations can be made for further research. Now only a proof of concept is made which demonstrated the possibility of creating physical surface textures using an MR fluid. The technology is in a too early stage to make it successful in industry and has to be developed furthermore in order to make it more attractive. This can be done by a possible bachelor project regarding some fundamentals of MR fluids influencing the performance of the bearing. More work can be done by possible master projects regarding modeling and a new demonstrator. When this is all done successfully and the results are promising, the next step towards industry is possible.

6-1 Fundamentals of the MR fluid (Bachelor project)

Investigation of the fundamentals of MR fluids can be done in a bachelor project. This can be done by making a simple set-up where different magnets in combination with different MR fluids can be tested, observing the behavior. The findings can be used in master projects in order to more efficiently model and experimentally validate different configurations. Taking this into consideration the following recommendations are suggested.

- Investigate the application of a ferrofluid based MR fluid [22].
- Investigate the material and magnetic properties of MR fluids.
- Investigate what parameters influence the sedimentation/diffusion of the magnetic particles.

6-2 Modeling of the MR fluid (Master thesis)

Making a good model can save time in optimizing the bearing configurations. This can be done in a master project implementing the findings in this thesis. Complete models can be optimized and used for designing a new demonstrator in which more configurations can be implemented. Taking this into consideration the following recommendations are suggested.

- Include the load capacity obtained at lower speeds due magnetization of the MR fluid in the models.
- Model the MR fluid as a thin-film flow combined with a modified Reynolds equation.
- Investigate the influence of material and magnetic properties of the MR fluid used on the performance of the bearing.
- Model the formation of the textures due sedimentation/diffusion in the fluid.
- Model a journal bearing using magnetorheological texturing.
- Make a complete model of the bearing which can be used for optimization.

6-3 Demonstrator using an MR fluid (Master thesis)

Disposing of a good demonstrator different concepts can easily be tested. In this demonstrator different configurations of magnets and different MR fluids can be tested resulting in different load carrying behavior. The performance of these configurations can be investigated also regarding friction, vibration dampening characteristics, and bearing life. Taking this into consideration the following recommendations are suggested.

- Design a new demonstrator in which the dimensions are not that limited and more configurations can be tested.
- Integrate different configurations of the magnetic field resulting in different configurations of self-acting hydrodynamic bearings.
- Investigate the amount of friction created during operation, especially at lower speeds.
- Investigate the vibration dampening characteristics in the bearing using an MR fluid.
- Investigate the bearing life and main causes of failure.
- Investigate the possibility to create virtual surface texturing instead of physical surface texturing.
- Implement a magnetic field that can be altered during operation in order to have active control over the performance of the bearing.

If the results are promising after testing different configurations taking the material and magnetic properties into consideration, the next step towards industry can be made. Now enough knowledge is developed in order to be able to make a first prototype. This can be done in collaboration with a company which is familiar with bearing technology. Especially successfully implementing the recommendation *"Implement a magnetic field that can be altered during operation in order to have active control over the performance of the bearing."* can be a huge selling point. Developing a prototype on a larger scale than done in research, possibly implementing the active control, can bring this technology to industry.

Appendix A

Literature

A-1 Magnetorheology

The magnetic properties of a magnetic liquid are obtained when particles that have magnetic properties are suspended in a carrier fluid. The most often used magnetic particle material for an MR fluid is iron, this is because the saturation magnetization of iron is 2.1 Tesla, this is the highest value of known elements [42]. This high saturation magnetization increases the maximum magnetorheological effect, this is due to the increase in maximum inter particle attraction. To achieve a stable suspension, the particles have to be protected against agglomeration due to van der Waals interaction. This stability can be achieved by coating the particles with long chained organic molecules as seen in figure A-1 or by electric charge stabilization [46]. Nonetheless mixing these particles in the carrier fluid can cause formation of clusters of these particles or the particles have the tendency to settle out of the fluid and come to rest against a certain barrier. This behavior will not be seen when the thermal energy of the particle will be in the same order of magnitude as the gravitational and magnetic energy of the particles [34]. Also a way of improving the stability is using additives. To enhance the redispersibility of MR fluid oleic acid can be used, but this cannot prevent particle settling. To counter the particle settling silica nanoparticles can be added, but this again makes the redispersion extremely difficult [30].

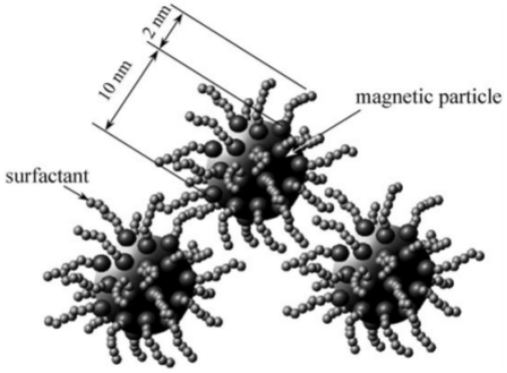

Figure A-1: A schematic view of the coated magnetic particles in a ferrofluid. Picture from [46].

MR fluids are fluids that can have a liquid behavior but can also act solid, depending on the strength of the magnetic field applied to it. If we look at ferrofluids it is seen that these fluids do not get as 'solid' as the MR fluids. MR fluids becoming a solid is due to the attractive dipolar forces between the particles which have been magnetized by the applied magnetic field. The strength of the solid phase is caused by the formation of certain structures

by particles, such as chain-like agglomerates [45] as schematically shown in figure A-2. An essential difference between ferrofluids and MR fluids is the size of the magnetic particles, where the particles of ferrofluids go up to 15 nanometer and of MR fluids are normally around the size of micrometers. Furthermore, the magnetic moment of the particles for an MR fluid is induced by the magnetic field, where the particles for a ferrofluid have permanent dipole moment. Also the particles for a ferrofluid perform intens thermal motion which limits the agglomerate formation, therefore there is no significant change in flow behavior when a field is induced. This aggregation process for an MR fluid is more intense in presents of a field, and that is why their flow behavior can be controlled [30]. These fluids are very attractive for applications in the industry, because the viscosity can easily be controlled by the application of a magnetic or electric field. For example it is really useful for damping as discussed before, or bearings where now the fluid is of constant viscosity.

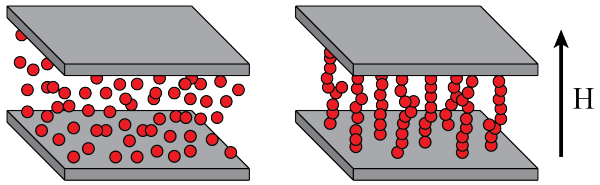

Figure A-2: Schematic overview of the formation of chain-like agglomerates when a magnetic field is applied. On the left there is no magnetic field applied and the MR fluid acts as a fluid. On the right a magnetic field in the direction of the arrow is applied, where the MR fluid acts as a solid.

A-2 Viscosity properties

Assuming a fixed magnetic moment within the particles and no interaction between the magnetic particles, applying a magnetic field to a MR fluid will cause the magnetic particles in the fluid to align in the direction of the magnetic field due to an alignment torque. This will increase the viscosity of the fluid (figure A-3). If a perpendicular shear force is applied to the field, an additional torque will be created which will reduce the effectiveness of the alignment torque which is now counteracted. Increasing the magnetic field will increase the alignment torque which increases resistance to the torque created by the shear stress. All in all, the free rotation of the particles is hindered and this causes the observation of increase in viscosity [34]. This is called rotational viscosity and can be expressed as in equation A-1 [46, 29].

$$\eta = \eta_0(1 + \frac{5}{2}\tilde{\phi}) \tag{A-1}$$

Equation A-1 only is valid when there is no field present ($\Delta\eta = 0$) and is called the Einstein formula where η_0 [Pa·s] is the viscosity of the carrier fluid and $\tilde{\phi}$ is the volume concentration including the surfactant. When there is a field present, $\Delta\eta$ is no longer equal to zero and the relation in equation A-2 is obtained:

$$\eta = \eta_0\left[1 + \frac{5}{2}\tilde{\phi} + \frac{3}{2}\tilde{\phi}\frac{\alpha - tanh(\alpha)}{\alpha + tanh(\alpha)}sin^2(\beta)\right] \tag{A-2}$$

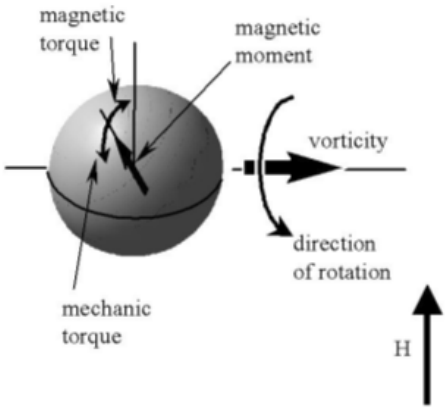

Figure A-3: The magnetic moment in the particle will align with the externally applied magnetic field which causes higher shear load. Picture from [48].

Here α is the Langevin parameter, β [rad] is the angle between the magnetic field and vorticity. The Langevin parameter shown in equation A-3 is the ratio of magnetic and thermal energy of the particles, and is used in the Langevin formula to calculate a theoretical magnetization curve [19]. If an appropriated model of inter particle interactions is chosen, this theoretical magnetization curve will agree with the experiments.

$$\alpha = \frac{\mu_0 m H}{k_B T} \tag{A-3}$$

Here μ_0 ($= 4\pi \cdot 10^{-7}$ [N/A^2]) is the permeability of vacuum, m [N·m/T] is the magnetic moment, H [A/m] is the magnetic field strength, k_B ($= 1.38064852 \cdot 10^{-23}$ [J/K]) is the Boltzmann's constant and T [K] the absolute temperature. As discussed before, applying a magnetic field will cause the magnetic particles in the fluid to align in a certain way. This alignment can be caused by one of the two processes: the Neel relaxation or the Brownian relaxation. For the Neel relaxation the particle itself is static, and therefore the magnetic moment which is inside the particle will align with the magnetic field. For the Brownian relaxation the magnetic moment inside the particle stays static instead of the particle itself, and so the particle aligns with the magnetic field. Both these processes have a time constant shown in equation A-4 (Neel) and A-5 (Brownian), and the process with the smallest time constant will occur [44].

$$\tau_N = \frac{1}{f_0} e^{\frac{KV}{k_B T}} \tag{A-4}$$

$$\tau_B = \frac{3\tilde{V}\eta}{k_B T} \tag{A-5}$$

Here f_0 [Hz] is the Larmor frequency of the magnetic moment in the anisotropy field of the particle, K is the anisotropy constant of the particles, V [m^3] is the volume of the magnetic core, and $\tilde{V}$ [m^3] is the volume of the particles including the surfactant layer. It is seen that for the Brownian relaxation the time constant is linearly dependent on the volume, where the Neel relaxation is exponentially dependent on the volume of the particle. This exponential

behavior causes the time constant of Neel to be higher after a critical size of the particle, this is shown in figure A-4.

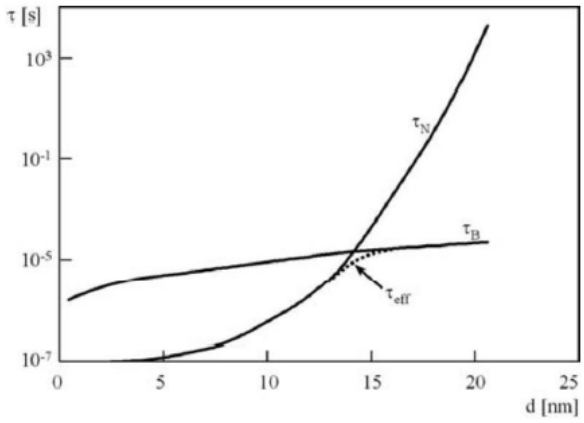

Figure A-4: Neelian and Brownian relaxation process as function of the diameter of the magnetic particle. Picture from [44].

As seen in figure A-4, when the diameter of the particle is around 13 nm the Brownian relaxation will dominate because of its smaller time constant, this diameter is called the critical diameter [44]. In figure A-5 the classification of magnetic fluids is seen [21]. The typical diameter of the particles in magnetorheological fluids are from 1 to 100 μm, preferably in the range of 1 to 10 μm. Particles larger than 100 μm can cause increased friction and accelerated wear [65, 23].

If ferrofluids are considered, the Neelian relaxation will dominate because here the particle size is below the critical diameter. Only a little part of the conventional ferrofluids will be influenced by the Brownian relaxation.

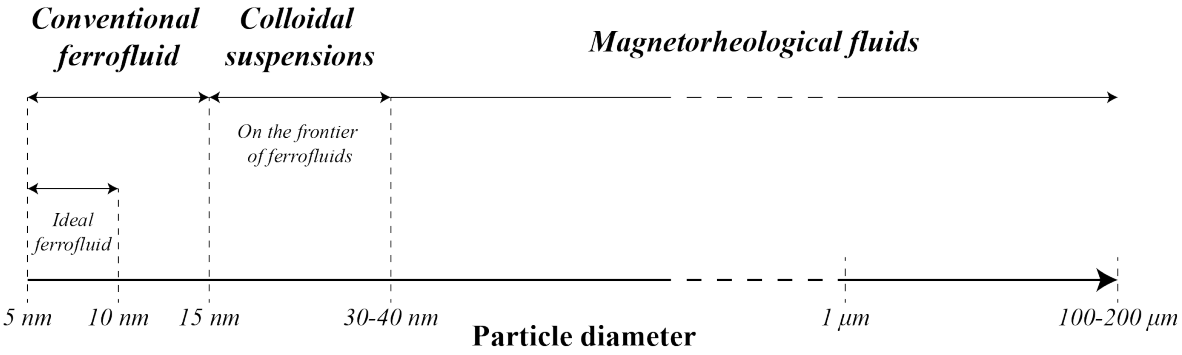

Figure A-5: Classification of magnetic fluids.

As stated before it is seen that the time constant for both the Brownian relaxation and the Neelian relaxation depend on a volume. For Brownian it is the volume of the particles including the surfactant layer, for Neelian it is the volume of the magnetic core. But the difference is that Brownian depends on the viscosity η of the fluid, where Neelian depends on the anisotropy constant K of the particles. Commonly the Neel particles and Brownian particles are called magnetically weak and magnetically hard particles respectively.

Additionally in figure A-6 experimental data of APG513A is shown and it shown that the increase of viscosity significantly depends on the shear rate. This cannot fully be explained by the theory of rotational viscosity, and therefore the term magnetoviscous effect is introduced [45]. This term is used to indicate concentrated suspensions, where inter particle interaction plays a significant role. For highly diluted suspensions with negligible particle interaction the term rotational viscosity will be used. From the experiments it is assumed that the leading component in the description of magnetoviscosity is the formation of chain-like aggregation or clusters of particles under the influence of a magnetic field. The strong increase of viscosity with the magnetic field strength is assumed to be caused by the hindrance of rotation of these agglomerates. Furthermore observed decrease in viscosity under shear strain can be explained by the rupture of the chains in a shear flow [47].

A model presented in [59] is used to investigate the influence of particle size distribution for the flow behavior of a magnetic fluid. Here it can be observed that not magnetically weak, but magnetically hard particles show an strong enough inter particle interaction to contribute significantly to a chain formation explained before.

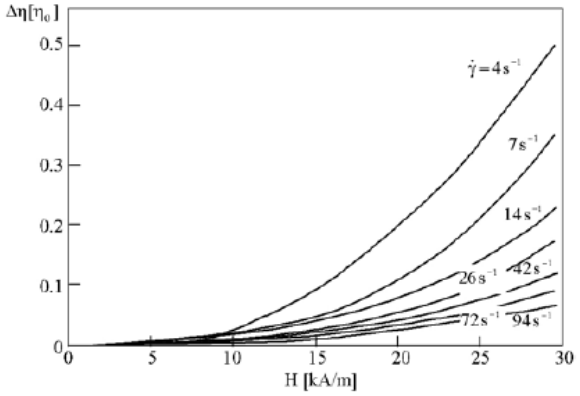

Figure A-6: The change of viscosity as a function of the magnetic field strength is shown of the APG513A for various shear rates. Picture from [45].

The appearance of the chain-like agglomerates that cause this magnetoviscous effect can be linked to the interaction parameter shown in equation A-6 [46]:

$$\lambda = \frac{\mu_0 M_0^2 V}{24 k_B T} \tag{A-6}$$

Here M_0 [A/m] is the spontaneous magnetization of the magnetic material. The chain-like aggregation will appear if this parameter is greater than one. For magnetic fluids there is the possibility that the particles are coated, this requires a modified interaction parameter which is as following [59]:

$$\lambda^* = \left(\frac{d}{d+2s}\right)^3 \lambda \tag{A-7}$$

Here s [m] is the parameter that represents the thickness of the surfactant layer and d [m] is the diameter of the particle. In figure A-7 the modified interaction parameter is shown for

particles with a diameter larger than 13 nm, the critical diameter. For these particles the parameter clearly exceeds 1, this is because of the strong magnetic dipole interaction.

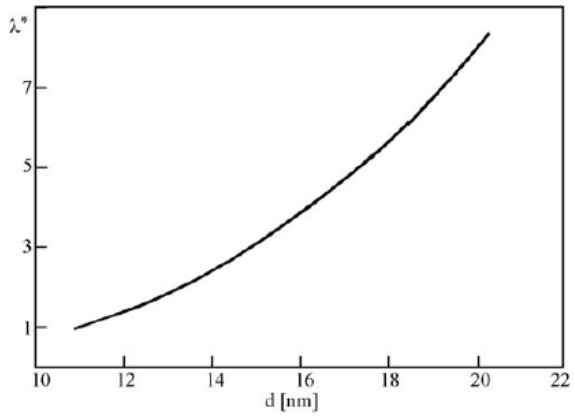

Figure A-7: The modified interaction parameter for particles with a 2 nm thick surfactant as a function of the particle diameter. Picture from [46].

Furthermore there is the Mason number, this number describes the viscosity changes against the relation of shear stress to magnetic interaction forces [39]. This Mason number is defined for electrorheological suspensions, where the electrostatic polarization forces and hydrodynamic forces are the main forces that govern the behavior. Considering this, the Mason number is defined as in equation A-8 [32].

$$Mn \equiv \frac{F^H}{F^E} = \frac{\eta_c \dot{\gamma}}{2\epsilon_0 \epsilon_c \beta^2 E^2} \tag{A-8}$$

Here ϵ_0 ($= 8.854210 \cdot 10^{-12}$ [F/m]) is the permittivity of free space, ϵ_c is the relative dielectric constant of the continuous phase, β is the relative polarizability, E [V/m] is the applied electric field strength, η_c [Pa·s] is the viscosity of the continuous phase, and $\dot{\gamma}$ [s^{-1}] is the macroscopic shear rate. In [32] an experiment is done where the relative viscosity as a function of $\dot{\gamma}$ for different currents was obtained as shown in figure A-8. Here the different currents indicate the different magnetic field strengths.

Using this experimental data and direct substitution of the magneto statics variables for electrostatic variables initially the Mason number for MR suspensions is defined as in equation A-9:

$$Mn(H) = \frac{\eta_c \dot{\gamma}}{2\mu_0 \mu_c \beta_M^2 H^2} \tag{A-9}$$

Here μ_c is the relative permeability of the continuous phase, and $\beta_M = (\mu_p - \mu_c)/(\mu_p + 2\mu_c)$ where μ_p is the relative permeability of the particle material. In [32] it is shown that shear viscosity data at various shear rates and magnetic field strengths do not collapse to the function shown here above. It appears that this is in part caused by nonlinear particle magnetization. What is done instead is that a Mason number defined in terms of the suspension magnetization M [A/m] is more useful and is seen equation A-10.

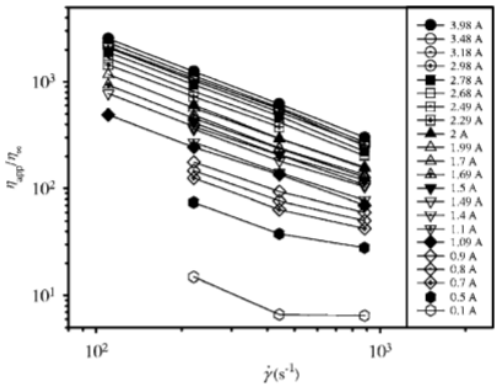

Figure A-8: The relative viscosity as a function of the macroscopic shear rate for different currents. The relative viscosity is defined by the apparent suspension viscosity η_{app} devided by the high shear rate viscosity η_∞ in the absence of an applied magnetic field. Picture from [32].

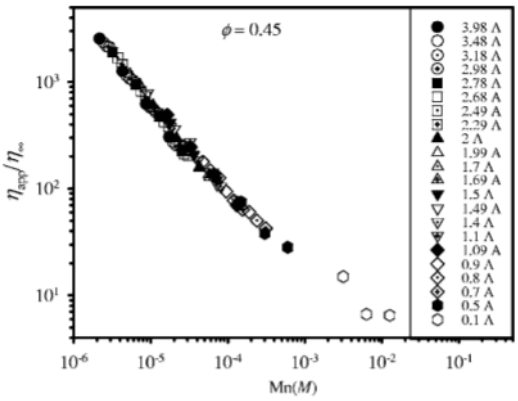

Figure A-9: Relative viscosity as a function of the Mason number which now depends on the suspension magnetization. Here the suspension magnetization was measured experimentally. Picture from [32].

$$Mn(M) = \frac{9\eta_c\dot{\gamma}\phi^2}{2\mu_0\mu_c\langle M\rangle^2} \tag{A-10}$$

Here ϕ represents the volume fraction of the magnetic particles. It is noted that every term in equation A-10 can be measured experimentally. In figure A-9 the experimental data is shown where the suspension magnetization was measured experimentally. The data collapses on to a single curve for all volume fractions. Now that these results are obtained, to describe the relation between the shear rate and field strength of the apparent viscosity of an MR suspension requires relatively few experiments.

A-3 Magnetic properties

The magnetic particle with relative magnetic permeability μ_p that is suspended in a non-magnetic fluid experiences a magnetic moment according to equation A-11 [45].

$$m = 4\pi\mu_0\mu_f\beta a^3 H_0 \tag{A-11}$$

Here μ_f is the relative permeability of the fluid, a [m] is the radius of the particle, H_0 [A/m] is the external magnetic field and $\beta = (\mu_p - \mu_f)/(\mu_p + 2\mu_f)$. When the relative permeability of the fluid is greater than that of the particle, there is the case of an inverse magnetic fluid [17]. Equation A-11 is the magnetic moment just for one particle and it can be used to obtain the interaction energy between two particles within the carrier liquid seen in equation A-12.

$$W = \frac{1}{4\pi\mu_0\mu_f}\left(\frac{m_\alpha m_\beta}{r^3} - \frac{3(m_\alpha r)(m_\beta r)}{r^5}\right) \tag{A-12}$$

Here r [m] is the separation vector between the centers of the two particles, and m_α & m_β are the magnetic moments of the different particles. The ratio of this interaction energy to kT is related to the certain formation of particles. This is called the interaction parameter shown in section A-2. To reach equilibrium in the structuration of an MR fluid, the way of increasing the magnetic field is important. Increasing the field too quickly will cause formation of labyrinths, but increasing it slowly will cause formation of separated columns [20, 41].

If the concepts of magnetism are considered the following parameters are important, the magnetic field strength H, the magnetic flux density B and the magnetization M. The magnetization is defined as the magnetic moment per unit volume [31]. The interpretation of B and H used is according to Faraday and Maxwell, H is the primary magnetic field that causes the field B in magnetizable matter [53]. In essence it can be said that the magnetic field strength is a measure of the force in free space, at contact surfaces with materials the experienced force is maximum. Over the distance of this material the force decreases, this is characterized by the magnetic flux. The relation between the three parameters is as in equation A-13:

$$B = \mu_0(H + M) \tag{A-13}$$

The direct relation between the magnetic field and the magnetic flux density is seen in equation A-14.

$$B = \mu H \tag{A-14}$$

Where $\mu = \mu_r\mu_0$ and the relative permeability is denoted with μ_r. This relative permeability is the ratio of the permeability of a specific medium to the permeability of free space and it is related to the magnetic susceptibility χ as in equation A-15.

$$\mu_r = 1 + \chi \tag{A-15}$$

This magnetic susceptibility indicates whether a material will be attracted to a magnetic field or will be repelled by the magnetic field. The magnetic susceptibility can be calculated with the use of a SQUID (Superconducting quantum interference device). With this device the hysteresis loop can be measured and from this the susceptibility can be calculated, using that magnetic susceptibility is the ratio between the magnetization of the material and the applied magnetic field strength: $\chi = M/H$ [9].

Also with the susceptibility it can be indicated whether a material is paramagnetic or diamagnetic. A positive value of the susceptibility indicates that the material is paramagnetic, and a negative value of the susceptibility indicates that the material is diamagnetic [31]. The paramagnetic materials are the ones that will be attracted by an externally applied field. Internally induced magnetic fields will be in the direction of the applied magnetic field. Diamagnetic materials will be repelled by externally applied magnetic fields and internally there will be a formation of induced magnetic field opposite to the direction of that applied magnetic field.

A-4 Magnetization model for an MR fluid

Different models are used for magnetic fluids. For ferrofluids the Newtonian model, $\tau = \eta\dot{\gamma}$, is used [1]. Here τ is the shear stress, η the dynamic viscosity, and $\dot{\gamma}$ the shear rate. For MR fluids this model is insufficient and a more complex model is used for example Bingham plastic [8], $\tau = \tau_y + \eta\dot{\gamma}$, and Herschel-Bulkley [23], $\tau = \tau_y + K\dot{\gamma}^n$. In [66] the herein-proposed magnetization model is developed to extend these models to describe the behavior of MR fluids. When the shear stress exceeds the yield stress, the Bingham plastic model assumes that the viscosity remains constant. The possibility is that this is not the case because of the shear-thinning/thickening effect, therefore the Herchel-Bulkley is introduced to incorporate this [7]. This effect is incorporated in the flow index n, for $n < 1$ the fluid is shear-thinning, and for $n > 1$ the fluid is shear-thickening, this can be seen in figure A-10. Furthermore the Bingham-Papanastasiou, $\tau = \tau_y(1 - exp(-m\dot{\gamma})) + \eta\dot{\gamma}$, can be used to model the magnetic behavior.

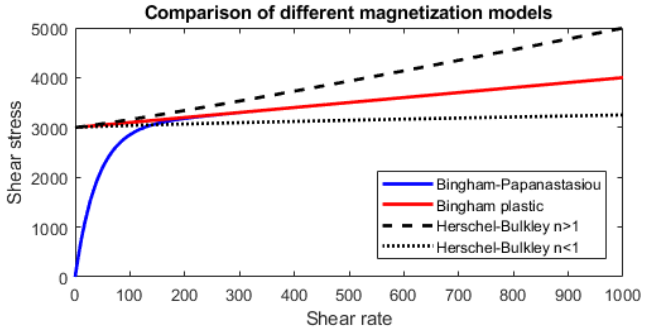

Figure A-10: The Herschel-Bulkley, Bingham plastic, and Bingham-Papanastasiou models compared to each other.

In figure A-10 the 3 main magnetization models are shown and compared to each other. It is seen in the figure that for the Herschel-Bulkley model shear-thinning and shear-thickening are incorporated. When n is equal to 1 and K is equal to the η, the Herschel-Bulkley will follow the Bingham plastic model. For numerical simulations these two models can be difficult to implement because for $\dot{\gamma} = 0$ the shear stress has two values, $\tau = 0$ and $\tau = \tau_y$. This is not the case for the Bingham-Papanastasiou model.

A-5 Fluid bearings

In this section categories in lubricated bearings will be discussed, the working principles and how they generally are designed. First a general introduction will be given, this will be followed up by a discussion about hydrostatic and hydrodynamic bearings.

A-5-1 Lubricated bearings

The biggest problem seen in systems which contain moving components is wear which is caused by contact between the bearing faces, this can lead to different failure modes. To avoid this the use of proper lubrication is very important. Two main bearings that can work with lubrication are the journal bearing and the thrust bearing, both are rotary bearings. The journal bearing is simply a shaft rotating in a bearing, where the shaft and bearing are separated by a layer of lubricant. Commonly they are used for supporting radial loads.

Thrust bearings are designed to support a predominately axial load. For this also lubricants can be used, which can support the axial thrust when pressurized. A few advantages of using lubricants are that they provide damping, reduce noise and reduce transmitted vibration [38].

In figure A-11 the Stribeck curve is shown which is used to describe the friction properties between two surfaces, for example for the hydrodynamic bearing which will be in the right region which describes fluid friction. The left region is for solid/boundary friction and the middle region for mixed friction [58]. For an MR fluid the viscosity can be altered by altering the magnetic field, this means the value of the Hersey number can be altered also.

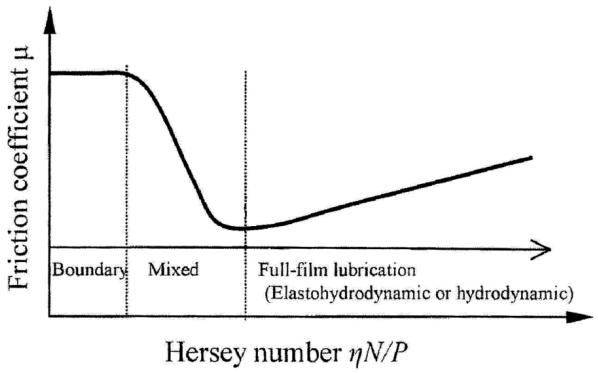

Figure A-11: Stribeck curve with the dimensionless lubrication parameter, the Hersey number, where η [Pa·s] is the dynamic viscosity, N [m/s] is the sliding speed, P [N] is the projected load. Picture from [24].

A-5-2 Hydrostatic bearing

If the purpose of bearings is considered it can be said that the main function of a bearing is to provide accurate movement between supported and supporting members. This movement is with low frictional resistance in the moving direction and good stiffness and damping in the supporting direction. In figure A-12 the basic working principle of a hydrostatic bearing is shown. First there is a constant pressure supply system which relies on a hydraulic pump that supplies the lubricants through a flow restrictor. Besides this, there also is a constant flow supply system which relies on a constant flow pump. In figure A-13 three structures are shown where hydrostatic bearings are based on, the journal bearing [51] which usually is combined with thrust bearings, and the linear guide way [57]. The advantage of a pressurized lubricant supply is that it can suppress lubricant heating and viscosity loss and it prevents contact between the brush and shaft of the bearing during starting and stopping [56].

There are different lubricant supply methods which will all influence the hydrostatic bearing static stiffness differently as seen in figure A-14. In practical use the constant flow supply system is not that common, because it requires expensive peripheral equipment [3]. Also for this system the load-carrying capacity and stiffness also change due to change of viscosity of the lubricant. For constant pressure systems the hydrostatic bearing stiffness strongly depends on the flow restrictor [5]. These bearings are designed for high stiffness and low energy consumption and this stiffness depends on the characteristics of the flow, the lubricant supply pressure, the geometry of the hydrostatic pad, compensator, and bearing clearance. By optimizing the flow restrictors according to the bearing clearance a high bearing stiffness can be obtained.

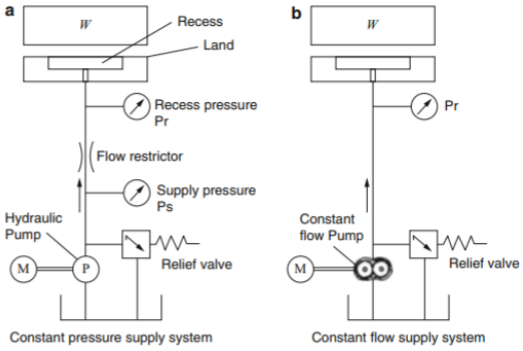

Figure A-12: Basic working principle of a hydrostatic bearing. In (a) a constant pressure supply system is shown and in (b) a constant flow supply system is shown. Picture from [3].

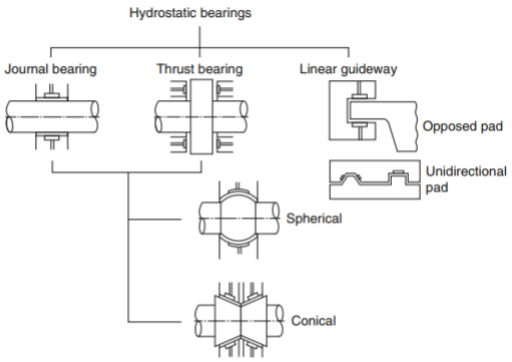

Figure A-13: Different structures of a hydrostatic bearing. Picture from [3].

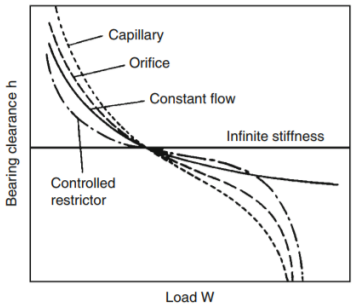

Figure A-14: The influence of different lubricant supply methods on the static stiffness of a hydrostatic bearing. Picture from [3].

A-5-3 Hydrodynamic bearing

Besides the hydrostatic bearing, there is the hydrodynamic bearing which does not require any supply pump for the lubricant. In the 19th century Beachamp Tower noticed leakage of the oil out of a hole located beneath the load. This hole was plugged with a cork, but oil could still go out. After replacing the cork with a wooden plug, this plug was still forced out by some pressure generated in the system [61]. The measurements Beachamp then did for the oil pressure gave experimental confirmation for hydrodynamic lubrication. He found that this could separate the sliding surfaces by a hydraulic force. Due to this Reynolds provided the first analytical proof that hydrodynamic pressure could separate the two sliding surfaces of a bearing. The friction coefficient of hydrodynamic bearings is very low, because the operating surfaces are fully separated by a lubricating film. Between the two moving surfaces a viscous liquid film is generated on the condition that the surfaces must move relatively to each other with sufficient velocity. Also the two moving surfaces have to be under an angle relatively to each other as seen in figure A-15, otherwise no pressure field will form to support the load [56]. Nevertheless it was found by Beauchamp that a bearing with two parallel surfaces with one of them having four radial grooves cut in it was able to carry loads [60].

Although hydrodynamic bearings do not require a supply pump, there are other disadvantages

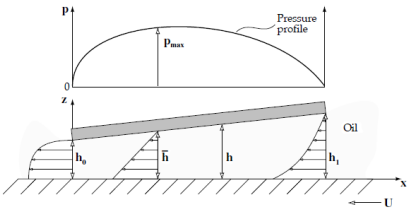

Figure A-15: Schematic illustraion of the pressure generation between two plates that are not parallel to each other. Picture from [56].

that are present and are as following:

- During starting and stopping, the bearing doesn't have any load capacity and this will cause the bearing surfaces to touch. Before load capacity is obtained, a non-zero sliding velocity is required.
- Because of the condition that it requires a non-zero sliding speed, damage during starting and stopping is inevitable.
- If the limits of the hydrodynamic lubrication are exceeded, for example by an excessive load or insufficient speed, the friction will rise and there is a possibility for bearing seizure.

A-6 Performance analysis

In this section the performance of lubricated bearings will be analyzed, different models can be used for this. The hydrodynamic lubrications will be analyzed with the use of the Reynolds equation. bearings will be discussed.

A-6-1 Hydrodynamic lubrication

In [56] the Reynolds equation is used to find most of the critical bearing design parameters such as the pressure distribution, load capacity, friction force and oil flow. This Reynolds equation is seen in equation A-16.

$$\frac{\partial}{\partial x}\left(\frac{h^3}{\eta}\frac{\partial p}{\partial x}\right)+\frac{\partial}{\partial y}\left(\frac{h^3}{\eta}\frac{\partial p}{\partial y}\right)=6\left(U\frac{\partial h}{\partial x}+V\frac{\partial h}{\partial y}\right)+12(w_h-w_0) \tag{A-16}$$

Equation A-16 is based on a column of lubricant as shown in figure A-16. Here q_x and q_y [m^3/s] are the rates at which the lubricant flows into the column horizontally and w_0 and w_h [m/s] are respectively the velocities at which the bottom and top of the column move up. In the Reynolds equation itself U and V [m/s] represent the surface velocities in x and y direction and h is a function that describes the specific film shape. This full equation is too complex for convenient use, that is why it has to be simplified. The approximations used in [56] to do this are:

1. **Undirectional velocity approximation**: here it is assumed that V is equal to zero, because there are not many cases that the journal bearing slides along a rotating shaft.
2. **Steady film thickness approximation**: here it is assumed there is no difference between w_h and w_0, which requires the distance between the surfaces to remain constant during operation.

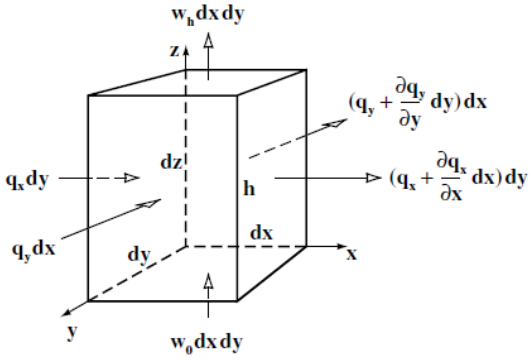

Figure A-16: Continuity of flow in a column. Picture from [56].

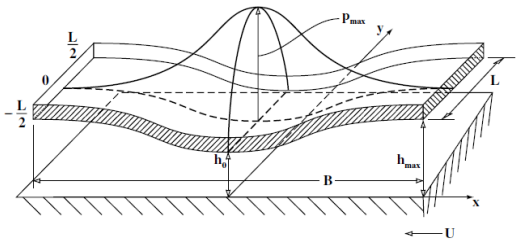

Figure A-17: Pressure distribution in the narrow bearing approximation. Picture from [56].

3. **Isoviscous approximation**: here it is assumed that the viscosity of the lubricant is constant over the film.
4. **Narrow bearing approximation** [13]: here it is assumed that the pressure gradient along the x axis is neglectable, because compared to the pressure gradient along the y axis it is very much smaller. This approximation was used in the analysis of load capacity in journal bearings [40]. So this means $\partial p/\partial x \ll \partial p/\partial y$, this all is represented in figure A-17.

Using all these approximations equation A-16 will come down to:

$$\frac{\partial}{\partial y}\left(h^3\frac{\partial p}{\partial y}\right) = 6U\eta\frac{\partial h}{\partial x} \tag{A-17}$$

Integrating this twice and using the boundary conditions zero pressure at the edge of the bearings and zero pressure gradient along the central plane of the bearing the pressure distribution is obtained in equation A-18.

$$p = \frac{3U\eta}{h^3}\frac{dh}{dx}\left(y^2 - \frac{L^2}{4}\right) \tag{A-18}$$

For the pressure distribution in terms of bearing geometry, lubricant viscosity and speed the Reynolds equation has to be integrated over the function $h = f(x, y)$. Furthermore different parameters can be found by integrating the pressure distribution, these are shown in table A-1.

For a hydrodynamic journal bearing the Reynolds equation can be obtained using an angular coordinate system as seen in equation A-19 [62]. Here the outflow in the sides is neglected and a purely circumferential flow is supposed, as well an infinitely long journal bearing is considered.

$$\frac{dp}{d\theta} = 6\eta R^2\omega\frac{h - h^*}{h^3} \tag{A-19}$$

Table A-1: Critical bearing design parameters obtained in [56].

Load Capacity	$W = \int_0^L \int_0^B p dx dy$
Friction force per unit length	$F = \int_0^L \int_0^B \tau dx dy \rightarrow \frac{F}{L} = \int_0^B \frac{h}{2}\frac{\partial p}{\partial x} dx - \int_0^B \frac{U\eta}{h} dx$
Coefficient of friction	$\mu = \frac{F}{W} = \frac{\int_0^L \int_0^B \tau dx dy}{\int_0^L \int_0^B p dx dy}$
Lubricant flow	$Q_x = \int_0^L q_x dy \quad \& \quad Q_y = \int_0^B q_y dx$

Here $dp/d\theta$ is there pressure gradient, R [m] is the radius, ω [rad/s] is the angular velocity, h [m] is the film thickness, and h^* [m] is the film thickness at the section where the fluid pressure and its gradient is zero.

Appendix B

Technologies and experiments

In this chapter the focus is mainly on information found in literature regarding bearings using magnetic fluids. For this both ferrofluids and MR fluids are considered in order to find the differences in performance. Doing this it can be found what already has been done and where improvement is required.

B-1 Center bearing assembly

In the application in [18] the MR fluid is not used as a bearing itself, but here it used for vibration dampening characteristics. The support member includes a bladder formed of an elastomeric material which contains an MR fluid as seen in figure B-1 and B-2. By varying the power a field will be created around the bladder, the viscosity of the MR fluid can be varied what will cause a change in vibration dampening characteristics.

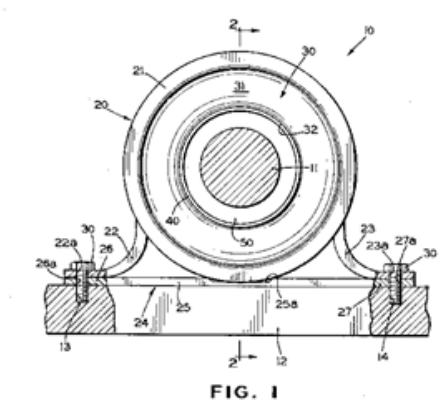

Figure B-1: The center bearing assembly including a support member (31) containing a rheological fluid. Picture from [18].

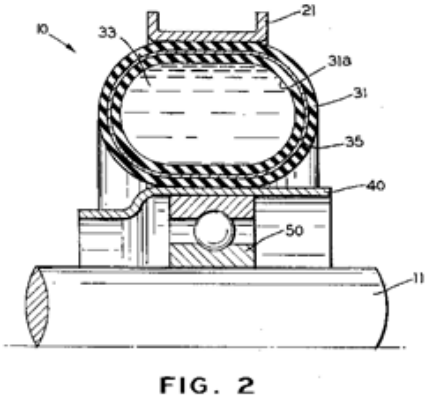

Figure B-2: A cross section of the center bearing assembly, where the support structure (31) containing the rheological fluid (33) is seen on top of the roller bearing. Picture from [18].

B-2 Magnetic fluid-based magnetorheological fluids

Normally in an MR fluid only the suspended particles are magnetic, and the carrier fluid is non-magnetic. In [22] an MR fluid is proposed where not only the suspended particles are magnetic, but where also the carrier fluid has magnetic properties because for this a ferrofluid is used. Due to the use of a ferrofluid as carrier fluid, the force between the magnetizable particles is enhanced. This causes the stiffness and viscosity of MR fluid to increase as shown

in figure B-3. By using this ferrofluid-based MR fluid in certain applications like clutches or dampers, the size of them can be reduced without reducing the generated forces.

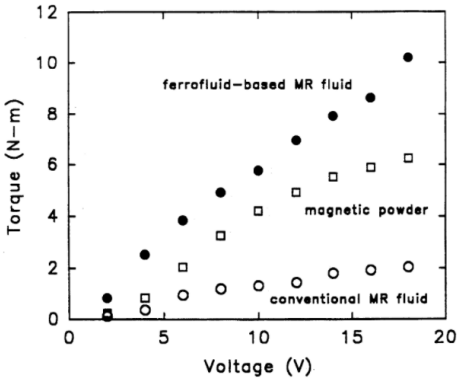

Figure B-3: Operational differences between a conventional MR fluid with a non-magnetic carrier fluid, and the ferrofluid-based MR fluid. Picture from [22].

B-3 Planar ferrofluid bearings

In [37, 36, 34, 11] planar ferrofluid bearings are demonstrated. Here a ferrofluid seal is used to encapsulate a pocket of air to carry a limited load. The bearings have low viscous friction and stick-slip is absent. Compared to traditional bearings a ferrofluid bearing is a passive, simple, and cost effective alternative. This is because no seals or active components are required, the fluid in the bearings in contained by a magnetic field that is generated by permanent magnets.

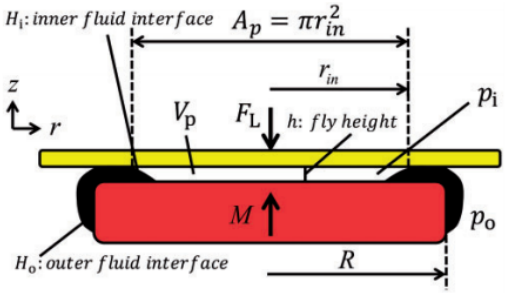

Figure B-4: The cross section of a disc-shaped magnet to define the parameters used in [36]

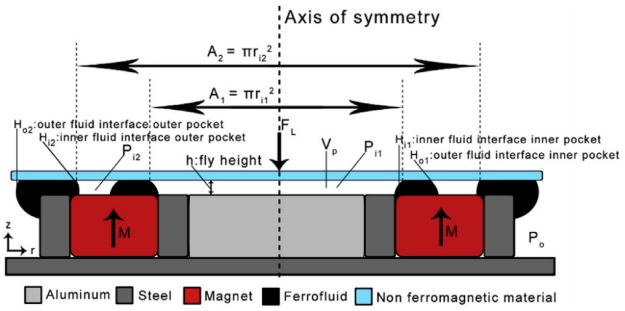

Figure B-5: The cross section of the ferrofluid bearing with the defined parameters in [11].

B-4 Journal ferrofluid bearings

In [33, 15, 49, 50] journal bearings lubricated with a ferrofluid are presented. It is observed that the bearing systems have an improved performance due to the magnetic fluid as compared to a conventional lubricant. By the application of a magnetic field the load carrying capacity of the bearings is increased, and with it the magnetic lubrication has negligible effect on the frictional force. But far from the conditions designed for, an insignificant effect is obtained for the magnetic lubrication.

B-5 Thrust bearing using a magnetic fluid lubricant under magnetic fields

In [43] a thrust bearing is presented which is using a magnetic fluid as a lubricant in combination with a constant magnetic field. The main focus in this work is the investigation of the critical pressure of the bearing using this magnetic fluid. It is shown that this bearing has advantages over normal thrust bearings that use normal oil lubrication. Due to the magnetic field the viscosity increases, the critical pressure increases compared to normal thrust bearings. This bearing can be used without a supply of fluid because along the circumferential side of the shaft a magnetic seal is created by the applied magnetic field.

B-6 Hydrodynamic bearing lubricated with magnetic fluids

In [62] a test bench (figure B-6) has been made to demonstrate that magnetic fluids can be used to develop active journal bearings. This is done because lubricated bearings main advantages are their low friction and very high precision, compared to rolling and friction bearings. A disadvantage of these lubricated bearings is the working velocity range as discussed before. From the results it is concluded that ferrofluids cannot be used for this purpose because the change in rheology and its effect in the bearing are not sufficient. Besides for the ferrofluid, also tests were done with an MR fluid where a stainless steel shaft and a carbon steel shaft is used. The results for the stainless steel shaft show that only at low speed and a lower eccentricity the magnetic effect was detectable. The results for the carbon steel shaft are more promising and show a high increase in bearing load capacity as shown in figure B-7.

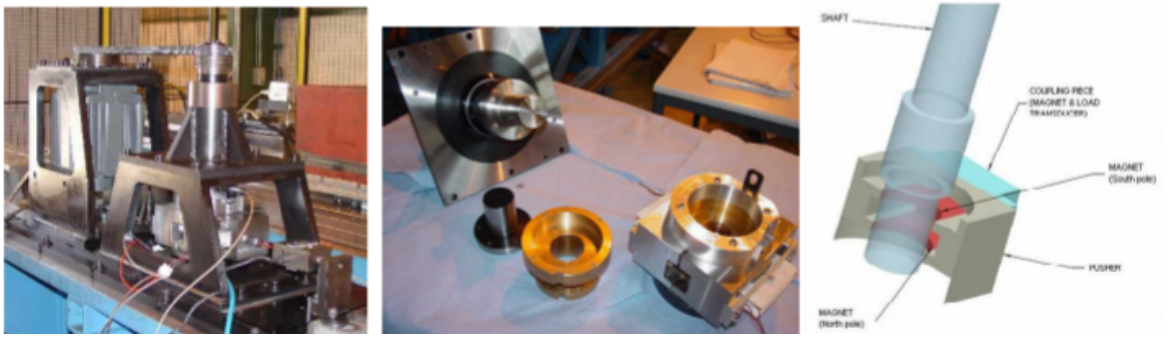

Figure B-6: From left to right the test bench, bearing with two shafts and magnetic pole view are shown. Picture from [62].

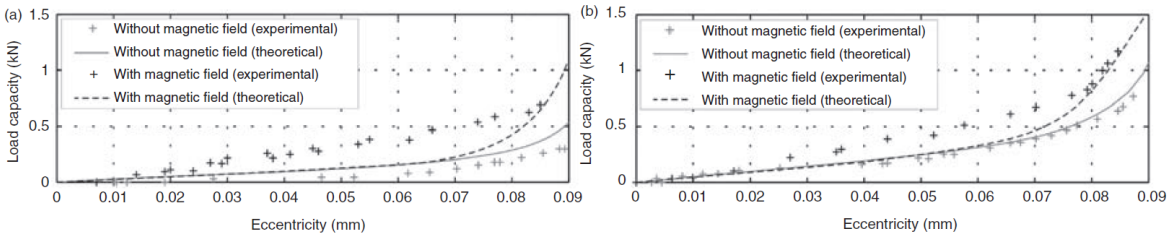

Figure B-7: The load capacity of the journal bearing with the carbon steel shaft which is lubricated with an MR fluid, in (a) the angular velocity is 50 rev/min and in (b) it is 200 rev/min. Picture from [62].

B-7 Active hydrostatic bearing with magnetorheological fluid

In [25] a new concept of hydrostatic bearings seen in figure B-8 is presented which makes use of an MR fluid. This is done because the disadvantage of hydrostatic bearings is the change in gap size with increasing payload. By using a MF fluid a constant gap size for alternating payloads can be achieved due to the fact that when MR fluids are exposed to the change of an external magnetic field the rheological properties change. The response time for this application will be short because there is no use for valves which were used for a change of the flow rate to compensate for the alternating payload. In figure B-9 the change in gap size h is shown for increasing current, and thus magnetic field. In figure B-10 the change in gap size h is shown for increasing payload. Combining these two it can be concluded that by changing the magnetic field, the same gap size can be achieved for different payloads and thus the gap size can be kept constant.

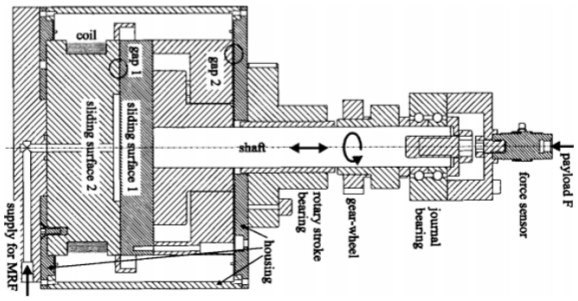

Figure B-8: The thrust bearing with MR fluid used used as a test setup. Picture taken from [25].

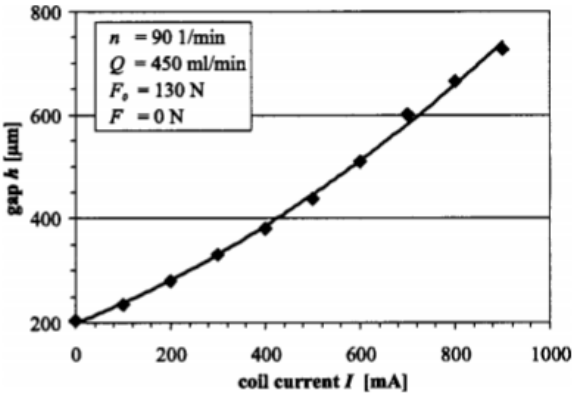

Figure B-9: Here the change of the bearing gap h with increasing coil current is shown. The load on the bearing was due to the self-weight of the bearing F_0 and no additional load F is present. Picture from [25].

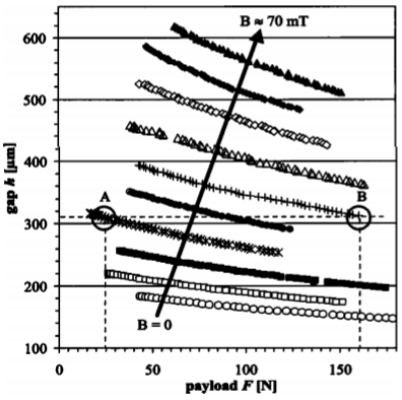

Figure B-10: Here the change of the bearing gap h is shown with increasing load F for different magnetic fields. Picture from [25].

B-8 Virtual Textured Bearing

In the work of [35] a bearing is proposed where the resistance is increased locally using a local variation of the viscosity of the lubricant. This can be realized with for example an

MR fluid or an electrorheological fluid. Here the local resistance over the whole bearing gap is obtained due to a constant magnetic field. The bearing presented is a combination of a hydrostatic and hydrodynamic bearing, and thus has a larger working regime. At low speeds it uses hydrostatic lubrication, and then at high speeds it naturally switches to hydrodynamic lubrication.

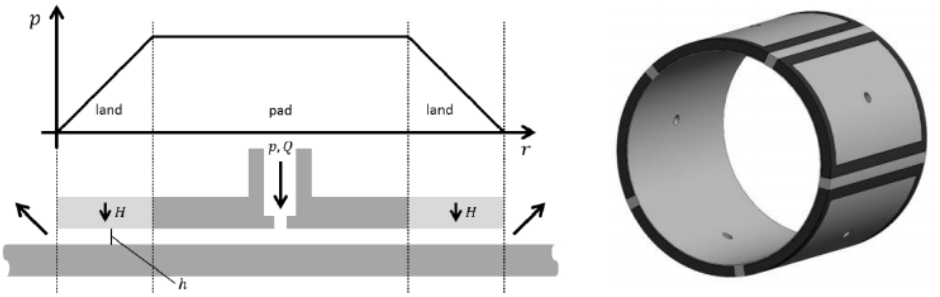

Figure B-11: The virtual textured hydrostatic bearing where a magnetic field and an MR fluid is used to increase the resistance locally. This can be implemented in a journal bearing, where in the dark zones a magnetic field is present in order to increase the resistance. Picture from [35].

B-9 Dynamic Characteristics of Magnetorheological Fluid Film Journal Bearing

In [10] results are shown of the experiments done with a constructed MR fluid film bearing. This bearing is capable of altering the rheological properties of the MR fluid using two lateral coils supplied with a direct current. The purpose of the experiments is to evaluate the dynamic properties of this bearing both in its active and its inactive state. The experimental setup consisted of a Bently Nevada Rk-4 rotorkit and an MR fluid bearing. The results in the paper show that the use of an MR fluid do enhance the dynamic characteristics of a journal bearing. Due to the use of an MR fluid influences the dynamic properties, the orbit of the shaft is reduced by 75% in both axes of motion and the amplitude of the journal motion is decreased by 45% within an overall time of 1.2 seconds.

B-10 Thrustbearing using an MR fluid

In [2] a porous slider bearing using a wedge, lubricated with a magnetic fluid, is discussed. Here a constant externally applied magnetic field is present. It is shown that the load capacity of the bearing is found to be greater than the configuration using a conventional lubricant seen in [52]. The research in [6] elaborated on [2] considering a slider consisting of an inclined pad and a flat pad. It was seen that the magnetic fluid increases the load capacity, and does not alter the friction.

B-11 Conclusion

It is seen that magnetic fluids have the potential to improve the performance of fluid bearings. A planar ferrofluid bearing is a passive, simple, and cost effective alternative, but the load is limited and trail formation is influencing the performance. The performance of journal bearings lubricated with a ferrofluid is modified significantly, like increase in stiffness and load capacity, but only for certain conditions. Far from these conditions, an insignificant

effect is obtained for the magnetic lubrication. It is seen that the rheological change of the ferrofluid is negligible for the purpose of a tunable lubricant. In contrary to an MR fluid which has good potential to be used as an tunable lubricant, and it is shown that the availability of control over the dynamic properties of a bearing can be enhanced. MR fluids improve the load capacity, stiffness, critical pressure, and can be used to maintain a constant bearing gap for different payloads. What the former concepts discussed all have in common is that the applied magnetic field is constant and/or applied globally and not locally. They all improve the performance to a certain extent, but do not discuss the wear which is generally caused by poor lubrications during high loading conditions or low speeds.

Appendix C

Schedule

The schedule as seen in figure C-1 will be discussed, this schedule will be followed to complete the research. The schedule is subdivided into different tasks with their own deliverables. The tasks are modeling, fabricating, measurement, optimization and finalizing the thesis. For every tasks some time is reserved and these tasks will be shortly explained here.

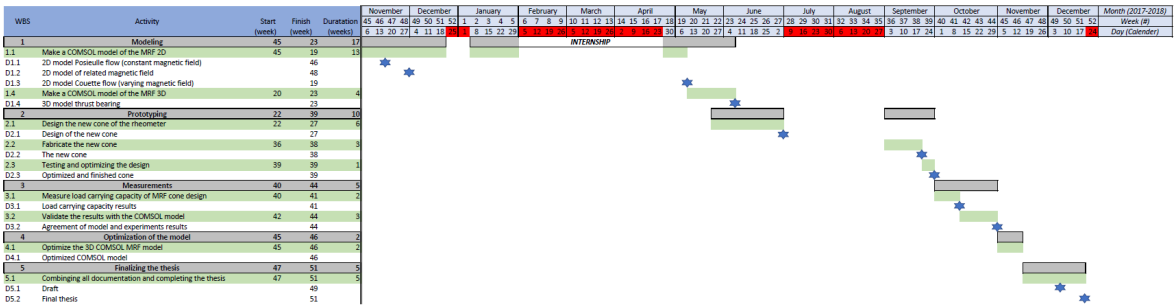

Figure C-1: Schedule used during the research on an MR fluid used in a bearing.

C-1 Modeling

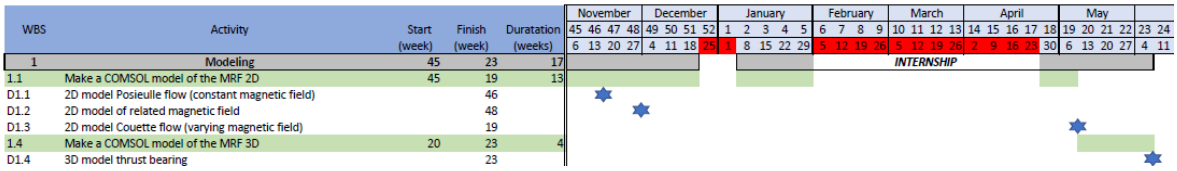

Figure C-2: Schedule used for the modeling.

In figure C-2 the schedule is seen for the modeling of the MR fluid in COMSOL. At first several 2D models will be made which include the model for the Posieulle flow, magnetic field and the Couette flow. For the Posieulle flow a constant magnetic field will be applied, which means a constant yield stress of the MR fluid. After this a magnetic field will be created in COMSOL which decreases across the height of the gap wherein the MR fluid is trapped. This varying magnetic field will be used in and related to the 2D model of the Couette flow. When the 2D models are finished, the 3D model which will represent the thrust bearing can be made. Here the MR fluid acts as lubrication and is also used to create local surface texturing. Seen in the schedule are parts indicated with red, in January this represents the Christmas break and the 3 months after that represent my internship at Van Oord.

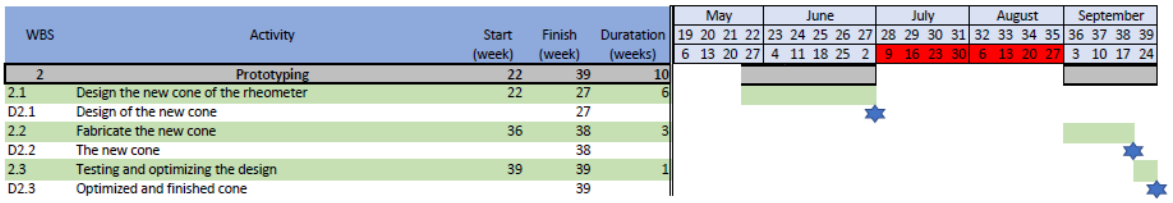

WBS	Activity	Start (week)	Finish (week)	Duratation (weeks)
2	Prototyping	22	39	10
2.1	Design the new cone of the rheometer	22	27	6
D2.1	Design of the new cone		27	
2.2	Fabricate the new cone	36	38	3
D2.2	The new cone		38	
2.3	Testing and optimizing the design	39	39	1
D2.3	Optimized and finished cone		39	

Figure C-3: Schedule used for the prototyping.

C-2 Prototyping

In figure C-3 the schedule is seen for the prototyping of the new cone which can be used in the rheometer. This cone is made in such a way that surface texturing is created using a specific magnetic field and the MR fluid. The design of the new cone starts during the time the 3D COMSOL model is made of the MR fluid. This is done because then these designs can be adjusted to each other to make them agree. The design of the cone is limited by the dimensions and other specifications of the rheometer, and this of course has to be taken into consideration. When the design is finished, the cone can be fabricated which will be done after the summer break indicated with red. In the end this new cone will be tested and optimized if required.

C-3 Measurements

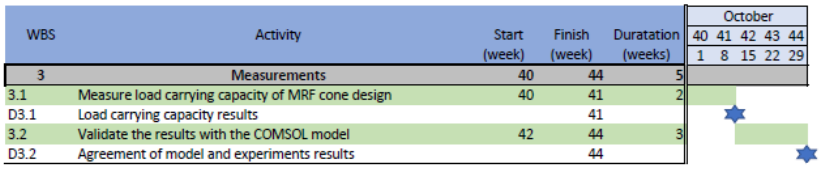

WBS	Activity	Start (week)	Finish (week)	Duratation (weeks)
3	Measurements	40	44	5
3.1	Measure load carrying capacity of MRF cone design	40	41	2
D3.1	Load carrying capacity results		41	
3.2	Validate the results with the COMSOL model	42	44	3
D3.2	Agreement of model and experiments results		44	

Figure C-4: Schedule used for the measurements.

In figure C-4 the schedule is seen for doing the measurements related to the fabricated new cone. This cone will be used in a rheometer which can measure the torque, rotating speed, and most importantly the load capacity. These experimental results can be compared to the results that come from the COMSOL model. This way it can be seen if the model is in agreement with the reality and can be used as a representative model which can be used for future designs.

C-4 Optimization of the model

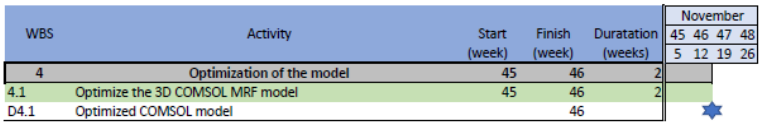

WBS	Activity	Start (week)	Finish (week)	Duratation (weeks)
4	Optimization of the model	45	46	2
4.1	Optimize the 3D COMSOL MRF model	45	46	2
D4.1	Optimized COMSOL model		46	

Figure C-5: Schedule used for the optimization of the model.

In figure C-5 the schedule is seen for the optimization of the 3D COMSOL model. If the experiments are in agreement with the results that come from the model and the model is

representative, it could be beneficial to optimize the model. This way the model can be more efficient and easier to work with for future work.

C-5 Finalizing the thesis

WBS	Activity	Start (week)	Finish (week)	Duratation (weeks)
5	Finalizing the thesis	47	51	5
5.1	Combinging all documentation and completing the thesis	47	51	5
D5.1	Draft		49	
D5.2	Final thesis		51	

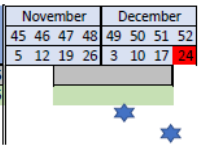

Figure C-6: Schedule used for the finalizing the thesis.

In figure C-6 the schedule is seen for finalizing the thesis. This is purely combining all documentation and writing the thesis. During all the other tasks documentation will be done also, but this of course have to be gathered and combined properly. It is planned to write a paper about the 2D models in this research, where also is proven that the concept of MR fluid bearings are a reality. Then an other paper is written about the 3D model based on the 2D models, combined with the experiments and results.

Appendix D

Flow mode with constant a magnetic field

In figure D-1 the shear stress and velocity profile in flow mode for both a Newtonian fluid and MR fluid are shown. The flow is caused by a difference in pressure at inlet and outlet. This flow mode is also referred to as Poiseuille flow. As seen in the figure, the velocity profile is hyperbolic for the Newtonian fluid but for the MR fluid it can be divided into three regions. The blue colored regions in figure D-1 represent the post-yield regions and the middle region represents the pre-yield region. The post-yield regions are near the walls of the channel, here the shear stress exceeds the yield stress ($|\tau| > \tau_y$) which causes the MR fluid to flow. In contrary, there is the pre-yield region at the center of the channel. Here the shear stress does not exceed the yield stress ($|\tau| \leq \tau_y$) and the MR fluid is in solid phase. In this region the velocity is constant and is also referred to as plug flow.

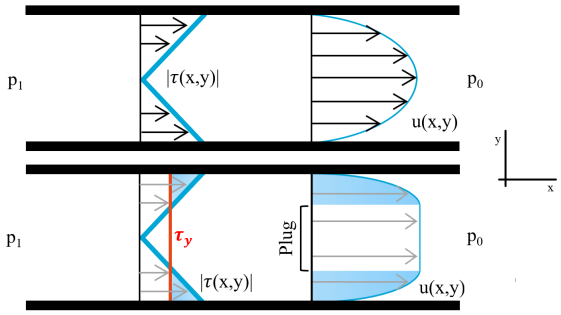

Figure D-1: Flow mode for a Newtonian fluid (top) and an MR fluid (bottom) between two fixed parallel surfaces. Here $p_1 > p_0$ which causes the fluid to flow.

Appendix E

Numerical simumlation

Here the different numerical simulations will be discussed required for the research done. At first the 2D numerical simulations will be discussed regarding the flow mode, shear mode, magnetic configuration, and step bearing configuration. Followed by the 3D numerical simulation regarding perfect mixture and complete sedimentation of the MR fluid.

E-1 Flow mode with a constant magnetic field

This simulation is based on the research in [16] and is used to validate that the Bingham-Papanastasiou model is implemented correctly in COMSOL Multiphysics. The Bingham-Papanastasiou model is implemented by adding a blank material to the study which has an apparent viscosity represented with the analytic function as seen in figure E-1.

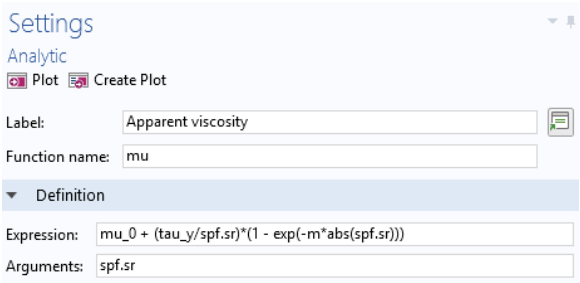

Figure E-1: Analytic function for the apparent viscosity implemented in COMSOL.

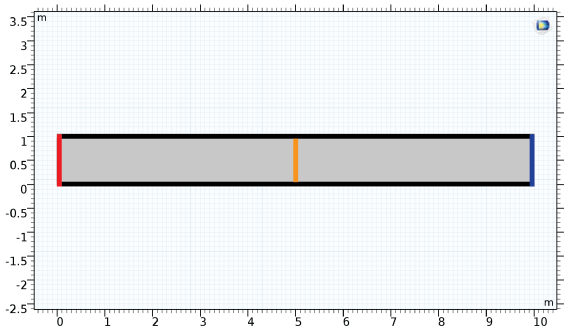

Figure E-2: Different boundary conditions applied to channel, and results taken along the orange line in the model.

Here mu_0 is the viscosity for no applied magnetic field of the MR fluid, tau_y is the constant yield applied to the fluid, and $spf.sr$ is the shear rate given by COMSOL. For the Poiseuille flow this shear rate is the only variable in the function, and the viscosity and yield stress will be known in advance. The normalized parameters used in this model are seen in table E-1. During the study a parametric sweep will be done for the yield stress, representing an increasing magnetic field.

The study that is chosen is the 'Creeping Flow (spf)', and a $P2 + P1$ discretization of fluids for the fluid flow. Different boundary conditions are applied to the system and are indicated in figure E-2. Indicated with red is the inlet where a pressure is applied, indicated with blue is the outlet where no pressure is applied, and a no slip boundary condition is applied to the walls indicated with black. The results for the velocity profile, stress, apparent viscosity, and

Table E-1: Normalized parameters from [16] used for simulating the MR fluid in flow mode

Parameters	
Channel (l x h) $[L_{norm} \cdot h]$	10 x 1
Regularization parameter $[m_{norm} \cdot h]$	1250
Viscosity $[\eta_{norm}]$	0.28
Pressure drop $[\Delta p_{norm} \cdot (1/h)]$	60
Yield stress $[\tau_{y,norm} \cdot (1/h)]$	0, 1,2, $\frac{13}{5}$, 3

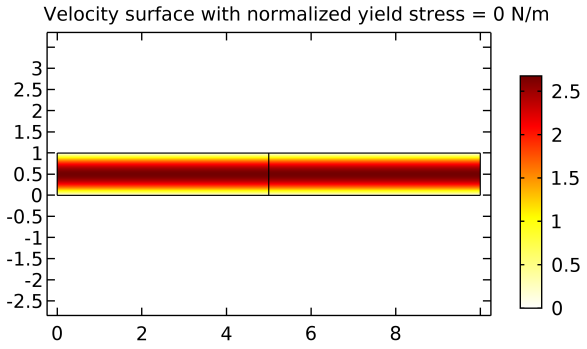

Figure E-3: Velocity surface for the Poiseuille flow where the normalized yield stress is $\tau_y = 0$ N/m.

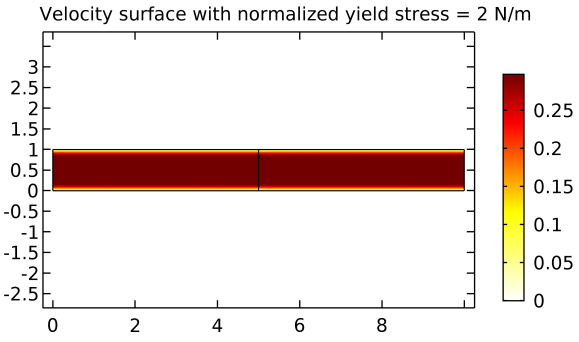

Figure E-4: Velocity surface for the Poiseuille flow where the normalized yield stress is $\tau_y = 2$ N/m.

shear rate are plotted along the orange line. Furthermore an extremely fine physics-controlled mesh is applied.

To visually check if the Bingham-Papanastasiou model is implemented correctly the velocity surface is plotted as seen in figure E-3 and E-4. For no applied yield stress no plug should be observed, only for a value greater than 0 for the yield stress should result in a plug. In figure E-3 no yield stress is applied and no plug is observed. In figure E-4 a yield stress is applied and here in the middle of the channel a constant velocity is observed indicating a plug flow.

E-2 Shear mode with a varying magnetic field

For these numerical simulations the study 'Creeping Flow (spf)' is used, and a $P2 + P1$ discretization of fluids for the fluid flow. The mesh applied is an extra fine physics-controlled mesh. The boundary conditions for the shear mode are indicated in figure E-5. Indicated with red is the inlet and indicated with blue is the outlet where for both no pressure is applied and normal flow is assumed. Indicated with black is the wall with a no slip condition, and indicated with green is a wall with a no slip condition and a certain velocity u_x representing the moving wall. The results for the velocity profile, stress, apparent viscosity, and shear rate are plotted along the orange line.

The shear mode is simulated for different velocities where the same analytical function as in E-1 is implemented. By applying a constant yield stress, and so a constant magnetic field, not the desired behavior is obtained. An analytical function for the apparent viscosity as in figure

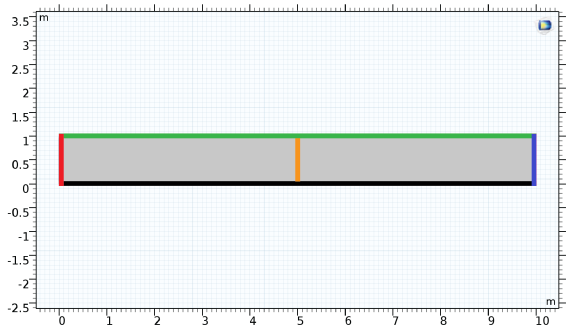

Figure E-5: Different boundary conditions for the flow mode applied to channel, and results taken along the orange line in the model.

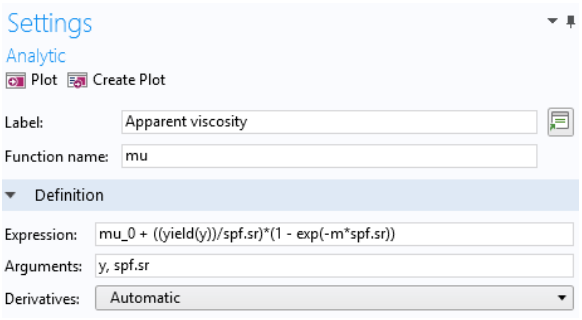

Figure E-6: Analytic function for the apparent viscosity implemented in COMSOL for the couette flow.

E-6 is implemented. Here the yield stress varies across the height of the channel and cannot be seen as a constant anymore and that is why the apparent viscosity now also depends on the height. For the normalized yield stress a linear decrease from 1 to 0 over the height of the channel is used. The normalized parameters used in this model are seen in table E-2.

Table E-2: Normalized parameters used for simulating an MR fluid in shear mode.

Parameters	
Channel (l x h) $[L_{norm} \cdot h]$	10 x 1
Regularization parameter $[m_{norm} \cdot h]$	10^4
Viscosity $[\eta_{norm}]$	1
Yield stress bottom $[\tau_{y,norm} \cdot (1/h)]$	1
Yield stress top $[\tau_{y,norm} \cdot (1/h)]$	1
Surface velocity $[u_{norm}]$	$\frac{1}{100}$, $\frac{3}{20}$, $\frac{3}{10}$, $\frac{3}{4}$, 2

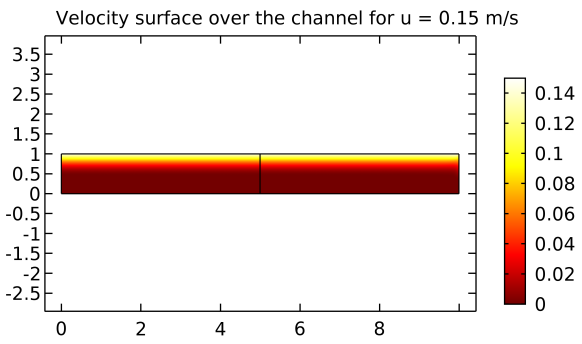

Figure E-7: Velocity surface for the shear mode where $u = 0.15$ m/s, the velocity of the wall.

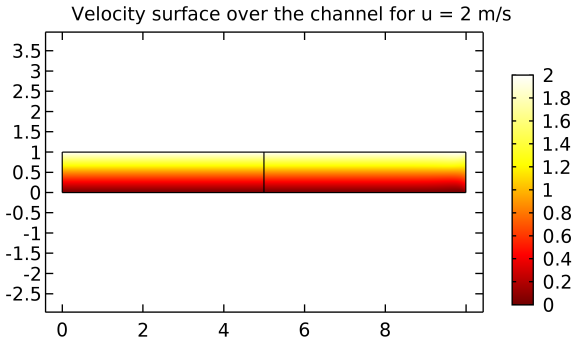

Figure E-8: Velocity surface for the shear mode where $u = 2$ m/s, the velocity of the wall.

To visually check if the Bingham-Papanastasiou model is implemented correctly the velocity

surface is plotted as seen in figure E-7 and E-8. Here the varying yield stress is applied over the whole length of the channel. Seen in figure E-7 is that at lower speeds a solid part now is created at the bottom of the channel, and when the velocity becomes significantly larger as seen in figure E-8 this solid part disappears because the yield stress in the fluid is overcome by the shear stress.

E-3 Magnetic configuration

For the magnetic configuration the Halbach array and a self created array are considered. The study 'Magnetic Fields, No Currents (mfnc)' is used in this model. A Halbach array is a special arrangement of permanent magnets as seen in figure E-10 that augments the magnetic field on one side of the array while cancelling the field to near zero on the other side. The self created array is an arrangement of permanent magnets and iron blocks which creates a high gradient in magnetic field.

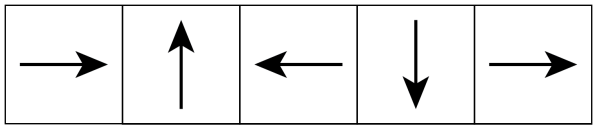

Figure E-9: Direction of the magnetic flux in each magnet used in the Halbach array.

Both the Halbach array and self created array are simulated in an environment representing a bearing as shown in figure E-10 and figure E-11. The different layers are indicated with the different colors.

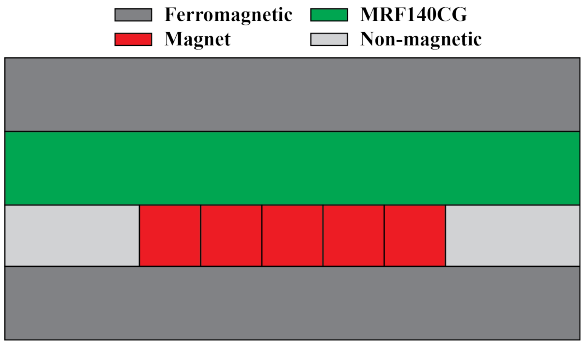

Figure E-10: The Halbach array in an environment representing a bearing.

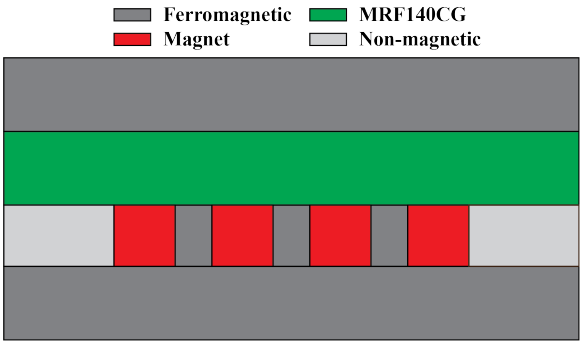

Figure E-11: The self created array in an environment representing a bearing.

To the corners of the magnets a small fillet is applied to obtain a better mesh around the corners (Fig. E-12), this is also done for the self created array seen in figure E-13. The mesh used for the magnetic studies is a finer physics-controlled mesh, and a cubic discretization for the magnetic scalar potential. Here the outer boundaries will be magnetically insulated and to one corner of this environment a zero magnetic scalar potential is applied. The direction of the magnetic flux inside each magnet of the self created array is in the positive y-direction. To obtain the magnetic field strength in the MR fluid, which can be used to calculate the yield stress in the MR fluid, the B-H curve and the relation between the magnetic field strength and yield stress is required. The relations used to calculate all this can be found in the datasheet of MRF140CG seen in appendix I. The normalized parameters used are seen in table E-3.

Using these parameters the magnetic field seen in figure E-14 and E-15 are obtained. The self created array is used in further research.

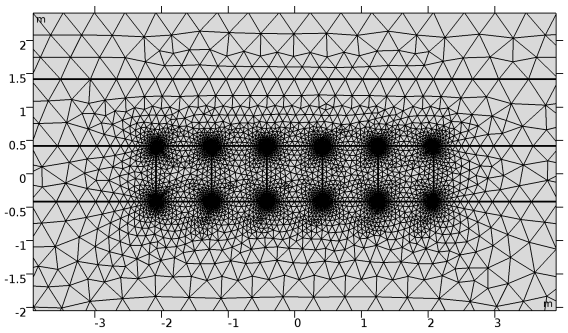

Figure E-12: Refinement of the mesh for the Halbach array around the corners of the magnets due to a fillet.

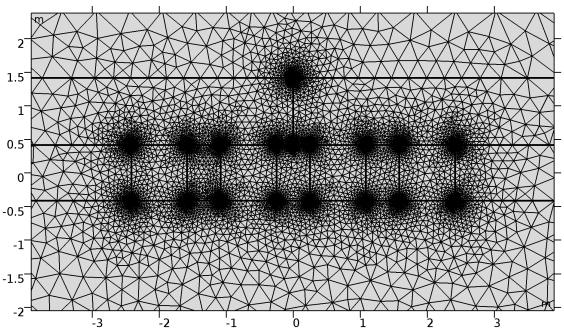

Figure E-13: Refinement of the mesh for the self created array around the corners of the magnets due to a fillet.

Table E-3: Normalized parameters used for simulating magnetic configurations.

Parameters	
Channel (l x h) $[L_{norm} \cdot h]$	15 x 1
Ferromagnetic layer (l x h) $[L_{norm} \cdot h]$	15 x 1
Magnets (l x h) $[L_{norm} \cdot h]$	$\frac{5}{6}$ x $\frac{5}{6}$
Ferromagnetic blocks (l x h) $[L_{norm} \cdot h]$	$\frac{1}{2}$ x $\frac{5}{6}$
Flux density	1 [T]

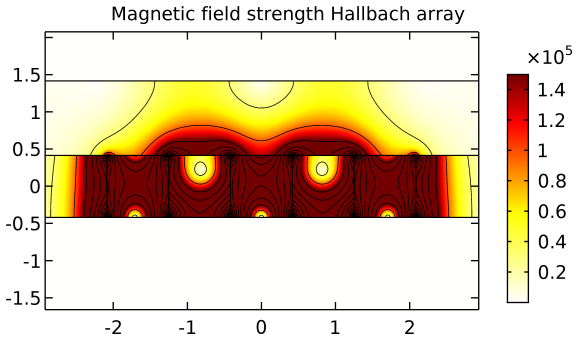

Figure E-14: Magnetic field strength using the Halbach array in an environment representing a bearing.

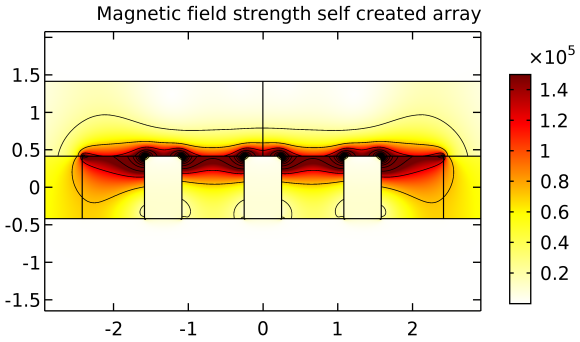

Figure E-15: Magnetic field strength using the self created array in an environment representing a bearing.

E-4 Step bearing configuration

It is wanted to create a step in the channel. For this the magnetic field must not act over the whole length of the channel as in section E-2, but only a certain part of it. To implement this the self created magnetic array in section E-3 is used. For this model the studies 'Magnetic Field, No Currents (mfnc)' and 'Creeping Flow (spf)' are combined. In the first study the magnetic field is simulated for the whole domain seen in figure E-11. Given every part has its own magnetic properties, the magnetic field is formed. After simulating the magnetic field, the fluid flow of the MR fluid is simulated in study 2 using the results obtained in study 1 as seen in figure E-16. This is done only for the domain where the MR fluid is present. Because the viscosity is depending on the local magnetic field, the results from the study regarding the magnetic field over the film height are obtained beforehand. The apparent viscosity shown in figure E-17 is implemented in the model. Here $mfnc.normH$ is the magnetic field strength obtained in study 1 and $spf.sr$ is the shear rate that will be obtained in study 2.

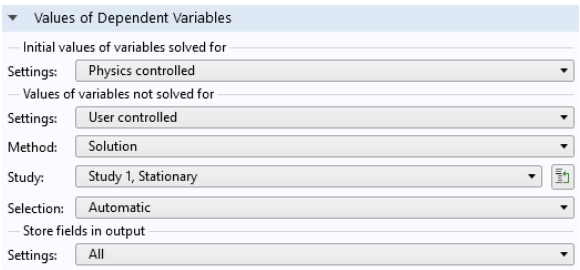

Figure E-16: Settings for the second study where the results from the first study regarding the magnetic field are known.

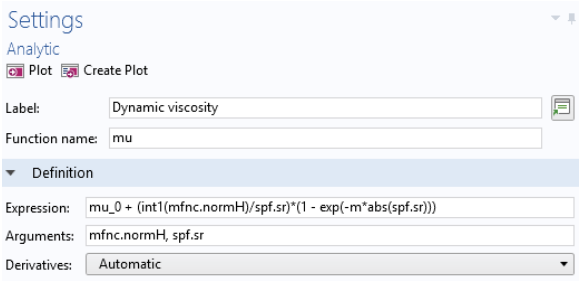

Figure E-17: Analytic function for the apparent viscosity implemented in COMSOL for the couette flow where a step is created.

For this study an extremely fine physics-controlled mesh is used, with a cubic magnetic scalar potential discretization for the magnetic field and a $P2 + P1$ discretization of fluids for the fluid flow. The boundary conditions for the magnetic domain are the same as in section E-3 and for the fluid domain the same as in section E-2. The normalized parameters used are seen in table E-4.

Table E-4: Normalized parameters used for simulating the MR fluid MRF140CG

Parameters	
Channel (l x h) $[L_{norm} \cdot h]$	15 x 1
Ferromagnetic layer (l x h) $[L_{norm} \cdot h]$	15 x 1
Magnets (l x h) $[L_{norm} \cdot h]$	$\frac{5}{6}$ x $\frac{5}{6}$
Ferromagnetic blocks (l x h) $[L_{norm} \cdot h]$	$\frac{1}{2}$ x $\frac{5}{6}$
Flux density $[B_{norm} \cdot (1/h)]$	10^{-5}
Regularization parameter $[m_{norm} \cdot h]$	10^{4}
Viscosity $[\eta_{norm}]$	1
Surface velocity $[u_{norm}]$	$\frac{1}{100}$, $\frac{3}{20}$, $\frac{3}{10}$, $\frac{3}{4}$, 2

To visually check if the Bingham-Papanastasiou model is implemented correctly the velocity

surface is plotted as seen in figure E-18 and E-19, here the magnetic field is applied over a certain length of the channel. In figure E-18 it seen that for a lower velocity a solid part, representing a step, is created in the middle of the channel. This solid part again disappears for a significantly higher value of the velocity as seen in figure E-19.

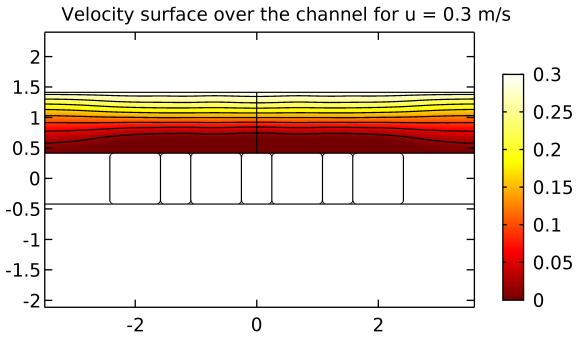

Figure E-18: Velocity surface for the couette flow where $u = 0.3$ m/s, the velocity of the wall. Here the magnetic field applied is obtained by the self created array.

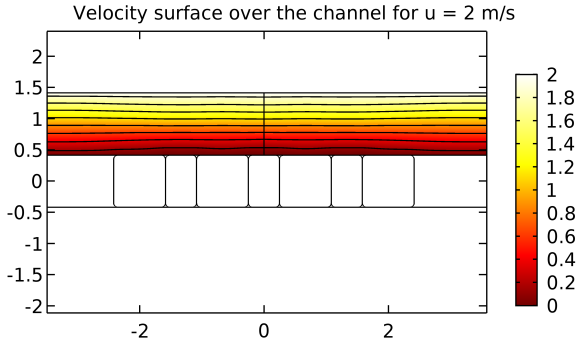

Figure E-19: Velocity surface for the couette flow where $u = 2$ m/s, the velocity of the wall. Here the magnetic field applied is obtained by the self created array.

E-5 Perfectly mixed MR fluid

This numerical simulation is a 3D model regarding perfect mixture of magnetic particles and carrier fluid. For this the studies 'Magnetic Field, No Currents (mfnc)' and 'Creeping Flow (spf)' are combined. Furthermore a cubic magnetic scalar potential discretization for the magnetic field and a $P2 + P1$ discretization of fluids for the fluid flow is used. The bearing is build up as in figure E-20, which is a 2D section as seen in figure E-21. In reality all the layers have a larger diameter than the MR fluid film, which is surrounded by air. All the parameters used in this model are seen in table E-5.

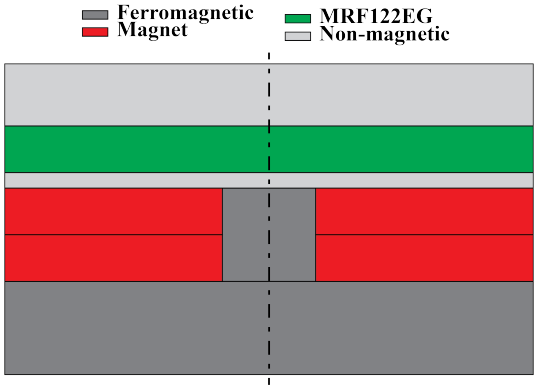

Figure E-20: 2D section at location A-A in figure E-21 of the geometry used in the numerical simulation for perfect mixture.

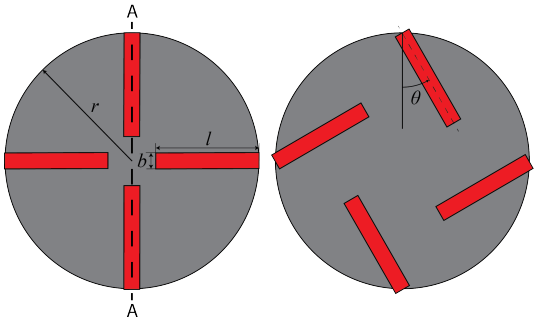

Figure E-21: Configuration of the magnets used in the numerical simulations and proof of concepts.

At first only the magnetic field will be simulated considering the whole domain. The bearing is simulated in a sphere of air of which its boundaries are magnetically insulated and the

Table E-5: Parameters used for simulating the perfectly mixed MR fluid.

Parameters	
Outer diameter bearing	30 [mm]
Ferromagnetic layer thickness	2 [mm]
Magnet (l x b x h)	7.5x1.1x1 [mm]
Flux density inside the magnet	1.28 [T]
Separation layer thickness	0.15 [mm]
MR fluid film height	0.2 [mm]
MR fluid film diameter	20 [mm]
Air surrounding MR fluid thickness	0.2 [mm]
Top layer thickness	2.2 [mm]
Viscosity MRF122EG	0.086 [Pa·s]
Regularization parameter	1
θ	0, 30, and 36 [degree]

to the top half a zero magnetic scalar potential is applied. Given every part has its own magnetic properties, a certain magnetic field will be formed over the model representing a bearing. Now this is done, the flow of the MR fluid can be simulated. This is done only for the domain where the MR fluid is present. For the boundary conditions for the fluid film an open boundary, no slip condition to the top and bottom surface, and a velocity given in polar coordinates applied to the top surface is considered. Because in the study for fluid flow the viscosity is depending on the local magnetic field, the results from the previous study regarding the magnetic field over the film height are now considered as known. The expression for the apparent viscosity implemented is the as seen in figure E-17 which was used for the step bearing configuration in section E-4.

The mesh used for the simulation has to be a trade-off between magnetics and fluid flow. For a magnetic study it is sufficient to have a high discretization and a normal mesh, but for a fluid flow it is desired to have have a dense mesh and many layers in the fluid film. Therefore a user-controlled mesh is applied. The sphere that represents the air surrounding the bearing has a extremely coarse free tetrahedral mesh. The bearing it self, excluding the fluid film, has an extra fine tetrahedral mesh. This is because it is adjacent to the fluid film. The fluid film itself has a free triangular mesh with a maximum element size of 1.87E-4 m and a minimum element size of 2.88E-6 m which is swept through the film resulting in a total of 10 layers.

In figure E-22 and B-2 the magnetic field strength over the length and width of the magnets is seen. Here it is seen that magnetic field strength decreases over the height of the fluid film, but does not reach 0 at the top. Also seen is that the magnetic field over the width of the magnet is different, and that is also why the magnetic and fluid study had to be combined for the 3D model.

In figure E-24 the different pressure distributions on the top bearing face obtained are seen. For obtaining the load capacity a surface integration for the pressure is done over this surface. For this a vapor pressure has to be implemented, otherwise no load capacity will be obtained for $\theta = 0$ because here the pressure distribution is antisymmetric. This vapor pressure will

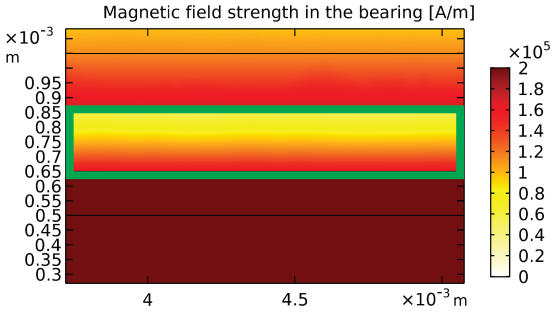

Figure E-22: Magnetic field strength over the length of the magnets. Here green indicates the fluid film.

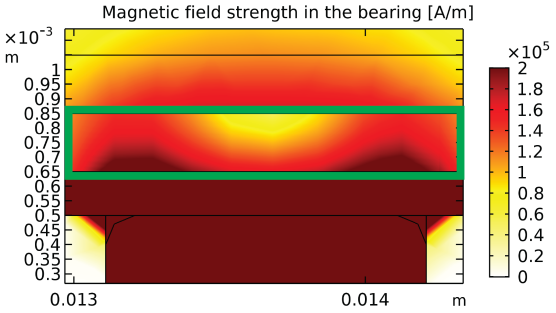

Figure E-23: Magnetic field strength over the width of the magnets. Here green indicates the fluid film.

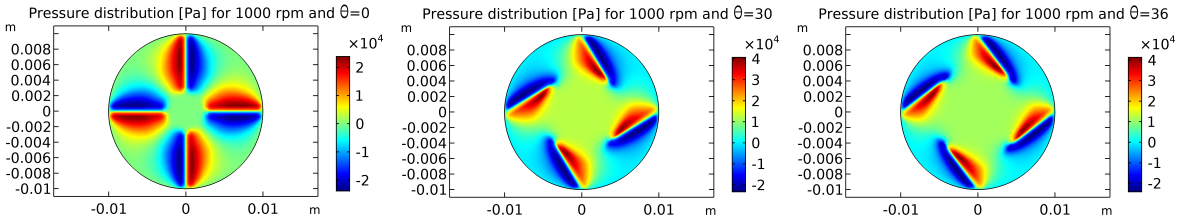

Figure E-24: Pressure distribution for 1000 rpm on the top bearing face for $\theta = 0, 30$ and 36.

be used as the cut-off ratio for the integration. When the pressure will be less than the vapor pressure, this value will be cut off and equal to the vapor pressure. For $\theta > 0$ already a load capacity will be obtained not considering a vapor pressure because here the positive pressure dominates.

E-6 Complete sedimentation

This numerical simulation is a 3D model regarding complete sedimentation of magnetic particles and carrier fluid. A model is made where physical steps are implemented over which a fluid flows with a viscosity equal to the carrier fluid. The physical steps modeled are based on results for the apparent viscosity in the 3D model seen in section E-5. Here the regions where $\eta > 1000$ are considered solid. The dimensions of this step do change for increasing velocity. This is why for the dimensions of the steps in the model average values are taken. Here the length of the step is equal to the length of the magnet, the width is equal to the twice the width of the magnet, and the height is taken equal to 180 μm. This corresponds to the volume fraction of iron in MRF122EG. An illustration of the model is seen in figure E-25, which is a 2D section as seen in figure E-21.

In this mode only the fluid film layer containing the steps is considered. For this model a 'Creeping Flow (spf)' was used with the same boundary conditions used for the model considering a perfectly mixed MR fluid in section E-5. Furthermore a cubic magnetic scalar potential discretization for the magnetic field and a $P2 + P1$ discretization of fluids for the fluid flow is used. Also for this model a user-controlled mesh is used. The model consists of two layers, one layer containing the steps and fluid (180 μm), and one layer of fluid (20 μm). For both a normal mesh is swept through it resulting in a total of 10 layers for the layer

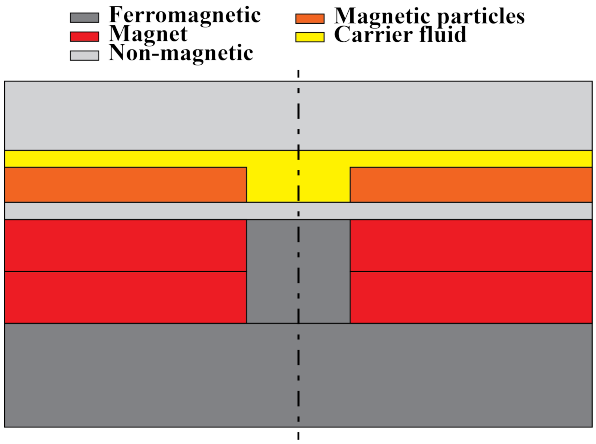

Figure E-25: 2D section at location A-A in figure E-21 of the geometry used in the numerical simulation for complete sedimentation

containing the steps and 5 layers for the layer of fluid.

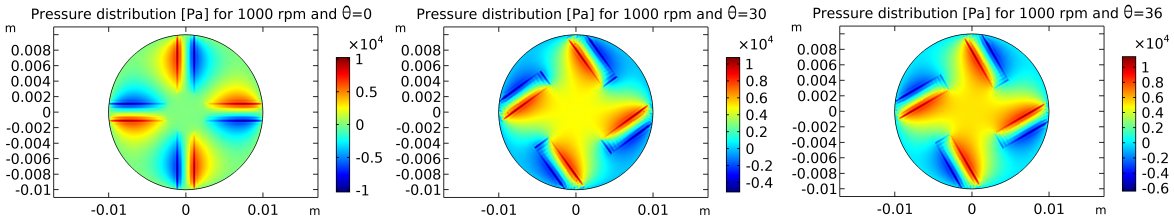

Figure E-26: Pressure distribution for 1000 rpm on the top bearing face for $\theta = 0, 30$ and 36.

In figure E-26 the different pressure distributions on the top bearing face obtained are seen. The sensitivity for a change in value of 10% for different dimensions of the steps, and the viscosity of the fluid is investigated in order to see which parameter has the most significant impact on the load capacity. In figure E-27 it is seen that for $\theta = 0$ a change in height of the step will have the most significant impact on the load capacity. For $\theta = 30$ and 36 the length of the step will have the most significant impact on the load capacity. In figure E-27 the reference line is the load capacity where $l = 7.5E-3$ mm, $b = 2.2E-3$ mm, $h = 1.8E-4$ mm, $\eta = 0.03$ Pa·s, and a vapor pressure of 0.965 atm.

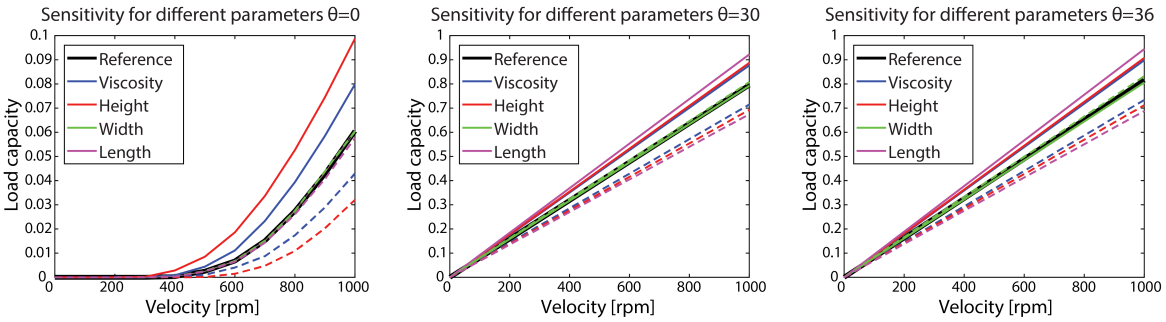

Figure E-27: Pressure distribution for 1000 rpm on the top bearing face for $\theta = 0, 30$ and 36.

E-7 Optimal angle

The configuration used in the numerical models and proof of concept seen in figure E-28 will have a different load capacity for a different angle θ. It is desired to obtain a configuration where the highest load capacity will be obtained. To obtain this angle, a simple numerical simulation is made where the angle is varied from 0 to 68 degrees. The maximum angle is chosen to be equal to 68, because at this angle the areas with a magnetic field will go past the outer radius of the measured circle. Two materials are implemented in the simulation, for one material the viscosity depends on the magnetic field and for the other material the viscosity is constant. The magnetic field strength is obtained from the numerical simulation for the thrust bearing in section E-5. This magnetic field is used to determine the yield stress and so being able to obtain the viscosity in the volumes highlighted in blue in figure E-28. For obtaining the viscosity the analytic function seen in figure E-29 is implemented. Here it is seen that the apparent viscosity depends on the yield stress which varies over the height of the fluid film, and the shear rate. The volume not highlighted in blue has a constant viscosity which is equal to the dynamic viscosity of the MR fluid.

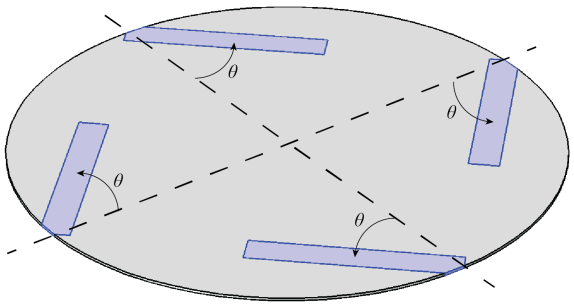

Figure E-28: Configuration of the prototype used in the numerical simulation.

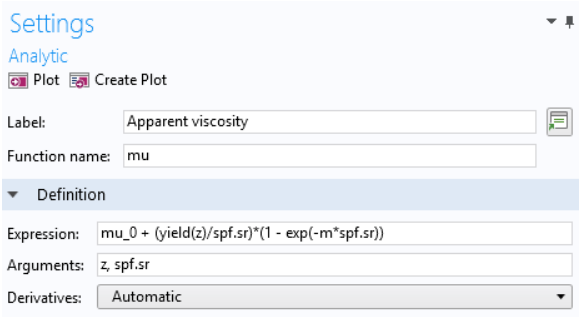

Figure E-29: Analytic function for the apparent viscosity implemented in COMSOL for obtaining the optimal angle.

The study 'Creeping Flow (spf)' is used and the same boundary conditions as used in section E-5 are applied, an open boundary, no slip condition to the top and bottom surface, and a velocity given in polar coordinates applied to the top surface. An user-controlled mesh is used, a coarser free triangular mesh is swept through the film resulting in a total of 10 layers.

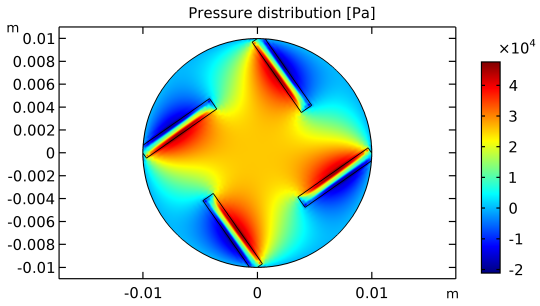

Figure E-30: Pressure distribution obtained for one configuration where $\theta = 36$ degrees.

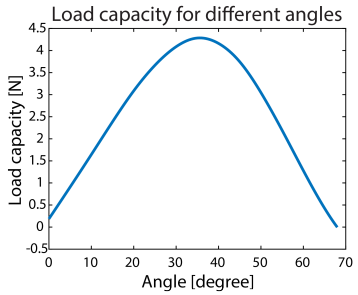

Figure E-31: Load capacity for different configurations of the magnets.

In figure E-30 the pressure distribution for one configuration is seen and in figure E-31 the change in load capacity is seen for an increasing angle θ. At an angle equal to 0 degrees, there already is a load capacity and if the angle is equal to 68 degrees the load capacity will be equal to 0. The maximum load capacity achievable is seen at an angle equal to 36 degrees. The magnitude of the load capacity in figure E-31 are not correct, but just an indication at which angle the maximum load capacity can be expected.

Appendix F

Experimental set-up

For the experiments the Anton Paar MCR 302 seen in figure F-1 is used. This rheometer is chosen because it was already available at the Delft University of Technology and it is able to measure a normal force which is desired for this research. Also the Viscotherm VT2 cool water bath and Julabo AWC100 circulation cooler are part of the set-up and a constant air pressure for the air bearing is required in the head of the rheometer. For the experiments a cone & plate, and a parallel plate spindle are used, both illustrated in figure F-2. The cone & plate spindle is used for measuring the viscosity of the fluid, and the parallel plate spindle is used for the measurements with the proof of concept where the normal force is measured. For the cone & plate only one measuring position equal to 0.085 mm can be measured, for the parallel plate the measuring position can be set to every desired value. For both the spindles the diameter over which is measured is equal to 20 mm and the angle for the cone is equal to 2 degrees.

Figure F-1: Experimental set-up where consisting of the Antor Paar MCR 302 rheometer, Viscotherm VT2 cool water bath, and Julabo AWC100 circulation cooler. A proof of concept is placed in the rheometer as seen at the right.

In figure F-3 the proof of concept used during the experiments are seen. Here three configurations are seen based on the configuration used in section E-5 and seen in figure E-21. Here again the angle under which the magnets lie are equal to 0, 30, and 36 degrees. As seen in the

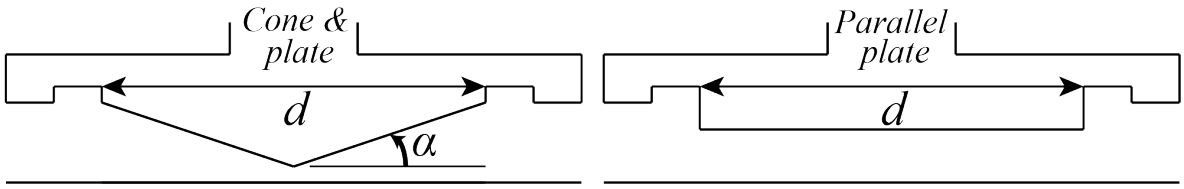

Figure F-2: Illustration of the cone & plate and parallel spindles used for the measurements.

figure one proof of concept is build out of 2 layers of 2 mm thick steel with diameter of 85 mm made with a laser cutter, a piece of 0.15 mm thick glass with a diameter of 25 mm indicated with red in te figure, 8 bar magnets indicated with blue (4 pairs of two) with dimensions 7.5x1.1x1 mm and a magnetic flux density of 1.28 tesla inside each magnet, 3 bolts, 3 flanges, and 3 nuts. The diameter of the steel layers is equal to the inner diameter of the 'tub' in the rheometer. As seen in figure F-3 one layer of steel, the bottom layer, is used to lock the proof of concept into place.

Figure F-3: Different proofs of concept used for the experiments on the top left, and the components used to make them on the bottom left (red and blue indicate the glass and magnets respectively). On the right is shown how the bottom layer of the proofs of concept locks in the rheometer.

For depositing the MR fluid on the proof of concept the Eppendorf Research plus, single-channel, variable, 20-200 μL, pipette is used. The volume that is deposited is equal to volume underneath the spindle. Before any measurement the rheometer has to be initialized and this is done without any spindle. The moment this is done, a spindle can be placed inside the head and the zero gap position can be set in order to determine the position of the proof of concept with respect to the spindle. This zero gap is set without any fluid present. For setting the zero gap the rheometer will lower the spindle until first contact is made, this position will be equal to a height of 0 mm.

When the machine is initialized and the zero gap is set, a fluid can be deposited on the proof of concept and a measurement can be initialized. Two test definitions are used for

the measurements as seen in figure F-5. One consisting of a procedure where the spindle is moved to the measuring position which is equal to the fly height of 0.2 mm, followed by the measurement. This is the definition where the measurements will not be zeroed. A second definition is also used where between the procedure for moving to the measuring position and measurement, a procedure is added where the normal force is balanced and set to zero. A measuring position of 0.2 mm was chosen. This is because when a lower position was chosen, the spindle could not lower to this position when an MR fluid was deposited on the proof of concept. Before the measuring position was reached already a normal force equal to 15 newton was sensed, and this limits the machine. This force is present due to the pressurization of the MR fluid due to the magnetic field. One time the machine was forced to a measuring position of 0.1 mm, but this resulted in failure of the proof of concept where the glass separating the fluid from the magnets broke as seen in figure F-4.

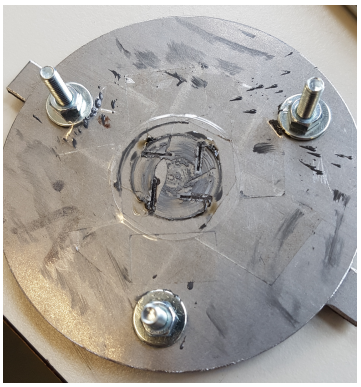

Figure F-4: Failure of the proof of concept where the glass separating the fluid from the magnets broke due to high normal forces.

In the measurement tab of the definition the parameters can be chosen that will be given as an input during the experiment. For these experiments it was chosen to set the rotational speed and let it increase linearly to 1000 as seen in figure F-5. The number of data points is set to 1000, and a constant interval between each point can be set. For the measurement an interval equal to 10 ms and 1000 ms was chosen. The measurement frequency of the sensor in the MCR 302 rheometer is equal to 512 Hz. For an interval of 10 ms the average of 5 data points will be displayed.

Also some measurements are done to check the viscosity of the MR fluid MRF122EG used for the experiments, and also for the carrier fluid. To obtain the carrier fluid from the MR fluid, the Eppendorf Centrifuge 5415 is used to separate the carrier fluid from the magnetic particles as seen in figure F-6. Little bottles designed for this centrifuge containing the MR fluid can be placed in the little holes in the centrifuge. The MR fluid is centrifuged for 10 minutes at a speed of 14000 rpm and the carrier fluid separated from the magnetic particles was obtained as seen in figure F-6. Both the results for MRF122EG and its carrier fluid are seen in figure F-7.

The viscosity obtained for MRF122EG is equal to 0.0856 Pa·s and that for the carrier fluid the viscosity is equal to 0.0302 Pa·s. Looking at the datasheet for MRF122EG in appendix J it is seen that the viscosity of the MR fluid does not correspond with the data provided on the sheet. The viscosity that is measured will be used during this research.

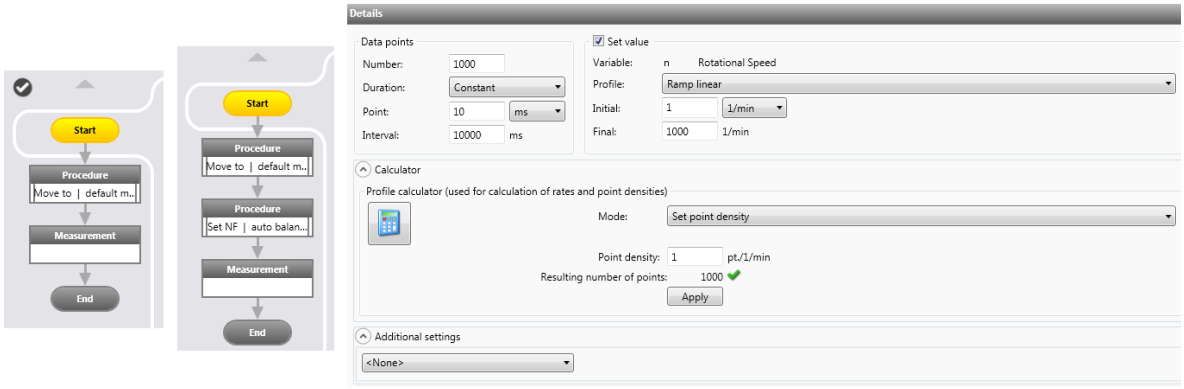

Figure F-5: Test definitions used for the experiments and details on how the measurement is done.

Figure F-6: Eppendorf Centrifuge 5415 used for separating the magnetic particles from the carrier fluid.

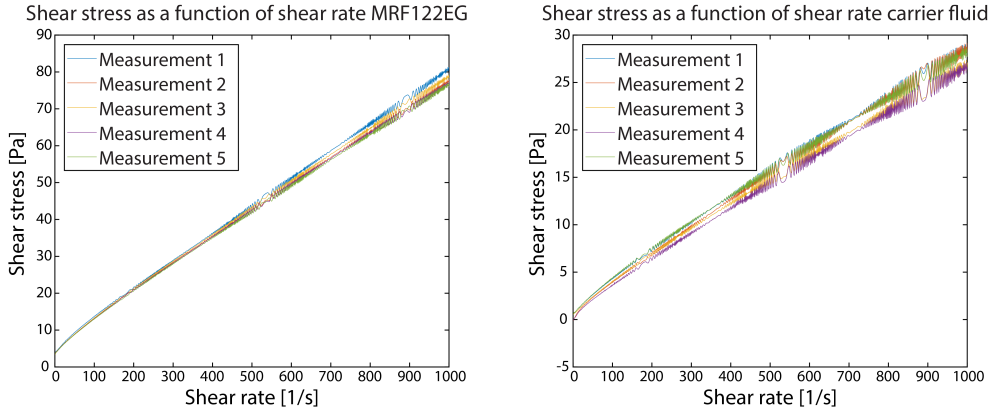

Figure F-7: Measurements done for MRF122EG and its carrier fluid for determining the viscosity. Here no magnetic field is applied.

Appendix G

Error

The shape of the surfaces in which between the MR fluid is captured can have an influence on the load capacity obtained. In a hydrodynamic thrust bearing where the parallel surfaces which have a velocity relatively to each other and have no surface texturing, the fluid will not be pressurized. When the two surfaces are not parallel due to any shape of one of the two surfaces, there is the possibility the fluid will be pressurized which can create a load carrying behavior. In figure G-1 three shapes of a surface are shown, a wedge, a parabolic cylinder, and an elliptic paraboloid are seen. Each shape can be described by an error which describes a length indicated with red in figure G-1.

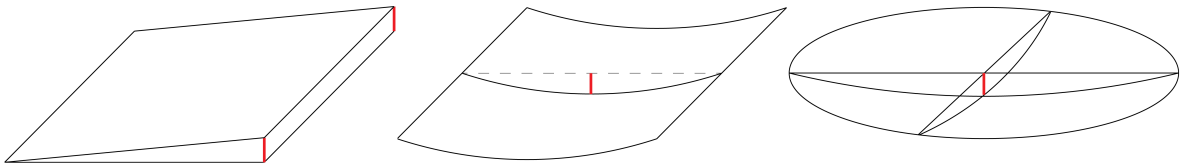

Figure G-1: Common shapes of a surface that can pressurize the liquid in a hydrodynamic bearing.

For being able to predict the possible error by the proof of concept, the surface has to be measured and this can be done with the Bruker white light interferometer. Knowing the shape, a numerical simulation will be used to see the contribution of the possible error.

G-1 Numerical simulation

For the numerical simulation a 'Thin-Film Flow, Shell (tffs)' study was used in combination with an extremely fine physics-controlled mesh. To the border of the surface a zero pressure border condition was applied. Because the surface is seen as a thin film, a height has to be given to the wall above reference plane and to the base below reference plane. The wall above reference plane represents the moving bearing face, and to the base below reference plane the error is applied. To the plane above reference a height of 200 μm is given, equal to the film height. To the base plane a height is given which is depending on x for the wedge and parabolic cylinder, and a height depending on x and y for the elliptic paraboloid. The height for the base plane for the wedge, parabolic cylinder, and elliptic paraboloid are seen in equations G-1, G-2, and G-3 respectively.

$$h_{b1} = -\frac{e}{2} + \frac{e}{20 \cdot 10^{-3}} x \tag{G-1}$$

$$h_{b2} = \frac{e}{r^2} \cdot x^2 - e \tag{G-2}$$

$$h_{b3} = \frac{e}{r^2} \cdot x^2 + \frac{e}{r^2} \cdot y^2 - e \tag{G-3}$$

In figure G-2, G-3, and G-4 the pressurization of the liquid due to a wedge shape, a parabolic cylinder shape, and a elliptic paraboloid are seen respectively. Here the viscosity is equal to the viscosity of MRF122EG when no magnetic field is applied, 0.085 P·s. For each result the film height is equal to 200 μm, and an error of 10 μm is applied. The velocity applied is 1000 rpm, which is equal to the maximum velocity applied during the experiments. Doing this an antisymmetric pressurization of the liquid is seen for the wedge and the parabolic cylinder. In contrary there is the elliptic paraboloid where no pressurization of the liquid is seen. The viscosity is sweeped from 0 to 1 resulting in different load capacities (Fig. G-5).

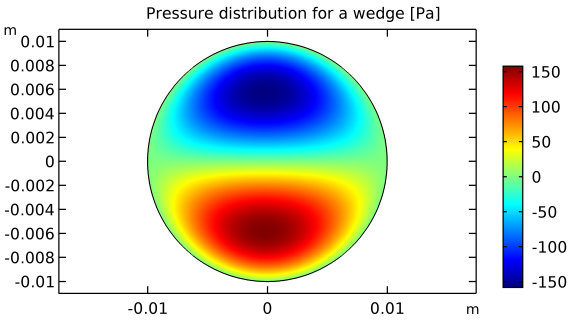

Figure G-2: Pressurization of the liquid due to a wedge shape.

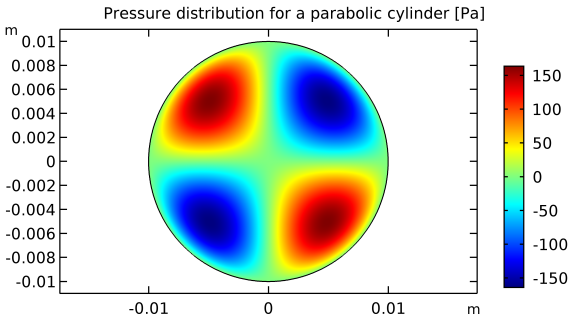

Figure G-3: Pressurization of the liquid due to a parabolic cylinder shape.

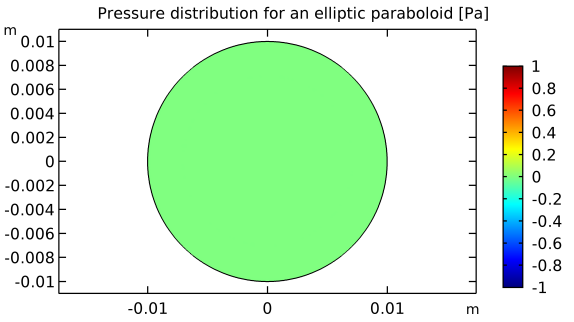

Figure G-4: Pressurization of the liquid due to an elliptic paraboloid shape.

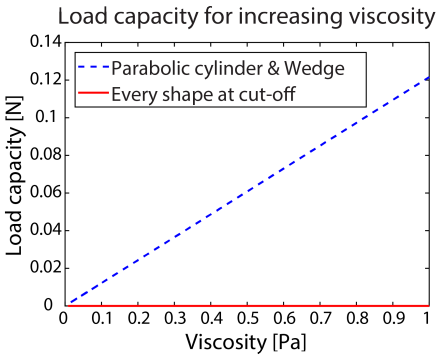

Figure G-5: Increasing load capacity due an increase in viscosity.

To obtain the load capacity due to the different shapes, the pressure distribution can be integrated over the top surface of the bearing. Because no cavitation is considered in the numerical models, no load capacity will be obtained due to the antisymmetric results. That is why the negative pressure is cut-off at 0.965 atm, in order to obtain an approximation for the load capacity. For a viscosity of 0.085 Pa·s and a velocity of 1000 rpm, no load capacity due to the error is obtained for any of the shapes as seen in figure G-5.

G-2 Shape of the proof of concept

In figure G-6 the tilted flatness of the proof of concept is seen, the area that is measured is the area which will be covered with MR fluid. The result is tilted because the table of the Bruker white light interferometer seen in figure G-7 on which the proof of concept is placed has to be leveled manually. So by tilting the result, the shape of the proof of concept can be obtained. It is seen that it is an elliptic paraboloid with a height of approximately 20 μm.

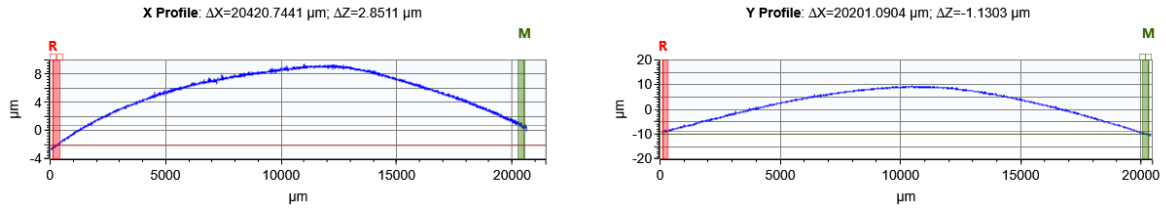

Figure G-6: Tilted result of the surface of the proof of concept.

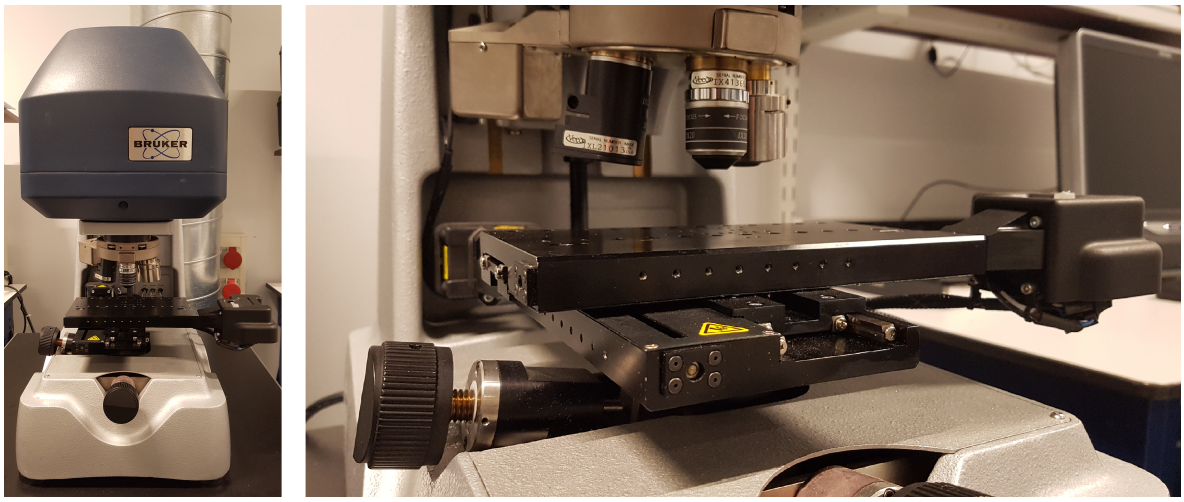

Figure G-7: Bruker White Light Interferometer, used to measure the surface of the proof of concept.

But because the results are tilted, a possible wedge will be ignored. In figure G-8 the untitled result is seen, and here it is seen that a wedge is present. The maximum measured is 76 μm and the minimum measured is -88 μm. But in this measurement also the possible wedge of the table of white light interferometer is measured. To obtain this error only a piece of glass which is used in the proof of concept is placed on the table, and the result is seen in figure G-9. Here the maximum measured is 81 μm and the minimum measured is -81 μm. Subtracting these results it can be stated that a wedge of approximately 3 μm is present in the proof of concept.

During experiments it was observed that the carrier fluid separates from the magnetic particles. This means that the fluid that has to be considered for causing an error in the load capacity has a lower viscosity than the MR fluid itself. Looking at the graph for the errors due to a wedge (Fig. G-5) it can be concluded that the effects of the shape of the proof of concept will not have an impact on the results.

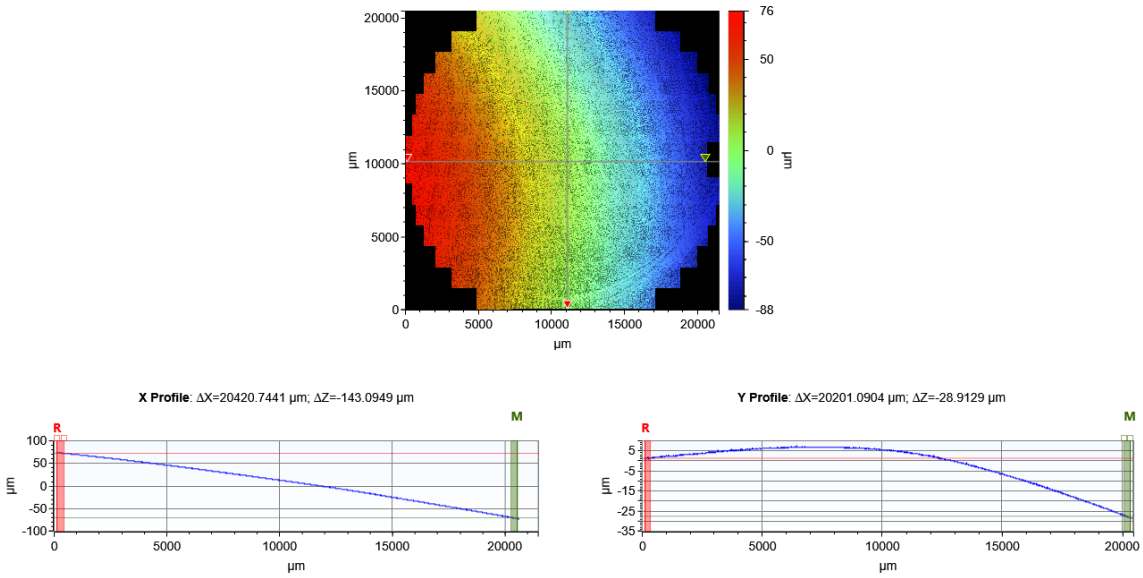

Figure G-8: Untilted result of the surface of the proof of concept.

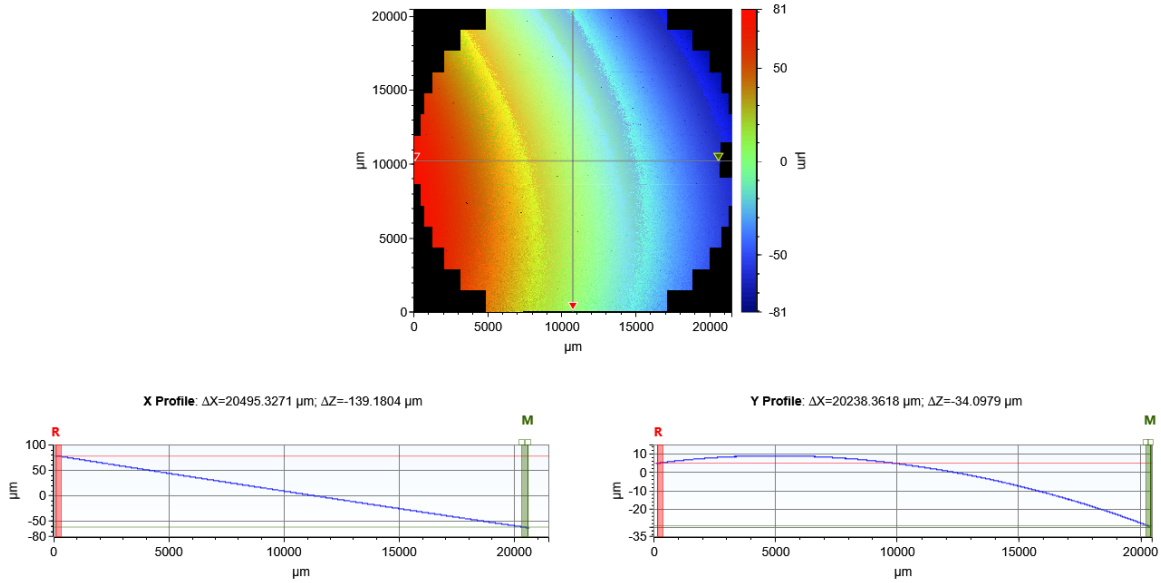

Figure G-9: Untiled result of the surface of glass used in the proof of concept.

Appendix H

Oil separation

During the experiments it was observed that carrier fluid was separating from the magnetic particles. This is seen for the different configurations used in figure H-1, H-2, and H-3. This separation resulted in different results for the load capacity than predicted with the numerical simulations.

Figure H-1: Oil separating from the magnetic particles during the experiments for $\theta = 0$ degrees.

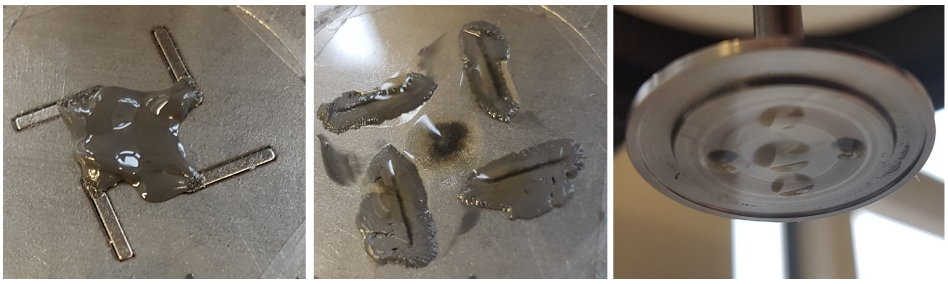

Figure H-2: Oil separating from the magnetic particles during the experiments for $\theta = 30$ degrees.

Figure H-3: Oil separating from the magnetic particles during the experiments for $\theta = 36$ degrees.

Appendix I

Datasheet MRF140CG

MRF-140CG Magneto-Rheological Fluid

Description

LORD MRF-140CG fluid is a hydrocarbon-based magneto-rheological (MR) fluid formulated for general use in controllable, energy-dissipating applications such as shocks, dampers and brakes.

MRF-140CG fluid is a suspension of micron-sized, magnetizable particles in a carrier fluid. When exposed to a magnetic field, the rheology of MRF-140CG fluid reversibly and instantaneously changes from a free-flowing liquid to a semi-solid with controllable yield strength. Altering the strength of the applied magnetic field precisely and proportionally controls the consistency or yield strength of the fluid.

MRF-140CG fluid can be used in *valve mode* (fluid flowing through an orifice) or in *shear mode* (fluid shearing between two surfaces). In the absence of a magnetic field, MRF-140CG fluid flows freely or allows free movement. Upon application of a magnetic field, the fluid's particles align with the direction of the field in chain-like fashion, thereby restricting the fluid's movement within the gap in proportion to the strength of the magnetic field.

Features and Benefits

Fast Response Time – responds instantly and reversibly to changes in a magnetic field.

Dynamic Yield Strength – provides high yield strength in the presence of a magnetic field and very low yield strength in the absence of a magnetic field; allows for a wide range of controllability.

Temperature Resistant – performs consistently throughout a broad temperature range, meeting the requirements of demanding applications such as automotive shock absorbers.

Hard Settling Resistant – provides high resistance to hard settling; easily redispersed.

Non-Abrasive – formulated to not abrade the devices in which the MR fluid is used.

Application

For more information on MR technology, refer to the MR Design Guides located on www.lord.com/mr.

Mixing – Under common flow conditions, no separation is observed between particles and the carrier fluid. However, a degree of separation may eventually occur under static conditions. If needed, use a paint shaker to redisperse the particles into a homogeneous state prior to use.

Storage

Keep container tightly closed when not in use.

Typical Properties*

Appearance	Dark Gray Liquid
Viscosity, Pa-s @ 40°C (104°F) Calculated as slope 800-1200 sec^{-1}	0.280 ± 0.070
Density	
g/cm^3	3.54-3.74
(lb/gal)	(29.5-31.2)
Solids Content by Weight, %	85.44
Flash Point, °C (°F)	>150 (>302)
Operating Temperature, °C (°F)	-40 to +130 (-40 to +266)

*Data is typical and not to be used for specification purposes.

LORD
AskUsHow™

Cautionary Information

Before using this or any LORD product, refer to the Material Safety Data Sheet (MSDS) and label for safe use and handling instructions.

For industrial/commercial use only. Not to be used in household applications. Not for consumer use.

Shear Stress as a function of Shear Rate with no Magentic Field applied at 40°C (104°F)

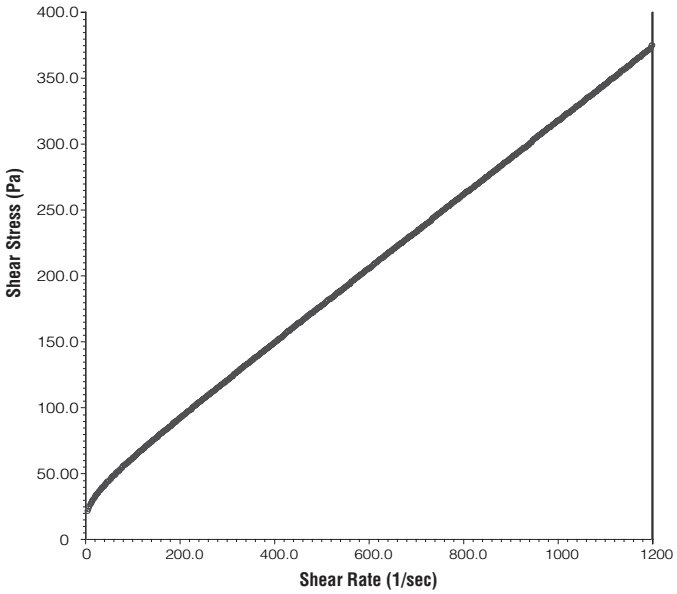

Yield Stress vs. Magnetic Field Strength

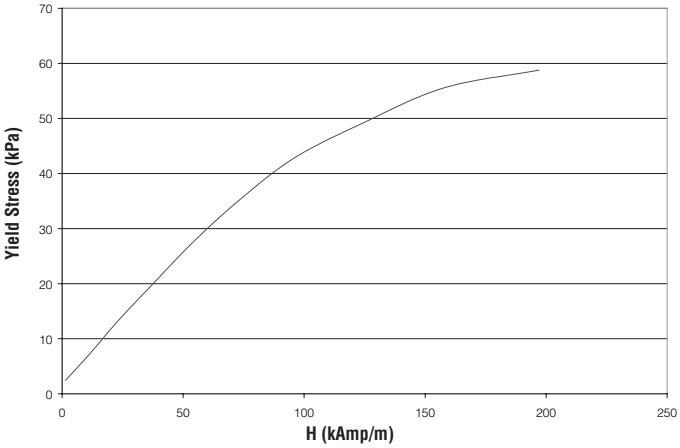

Typical Magnetic Properties

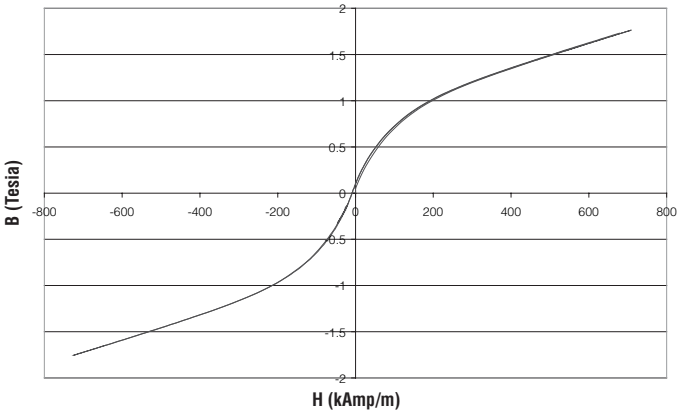

Values stated in this technical data sheet represent typical values as not all tests are run on each lot of material produced. For formalized product specifications for specific product end uses, contact the Customer Support Center.

Information provided herein is based upon tests believed to be reliable. In as much as LORD Corporation has no control over the manner in which others may use this information, it does not guarantee the results to be obtained. In addition, LORD Corporation does not guarantee the performance of the product or the results obtained from the use of the product or this information where the product has been repackaged by any third party, including but not limited to any product end-user. Nor does the company make any express or implied warranty of merchantability or fitness for a particular purpose concerning the effects or results of such use.

LORD provides valuable expertise in adhesives and coatings, vibration and motion control, and magnetically responsive technologies. Our people work in collaboration with our customers to help them increase the value of their products. Innovative and responsive in an ever-changing marketplace, we are focused on providing solutions for our customers worldwide . . . Ask Us How.

LORD Corporation
World Headquarters
111 Lord Drive
Cary, NC 27511-7923
USA

Customer Support Center (in United States & Canada)
+1 877 ASK LORD (275 5673)

www.lord.com

LORD
Ask Us How™

Appendix J

Datasheet MRF122EG

MRF-122EG Magneto-Rheological Fluid

Description

LORD MRF-122EG fluid is a hydrocarbon-based magneto-rheological (MR) fluid formulated for general use in controllable, energy-dissipating applications such as shocks, dampers and brakes.

MRF-122EG fluid is a suspension of micron-sized, magnetizable particles in a carrier fluid. When exposed to a magnetic field, the rheology of MRF-122EG fluid reversibly and instantaneously changes from a free-flowing liquid to a semi-solid with controllable yield strength. Altering the strength of the applied magnetic field precisely and proportionally controls the consistency or yield strength of the fluid.

MRF-122EG fluid can be used in *valve mode* (fluid flowing through an orifice) or in *shear mode* (fluid shearing between two surfaces). In the absence of a magnetic field, MRF-122EG fluid flows freely or allows free movement. Upon application of a magnetic field, the fluid's particles align with the direction of the field in chain-like fashion, thereby restricting the fluid's movement within the gap in proportion to the strength of the magnetic field.

Features and Benefits

Fast Response Time – responds instantly and reversibly to changes in a magnetic field.

Dynamic Yield Strength – provides high yield strength in the presence of a magnetic field and very low yield strength in the absence of a magnetic field; allows for a wide range of controllability.

Temperature Resistant – performs consistently throughout a broad temperature range, meeting the requirements of demanding applications such as automotive shock absorbers.

Hard Settling Resistant – provides high resistance to hard settling; easily redispersed.

Non-Abrasive – formulated to not abrade the devices in which the MR fluid is used.

Application

For more information on MR technology, refer to the MR Design Guides located on www.lord.com/mr.

Mixing – Under common flow conditions, no separation is observed between particles and the carrier fluid. However, a degree of separation may eventually occur under static conditions. If needed, use a paint shaker to redisperse the particles into a homogeneous state prior to use.

Storage

Keep container tightly closed when not in use.

Typical Properties*

Appearance	Dark Gray Liquid
Viscosity, Pa-s @ 40°C (104°F) Calculated as slope 500-800 sec^{-1}	0.042 ± 0.020
Density	
g/cm^3	2.28-2.48
(lb/gal)	(19.0-20.7)
Solids Content by Weight, %	72
Flash Point, °C (°F)	>150 (>302)
Operating Temperature, °C (°F)	-40 to +130 (-40 to +266)

*Data is typical and not to be used for specification purposes.

LORD
AskUsHow™

Cautionary Information

Before using this or any LORD product, refer to the Material Safety Data Sheet (MSDS) and label for safe use and handling instructions.

For industrial/commercial use only. Not to be used in household applications. Not for consumer use.

Yield Stress vs. Magnetic Field Strength

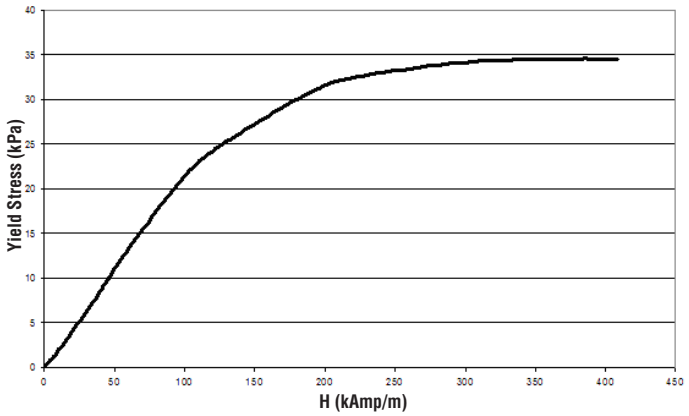

Shear Stress as a function of Shear Rate with no Magnetic Field applied at 40°C (104°F)

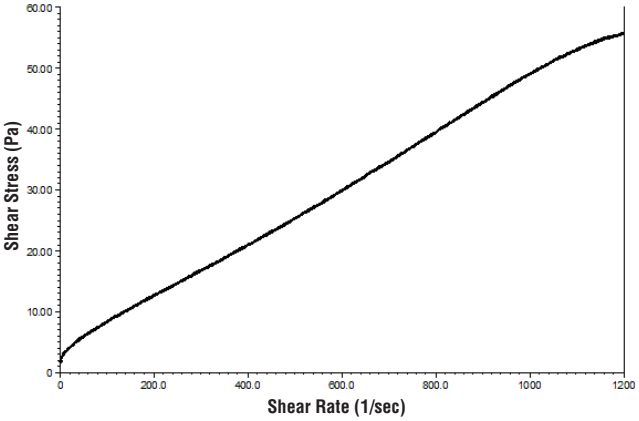

Typical Magnetic Properties

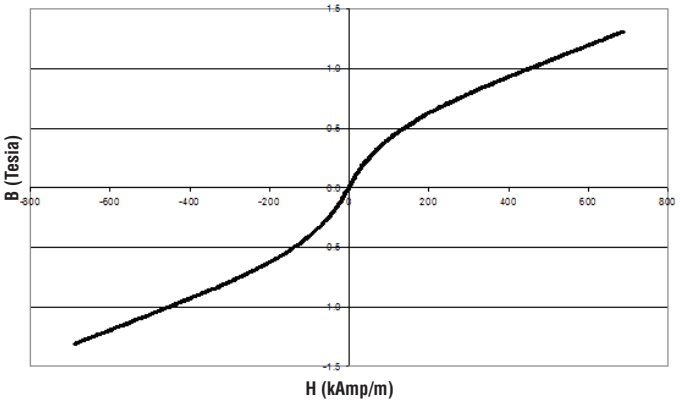

Values stated in this technical data sheet represent typical values as not all tests are run on each lot of material produced. For formalized product specifications for specific product end uses, contact the Customer Support Center.

Information provided herein is based upon tests believed to be reliable. In as much as LORD Corporation has no control over the manner in which others may use this information, it does not guarantee the results to be obtained. In addition, LORD Corporation does not guarantee the performance of the product or the results obtained from the use of the product or this information where the product has been repackaged by any third party, including but not limited to any product end-user. Nor does the company make any express or implied warranty of merchantability or fitness for a particular purpose concerning the effects or results of such use.

LORD provides valuable expertise in adhesives and coatings, vibration and motion control, and magnetically responsive technologies. Our people work in collaboration with our customers to help them increase the value of their products. Innovative and responsive in an ever-changing marketplace, we are focused on providing solutions for our customers worldwide . . . Ask Us How.

LORD Corporation
World Headquarters
111 Lord Drive
Cary, NC 27511-7923
USA

Customer Support Center (in United States & Canada)
+1 877 ASK LORD (275 5673)

www.lord.com

LORD Ask Us How™

Bibliography

[1] Ö. B. Adıgüzel and K Atalık. "Magnetic field effects on Newtonian and non-Newtonian ferrofluid flow past a circular cylinder". In: *Applied Mathematical Modelling* 42 (2017), pp. 161–174.

[2] V.K. Agrawal. "Magnetic-fluid-based porous inclined slider bearing". In: *Wear* 107.2 (1986), pp. 133–139.

[3] Tojiro Aoyama. "Hydrostatic bearing". In: *CIRP Encyclopedia of Production Engineering*. Springer, 2014, pp. 682–687.

[4] H. A. Barnes, J. F. Hutton, and K. Walters. *An introduction to rheology*. Elsevier, 1989.

[5] R. Bassani and B. Piccigallo. *Hydrostatic lubrication*. Vol. 22. Elsevier, 1992.

[6] M.V. Bhat and G.M. Deheri. "Porous composite slider bearing lubricated with magnetic fluid". In: *Japanese journal of applied physics* 30.10R (1991), p. 2513.

[7] S. N. Bhore and N. D. Khaire. "Analytical and Experimental investigation of Magnetorheological Fluid in Hydrodynamic journal bearing". In: *International Engineering Research Journal* (), pp. 271–277.

[8] E. C. Bingham. *An investigation of the laws of plastic flow*. 278. US Government Printing Office, 1917.

[9] A.J.F. Bombard et al. "Magnetic susceptibility and saturation magnetization of some carbonyl iron powders used in magnetorheological fluids". In: *Materials science forum*. Vol. 416. Transtec Publications. 2003, pp. 753–758.

[10] D.A. Bompos and P.G. Nikolakopoulos. "Experimental and analytical investigations of dynamic characteristics of magnetorheological and nanomagnetorheological fluid film journal bearing". In: *Journal of Vibration and Acoustics* 138.3 ().

[11] A.S.T. Boots et al. "Increasing the load capacity of planar ferrofluid bearings by the addition of ferromagnetic material". In: *Tribology International* 129 (2019), pp. 46–54.

[12] "BWI MagneRide: Magneto-rheological damping". In: *The Automotive Suspension Systems Report* (2013), pp. 59–60.

[13] A. Cameron and F.W. Ocvirk. *Principles of lubrication*. 1967.

[14] J.D. Carlson, W. Matthis, and J.R. Toscano. "Smart prosthetics based on magnetorheological fluids". In: *Smart Structures and Materials 2001: Industrial and Commercial Applications of Smart Structures Technologies*. Vol. 4332. International Society for Optics and Photonics. 2001, pp. 308–317.

[15] C.Q. Chi, Z.S. Wang, and P.Z. Zhao. "Research on a new type of ferrofluid-lubricated journal bearing". In: *Journal of Magnetism and Magnetic Materials* 85.1-3 (1990), pp. 257–260.

[16] G. Daniel et al. "Bingham-papanastasiou and approximate parallel models comparison for the design of magneto-rheological valves". In: *Advanced Intelligent Mechatronics (AIM), 2014 IEEE/ASME International Conference on*. Ieee. 2014, pp. 168–173.

[17] B.J. De Gans et al. "Preparation and magnetisation of a silica-magnetite inverse ferrofluid". In: *Journal of magnetism and magnetic materials* 201.1-3 (1999), pp. 11–13.

[18] J.A. Duggan. *Center bearing assembly including support member containing rheological fluid*. US Patent 5,452,957. 1995.

[19] S.V. D'yachenko and A.I. Zhernovoi. "The Langevin formula for describing the magnetization curve of a magnetic liquid". In: *Technical Physics* 61.12 (2016), pp. 1835–1837.

[20] M. Fermigier and A.P. Gast. "Structure evolution in a paramagnetic latex suspension". In: *Journal of Colloid and Interface Science* 154.2 (1992), pp. 522–539.

[21] S. Genc and B. Derin. "Synthesis and rheology of ferrofluids: a review". In: *Current Opinion in Chemical Engineering* 3 (2014), pp. 118–124.

[22] J.M . Ginder, L.D. Elie, and L.C. Davis. *Magnetic fluid-based magnetorheological fluids*. US Patent 5,549,837. 1996.

[23] J. Gołdasz and B. Sapiński. *Insight into magnetorheological shock absorbers*. Springer, 2015.

[24] T. He et al. "Experimental and Numerical Investigations of the Stribeck Curves for Lubricated Counterformal Contacts". In: *Journal of Tribology* 139.2 (2017), p. 021505.

[25] J.A.K.C. Hesselbach and C. Abel-Keilhack. "Active hydrostatic bearing with magnetorheological fluid". In: *Journal of applied physics* 93.10 (2003), pp. 8441–8443.

[26] G.J. Hiemenz, Y. Choi, and N.M. Wereley. "Semi-active control of vertical stroking helicopter crew seat for enhanced crashworthiness". In: *Journal of aircraft* 44.3 (2007), pp. 1031–1034.

[27] T.E. Il'ina and N.V. Prodan. "Element Design for an Inkjet System of Hydrostatic Gas Bearing Control". In: *Naučno-tehničeskij Vestnik Informacionnyh Tehnologij* 15.5 (2015), pp. 921–929.

[28] R. Jacob. *High-speed magnetic fluid clutch*. US Patent 2,622,713. 1952.

[29] S. JP and M. Doi. "Effective viscosity of magnetic fluids". In: *Journal of the Physical Society of Japan* 59.1 (1990), pp. 111–117.

[30] I.G. Kim et al. "Nano-sized Fe soft-magnetic particle and its magnetorheology". In: *Colloid and Polymer Science* 289.1 (2011), pp. 79–83.

[31] C. Kittel. *Introduction to solid state physics*. Vol. 8. Wiley New York, 1976.

[32] D.J. Klingenberg, J.C. Ulicny, and M.A. Golden. “Mason numbers for magnetorheology”. In: *Journal of Rheology* 51.5 (2007), pp. 883–893.

[33] D.C. Kuzma. “The magnetohydrodynamic journal bearing”. In: *Journal of Basic Engineering* 85.3 (1963), pp. 424–427.

[34] S.G.E. Lampaert. “Planar Ferrofluid Bearings: Modelling and Design Principles”. In: (2015).

[35] S.G.E. Lampaert and R.A.J van Ostayen. “Virtual Textured Hybrid Bearings”. In: *44th Leeds-Lyon Symposium on Tribology* (2017).

[36] S.G.E. Lampaert, J.W. Spronck, and R.A.J. van Ostayen. “Load and stiffness of a planar ferrofluid pocket bearing”. In: *Proceedings of the Institution of Mechanical Engineers, Part J: Journal of Engineering Tribology* 232.1 (2018), pp. 14–25.

[37] S.G.E. Lampaert et al. “In-plane friction behaviour of a ferrofluid bearing”. In: *Precision Engineering* 54 (2018), pp. 163–170.

[38] M. Leader. “Understanding journal bearings”. In: *Vibration Institute Annual Conference Proceedings*. 2012.

[39] J.E. Martin and R.A. Anderson. “Chain model of electrorheology”. In: *The Journal of chemical physics* 104.12 (1996), pp. 4814–4827.

[40] A.G.M. Michell. “The lubrication of plane surfaces”. In: *Transactions of the Institution of Engineers, Australia. Mechanical engineering* 12.3-4 (1988), pp. 48–62.

[41] T. Mou et al. “The evolution of field-induced structure of confined ferrofluid emulsions”. In: *International Journal of Modern Physics B* 8.20 (1994), pp. 2779–2787.

[42] Aslam Muhammad, Xiong-liang Yao, and Zhong-chao Deng. “Review of magnetorheological (MR) fluids and its applications in vibration control”. In: *Journal of Marine Science and Application* 5.3 (2006), pp. 17–29.

[43] K. Nagaya et al. “Thrust bearing using a magnetic fluid lubricant under magnetic fields”. In: *Tribology international* 26.1 (1993), pp. 11–15.

[44] S. Odenbach. *Colloidal magnetic fluids: basics, development and application of ferrofluids*. Vol. 763. Springer, 2009.

[45] S. Odenbach. *Ferrofluids: magnetically controllable fluids and their applications*. Vol. 594. Springer, 2008.

[46] S. Odenbach. “Recent progress in magnetic fluid research”. In: *Journal of physics: condensed matter* 16.32 (2004), R1135.

[47] S. Odenbach and H. Störk. “Shear dependence of field-induced contributions to the viscosity of magnetic fluids at low shear rates”. In: *Journal of magnetism and magnetic materials* 183.1-2 (1998), pp. 188–194.

[48] S. Odenbach and S. Thurm. “Magnetoviscous effects in ferrofluids”. In: *Ferrofluids*. Springer, 2002, pp. 185–201.

[49] T.A. Osman, G.S. Nada, and Z.S. Safar. “Static and dynamic characteristics of magnetized journal bearings lubricated with ferrofluid”. In: *Tribology International* 34.6 (2001), pp. 369–380.

[50] N.S. Patel, D.P. Vakharia, and G.M. Deheri. "A study on the performance of a magnetic-fluid-based hydrodynamic short journal bearing". In: *ISRN mechanical engineering* 2012 (2012).

[51] H. Peeken. "Hydrostatische querlager [Hydrostatic Journal Bearing]". In: *Konstruktion [Design]* 16.7 (1964), pp. 266–276.

[52] J. Prakash and S.K. Vij. "Hydrodynamic lubrication of a porous slider". In: *Journal of Mechanical Engineering Science* 15.3 (1973), pp. 232–234.

[53] J.J. Roche. "B and H, the intensity vectors of magnetism: A new approach to resolving a century-old controversy". In: *American Journal of Physics* 68.5 (2000), pp. 438–449.

[54] W.B. Rowe. *Hydrostatic, aerostatic, and hybrid bearing design*. Elsevier, 2012.

[55] K. Saraswathamma, S. Jha, and P.V. Rao. "Rheological behaviour of Magnetorheological polishing fluid for Si polishing". In: *Materials Today: Proceedings* 4.2 (2017), pp. 1478–1491.

[56] G. Stachowiak and A.W. Batchelor. *Engineering tribology*. Butterworth-Heinemann, 2013.

[57] F.M. Stansfield. *Hydrostatic bearings for machine tools and similar applications*. Machinery Publishing London, 1970.

[58] R. Stribeck. "The basic properties of sliding and rolling bearings". In: *(Die Wesentlichen Eigenschaften der Gleit-und Rollenlager) Zeitschrift des Vereins Deutscher Ingenieure* 46.36 (2002), pp. 1341–1348.

[59] S. Thurm and S. Odenbach. "Particle size distribution as key parameter for the flow behavior of ferrofluids". In: *Physics of Fluids* 15.6 (2003), pp. 1658–1664.

[60] B. Tower. "Experiments on Pivot Friction". In: (1891).

[61] B. Tower. "First report of friction experiments". In: (1883).

[62] H. Urreta et al. "Hydrodynamic bearing lubricated with magnetic fluids". In: *Journal of intelligent material systems and structures* 21.15 (2010), pp. 1491–1499.

[63] A. Vincent. "Iron Man suit for US military - thanks to Hollywood costumers". In: *The Telegraph* (2014).

[64] W.M. Winslow. "Induced fibration of suspensions". In: *Journal of applied physics* 20.12 (1949), pp. 1137–1140.

[65] Q. Zhang et al. "Effect of particle size on the wear property of magnetorheological fluid". In: *Advances in Materials Science and Engineering* 2016 (2016).

[66] M. Zubieta et al. "Magnetorheological fluids: characterization and modeling of magnetization". In: *Smart Materials and Structures* 18.9 (2009), p. 095019.